

**UNDERSTANDING THE MECHANISM OF SIMULTANEOUSLY
OLEOPHOBIC/HYDROPHILIC PERFLUOROPOLYETHER (PFPE) NANO-
COATINGS**

by

Yongjin Wang

B.S., Dalian University of Technology, 2010

Submitted to the Graduate Faculty of
The Swanson School of Engineering in partial fulfillment
of the requirements for the degree of
Doctor of Philosophy

University of Pittsburgh

2016

UNIVERSITY OF PITTSBURGH
SWANSON SCHOOL OF ENGINEERING

This dissertation was presented

by

Yongjin Wang

It was defended on

January 21th, 2016

and approved by

Robert M. Enick, Ph.D., Professor, Department of Chemical and Petroleum Engineering

Di Gao, Ph.D., Associate Professor, Department of Chemical and Petroleum Engineering

Haitao Liu, Ph.D., Assistant Professor, Department of Chemistry

Dissertation Director: Lei Li, Ph.D., Assistant Professor, Department of Chemical and

Petroleum Engineering

Copyright © by Yongjin Wang

2016

**UNDERSTANDING THE MECHANISM OF SIMULTANEOUSLY
OLEOPHOBIC/HYDROPHILIC PERFLUOROPOLYETHER (PFPE) NANO-
COATINGS**

Yongjin Wang, PhD

University of Pittsburgh, 2016

This dissertation is focused on understanding the mechanism of simultaneously oleophobic/hydrophilic perfluoropolyether (PFPE) nano-coatings. Four specific topics are presented: 1) investigate why can a nanometer-thick polymer coated surface be more wettable to water than to oil; 2) discuss the effect of end-groups on simultaneous oleophobicity/hydrophilicity and testify the anti-fogging performance of nanometer-thick PFPEs; 3) Fabricate nanometer-thick simultaneously oleophobic/hydrophilic coatings via a cost-effective photochemical approach; 4) study the role of the interfacial interaction in the slow relaxation of nanometer-thick polymer melts on a solid surface.

Specifically, chapter 2 and chapter 3 indicate that the simultaneously oleophobic/hydrophilic behavior is kinetic in nature and results from the combination of nanoscale and interfacial phenomena. The end-groups of the nanometer-thick PFPEs are critical to this peculiar wetting behavior: PFPE polymers with different end-groups can interact with the substrate in very different ways, resulting in different packing orders and thus different inter-chain distances within the polymer nanofilms. If the inter-chain distance is appropriately small, smaller water molecules penetrate the nanofilms quickly while larger oil molecules penetrate the nanofilms much more slowly. As a result, the surface shows a higher oil contact angle (OCA)

than water contact angle (WCA). Moreover, the effect of simultaneous oleophobicity/hydrophilicity on the long-term anti-fogging capability has been studied by X-ray photoelectron spectroscopy (XPS) and anti-fogging tests. The results indicated that the unique simultaneous oleophobicity/hydrophilicity reduces the airborne hydrocarbon contamination and therefore improves the long-term anti-fogging performance. In chapter 4, an UV-based photochemical approach has been developed to fabricate nanometer-thick simultaneously oleophobic/hydrophilic coatings using cost-effective PFPEs without polar end-groups and the anti-fogging performance and mechanical robustness of the coating were studied. The photochemical approach established here potentially can be applied on many other polymers and greatly accelerates the development and application of simultaneously oleophobic/hydrophilic coatings. In chapter 5, the relaxation of nanometer-thick PFPE melts on a silicon wafer has been investigated by water contact angle measurement. This work reports that the relaxation of nanometer-thick polymer melts on a solid surface is much slower than in the bulk, which has been attributed to the low mobility of the anchored polymer chains and the motional cooperativity between anchored and free polymer chains in the nanometer-thick films.

TABLE OF CONTENTS

PREFACE	XV
1.0 INTRODUCTION	1
1.1 OVERVIEW	1
1.1.1 Background	2
1.1.2 Literature Review	4
1.1.2.1 Simultaneously hydrophilicity/oleophobicity: previously proposed mechanism	4
1.1.2.2 Application in anti-fogging coatings	5
1.1.2.3 Mechanism of ultraviolet (UV) bonding of PFPEs	7
1.2 EXPERIMENTS	9
1.2.1 Materials and chemicals	9
1.2.2 Fabrication of nanometer-thick films	10
1.2.3 Characterization	12
1.2.3.1 Contact angle measurement	12
1.2.3.2 X-ray Photoelectron Spectroscopy (XPS)	16
1.2.3.3 Scanning Probe Microscope (SPM)	17
1.2.3.4 Spectroscopic ellipsometry	20
1.2.3.5 Thermogravimetric analysis (TGA)	23

2.0	WHY CAN A NANOMETER-THICK POLYMER COATED SURFACE BE MORE WETTABLE TO WATER THAN TO OIL	25
2.1	CHAPTER PREFACE	25
2.2	INTRODUCTION	26
2.3	EXPERIMENTAL SECTION.....	30
2.3.1	Materials.....	30
2.3.2	Fabrication of nanometer-thick films	31
2.3.3	Characterizations.....	31
	2.3.3.1 PFPE thin films characterization	31
	2.3.3.2 Water contact angle characterization	34
2.4	RESULTS	35
2.5	DISCUSSION.....	40
2.6	CONCLUSIONS	44
3.0	EFFECT OF END-GROUP ON SIMULTANEOUS OLEOPHOBICITY/HYDROPHILICITY AND ANTI-FOGGING PERFORMANCE OF NANOMETER-THICK PERFLUOROPOLYETHERS (PFPEs).....	45
3.1	CHAPTER PREFACE	45
3.2	INTRODUCTION	46
3.3	EXPERIMENTAL SECTION.....	49
3.4	RESULTS	52
	3.4.1 Thickness of PFPE nanofilms.....	52
	3.4.2 Topography of PFPE nanofilms.....	52
	3.4.3 Static and time-dependent contact angle tests	53
	3.4.4 Evaporation effect on time-dependent contact angles (CA)	56

3.4.5	Advancing contact angle (ACA) and receding contact angle (RCA)	56
3.4.6	Effect of molecular weight (MW) on contact angle results.....	57
3.4.7	XPS and anti-fogging tests.....	58
3.4.7.1	Anti-fogging tests.....	58
3.4.7.2	XPS results.....	59
3.4.7.3	XPS peaks assignments.....	61
3.4.7.4	Calculation of the amount (%) of airborne hydrocarbon contaminants	63
3.5	DISCUSSIONS.....	65
3.5.1	Underlying mechanisms of simultaneous oleophobicity/hydrophilicity ...	65
3.5.2	Airborne hydrocarbon contamination and anti-fogging performance	69
3.6	CONCLUSIONS	72
4.0	FABRICATING NANOMETER-THICK SIMULTANEOUSLY OLEOPHOBIC/HYDROPHILIC COATINGS VIA A COST-EFFECTIVE PHOTOCHEMICAL APPROACH	73
4.1	CHAPTER PREFACE	73
4.2	INTRODUCTION	74
4.3	EXPERIMENTAL SECTION.....	76
4.3.1	Materials and sample fabrication	76
4.3.2	UV treatment.....	76
4.3.3	Characterizations.....	77
4.3.3.1	Contact angle tests.....	77
4.3.3.2	Ellipsometry	77
4.3.3.3	XPS	77
4.3.3.4	Anti-fogging tests.....	78

4.3.3.5	Detergent-free cleaning.....	78
4.3.3.6	Mechanical wipe test.....	78
4.4	RESULTS AND DISCUSSIONS.....	79
4.4.1	Simultaneous oleophobicity/hydrophilicity:.....	79
4.4.2	Anti-fogging:	84
4.4.3	Detergent-free cleaning:	86
4.4.4	Mechanical robustness:.....	87
4.5	CONCLUSIONS	88
5.0	THE ROLE OF THE INTERFACIAL INTERACTION IN THE SLOW RELAXATION OF NANOMETER-THICK POLYMER MELTS.....	90
5.1	CHAPTER PREFACE	90
5.2	INTRODUCTION	91
5.3	EXPERIMENTAL SECTION.....	94
5.3.1	Materials.....	94
5.3.2	Fabrication of nanometer-thick films	95
5.3.3	Characterization	96
5.3.3.1	Spectroscopic ellipsometer	96
5.3.3.2	Scanning probe microscope (SPM).....	96
5.3.3.3	XPS results	96
5.3.3.4	Water contact angle	97
5.4	RESULTS	99
5.5	DISCUSSION.....	108
5.5.1	Thermodynamic Driving Force of the Relaxation.....	108
5.5.2	Kinetics of the Relaxation.....	110

5.6	CONCLUSION	114
6.0	SUMMARY & OUTLOOK	115
6.1	SUMMARY	115
6.1.1	The mechanism of simultaneous oleophobicity/hydrophilicity	115
6.1.2	The applications of simultaneous oleophobicity/hydrophilicity	116
6.1.3	The photochemical approach of simultaneous oleophobic/hydrophilic substrates	116
6.2	OUTLOOK.....	117
6.2.1	Clarify the effect of “hole” on simultaneous oleophobic/hydrophilic substrates	117
6.2.2	Optimize the polymer to achieve a better application performance.....	118
APPENDIX A		119
APPENDIX B		121
BIBLIOGRAPHY		122

LIST OF TABLES

Table 1. Roughness (Ra) and PFPE thickness on Si Wafers	32
Table 2. Static water and hexadecane contact angles	35
Table 3. The thickness of PFPE nanofilms on silica surfaces	52
Table 4. Static water and hexadecane contact angle on different surfaces.	53
Table 5. The decrease of diameter of water and hexadecane droplet.	56
Table 6. Dynamic contact angles of PFPEs coated on silica surfaces.	57
Table 7. WCA and HCA on different ZDOL nanofilms with different molecular weights	57
Table 8. XPS C1s curve fitting results for different PFPEs coated glass slides on the 1st day (a) and the 14th day (b) after the samples were fabricated	64
Table 9. Contact angles on the Z-03/Silica.....	79
Table 10. Roughness and PFPE Thickness	99
Table 11. List of abbreviations	121

LIST OF FIGURES

Figure 1. The schematic diagrams of the presumed bonding mechanisms.....	8
Figure 2 One possible bonding reaction between PFPEs and Si substrates.....	8
Figure 3. The Chemical Structures of PFPE polymers	9
Figure 4. Dip-coating instrument	11
Figure 5. Formation mechanism of ZDOL polymers on the polar surface during dip-coating (Schematic not shown to scale).....	12
Figure 6. Schematic of a sessile-drop contact angle system.	13
Figure 7. VCA optima XE video contact angle system	14
Figure 8. The measurement of advancing and receding contact angle	15
Figure 9. Basic components of a monochromatic XPS system.	16
Figure 10. X-ray photoelectron spectroscopy	17
Figure 11. Scheme for an atomic force microscope.....	18
Figure 12. Block diagram of atomic-force microscope.	19
Figure 13. Atomic force microscopy	20
Figure 14. Schematic of ellipsometer configuration with a polarizer to define the incoming polarization and a rotating analyzer after light reflection. Reprinted with permission	21
Figure 15. Alpha-SE ellipsometer.....	22
Figure 16. Typical fitting result of PFPE nanofilm on the silica surface.....	23

Figure 17. Thermogravimetric analysis.	24
Figure 18. Images of contact angles of water and hexadecane.	28
Figure 19. The Chemical Structures of ZDOL and Z-03 polymers.	30
Figure 20. XPS C1s spectra and curve-fitting results.	34
Figure 21. Change in hexadecane contact angles with time on ZDOL (0.9 nm)/Si (From left to right: 5 min, 300 min and 1440 min).	36
Figure 22. Time dependence of $\cos \theta$ of hexadecane on various surfaces.	36
Figure 23. TGA results of hexadecane (room temperature in air).	37
Figure 24. KWW Fitting results of $\cos \theta$ of hexadecane on ZDOL (0.9 nm)/Si (top) and ZDOL (1.8 nm)/Si (bottom).	39
Figure 25. Schematic show of the “penetration” mechanism (not to scale).	40
Figure 26. The chemical structures of PFPE polymers.	49
Figure 27. Sealed cuvette with needle piercing rubber septum.	51
Figure 28. AFM images of PFPE nanofilms on silica surfaces.	53
Figure 29. $\cos \theta$ ((a) hexadecane, (b) water) vs. time on different PFPE nanofilms.	55
Figure 30. Anti-fogging testing results of PFPE-coated glass slides.	58
Figure 31. XPS C1s spectra of PFPE-coated glass.	60
Figure 32. Molecular formula of PFPEs.	61
Figure 33. XPS C1s spectra and curve-fitting results (a) ZDOL, (b) Z-tetraol, (c) Z-03.	63
Figure 34. Schematic bonding models of PFPE polymers on silica surfaces (not shown to scale).	66
Figure 35. Schematic show of the “penetration” mechanism of water and hexadecane on ZDOL/Si (not shown to scale).	69
Figure 36. (a) (top) HCA and WCA on Z-03/Silica as a function of UV treatment time. (b) (middle) Bonded thickness as a function of UV time. (c) (bottom) Fluorine element percentage of Z-03/Silica (bonded) as a function of UV exposure time.	81

Figure 37. Schematic bonding models of Z-03 polymers on silica substrate during UV irradiation (not shown to scale)	82
Figure 38. HCA change with time on Z-03/Silica wafer without UV treatment and with 10 minutes' UV treatment.	83
Figure 39. (a) (top) Anti-fogging testing results of Z-03 polymer coated glass slides without and with 10-minutes UV irradiation. (b) (bottom) XPS C1s spectra of Z-03 polymer coated glass slides without and with 10-minutes UV irradiation: Fresh (left) and Aged (right). (The time period between the fresh and aged samples is 14 days)	85
Figure 40. Detergent-free cleaning testing results of Z-03 polymer coated glass slides without and with 10-minutes UV irradiation: (a) with hexadecane on the surfaces. (b) after rinse with DI water	87
Figure 41. (a) (top) Thickness of Z-03 before and after wiping. (b) (bottom) XPS results of Z-03 before and after wiping.	88
Figure 42. The Chemical Structures of ZDOL and Z-03 polymers	94
Figure 43. AFM image of the Z-03 1.3 nm/Si wafer.	100
Figure 44. XPS C1s spectra (solid line) and curve-fitting (dotted line) results of a 1.8 nm ZDOL/Si samples.	101
Figure 45. Water contact angle of PFPE-coated Si wafers vs aging time.	102
Figure 46. Water contact angle of Z-03 on different Si wafers.	103
Figure 47. Water contact angle of 100% bonded ZDOL on different Si wafers.	103
Figure 48. $\cos\theta$ (θ is water contact angle) of ZDOL/Si and bare Si with aging time.	105
Figure 49. $\cos\theta$ (θ is water contact angle) of ZDOL/Si and bare Si with a ging time (Zoom: initial 24 hours).	105
Figure 50. KWW fitting result of the relaxation of ZDOL 1.2 nm ($\cos \theta_0 = 0.93$, $\cos \theta_e = 0.67$, $\tau = 3871$ min, $\beta = 0.60$).	107
Figure 51. Formation mechanism of ZDOL polymers on the Si wafer during dip-coating (Schematic not shown to scale)	109
Figure 52. Proposed relaxation mechanism of ZDOL polymers on the Si wafer (schematic not shown to scale).	110

PREFACE

Foremost, I would like to express my sincere gratitude to my research advisor, Professor Lei Li, for his support over the past five years. I would like to thank him for his contributions of time, ideas and funding to make my Ph.D. experience productive and stimulating. As a tremendous mentor for me, Professor Li. always showed me his patience, diligence and painstaking attention to research, which encourages me a lot in my research.

I want to acknowledge Professor Haitao Liu for providing me the opportunity of doing research in his lab. He recommended many good papers and books, which helps me greatly during my Ph.D. research.

I am also grateful to Professor Di Gao and Professor Robert Enick, for serving as my committee members. I would like to thank them for their insightful comments and suggestions.

I would like to thank to all of my colleague members and collaborators, including Andrew Kozbial, Dr. Xiao Gong, Dr. Vahid Vahdat, Zhiting Li, Feng Zhou, James Knapp, Aleigh Legere, Jacob Raney, Cassandra Gallaschun, Timothy Risch, Michael Dugan and Brian Urbaniak. It is my great pleasure to work with all of you and I wish you all the best.

I would like to thank Dr. Susheng Tan, Mike McDonald, and Matthew France for training me on Scanning Electron Microscope (SEM), Scanning Probe Microscopy Station (SPM), and Fourier Transform Infrared Spectroscopy (FT-IR). I am also grateful to Dr. Joel Gillespie for providing great X-ray photoelectron spectroscopy (XPS) training on me. I would like to thank

Dr. Jianing Sun for her help on Ellipsometer usage. I also want to thank Dr. Jacqueline Sturgeon from RJ Lee Group, Inc. for performing XPS analysis.

Lastly and above all, I would like to express my great gratitude to my parents. I always remember their words: go ahead to do anything that you want, we are always supporting you in behind. I want to thank them for giving birth to me, raising me up, and providing me comfortable life and endless love. Also I want to thank myself for never giving up no matter how difficult it is in both research and life. This dissertation is really the best gift to myself to memorize my past five years - graduate research's year.

1.0 INTRODUCTION

1.1 OVERVIEW

The previous research showed that, in general, a solid surface is more wettable to oil than to water. In other words, for a given solid surface, water contact angle (WCA) is higher than oil contact angle (OCA) and the simultaneous oleophobicity/hydrophilicity is unlikely. However, a few recent studies indicated that it is possible to achieve simultaneous oleophobicity/hydrophilicity by applying some polymer nanofilms on some solid substrates. Unfortunately, to date, the underlying mechanism is still unclear.

Meanwhile, simultaneously oleophobic/hydrophilic surfaces are highly desirable in many important applications, such as anti-fogging. Traditional anti-fogging surfaces are hydrophilic and they can be easily contaminated by the airborne hydrocarbons, which will make the surface more hydrophobic and not anti-fogging any more. A promising approach to address this issue is to make the surface simultaneously oleophobic/hydrophilic. In this way, the airborne hydrocarbon contaminants should be effectively reduced and the long-term anti-fogging performance will be improved. However, to date, such coatings have been rarely reported and the underlying mechanisms remain unclear.

1.1.1 Background

When a liquid is placed on a solid surface, the equilibrium contact angle (θ) is related to liquid surface tension (γ_l), solid surface tension (γ_s) and solid-liquid interfacial tension (γ_{sl}), which can be described by Young's equation:

$$\gamma_l \cos\theta + \gamma_{sl} = \gamma_s$$

As only γ_l and θ can be determined experimentally, there are two unknowns in Young's equation. Since the "classic" surface tension models relating γ_{sl} to γ_l and γ_s , such as Owens & Wendt model¹ and Neumann model,² are still a matter of debate, the exact quantitative relationship among θ , γ_l and γ_s is not available at present.³⁻⁵ However, according to previous experimental results, it is generally accepted that the higher the liquid surface tension, the larger the contact angle is on a given solid surface. For example, hexadecane has much lower surface tension than water, thus WCA is larger than hexadecane contact angle (HCA) on the same solid surface.⁶⁻⁷ Since the contact angle is an inverse measure of wettability,⁶ a solid surface is expected to be more wettable to oil than to water. In other words, if a solid surface is hydrophilic, it cannot be oleophobic. However, a simultaneously oleophobic/hydrophilic surface is highly desirable in many important applications.⁸⁻¹¹ For example, such a surface can be cleaned with just water (no detergent is needed) because water can easily replace the oil-type contaminants at the liquid-solid interface and flushes the oil away from the surface.⁸⁻¹¹ This "detergent-free" surface will largely reduce the consumption of detergents that will protect the environment from the detergent-related pollution and conserve the valuable energy resource, petroleum, which is the raw material for detergents. If the surface of an oil-water separating membrane is more

wettable to water than to oil, the separation efficiency will be enhanced since the water permeability will increase relative to the oil permeability.¹²⁻¹³ This improved water-oil separation efficiency will benefit oil, metal and food processing industries.¹²⁻¹³ Moreover, simultaneous oleophobicity/hydrophilicity is also highly desirable for anti-fogging, which is critical to glasses, goggles, camera lenses, automobiles, greenhouse windows, analytical and medical instruments and solar energy devices.^{10-11, 14-15} The question is: Can we fabricate simultaneously hydrophilic/oleophobic surfaces?

1.1.2 Literature Review

1.1.2.1 Simultaneously hydrophilicity/oleophobicity: previously proposed mechanism

Indeed, a few recent reports indicated that it is possible to achieve simultaneous oleophobicity/hydrophilicity with nanometer-thick amphiphilic coatings on hydrophilic substrates.^{8-11, 16-17} For example, polyelectrolyte plasma polymer substrates, coated with ionic amphiphilic fluoro-surfactants, were reported to be more wettable to water than to oil.⁸⁻⁹ Badyal et al.⁸⁻¹¹ proposed that the amphiphilic polymer molecule takes a conformation that the perfluorinated segments stay on the very top of the monolayer surface repelling hexadecane, which results in a higher HCA. They also speculated⁸⁻⁹ that water molecules “contact” with the substrate with high surface energy, which results in a lower WCA. Youngblood and Howarter⁸⁻⁹ covalently bonded a nanometer-thick perfluorinated amphiphilic polymer with a polyethylene glycol (PEG) head-group to an isocyanate-modified silica surface and found that the receding contact angle of hexadecane is higher than the advancing contact angle of water. Since the PEG segments are covalently bonded to the substrate, the “flip-flop” type of switching mechanism is highly unlikely. They speculated¹⁰⁻¹¹ that the low WCA results from the swelling of PEG layer by water penetrating the perfluorinated constituent driven by the attraction between water and hydrophilic PEG segments. They¹⁰⁻¹¹ also hypothesized that, since there is no attraction between PEG segments and hexadecane, the hexadecane prefers to stay on top of the perfluorinated segments and this results in the higher hexadecane contact angle. Badyal and Youngblood⁸⁻¹¹ proposed that hexadecane would stay on top of the fluorinated moiety and water could penetrate the fluorinated segments and swell the subsurface, which is either hydrophilic segments of the amphiphilic polymer or the substrate with high surface energy. The implication in both cases is

that macroscopic hexadecane and water droplets selectively “see” different molecular moieties at the same macroscopic surface under equilibrium state. Since the contact angle test itself is macroscopic in nature, these previously proposed mechanisms⁸⁻¹¹ contradict the “classic” theories^{1-2, 18} because, a given macroscopic surface should have only one fixed surface tension value no matter how complicated the molecular-level structure is.

Recently, Badyal¹⁹ proposed another mechanism to explain the wetting behavior of simultaneously oleophobic/hydrophilic. Solvent-cast copolymers modified with fluorosurfactant surfaces are found to display oleophobic/hydrophilic switching behavior. The change of static WCA in 10 seconds is attributed to the penetration of water through defects in the fluorinated outermost layer toward the hydrophilic subsurfaces, resulting in the water faces a hydrophilic surface instead of hydrophobic surface. Since oil molecules are much larger than water molecules, they are unable to penetrate the fluorinated top layer, therefore, leaving the surface to be oleophobic.¹⁹

1.1.2.2 Application in anti-fogging coatings

To understand the fogging mechanism, Briscoe¹⁵ studied the condensation of water vapor on some solid surfaces, including polyethylene and glass, and found that: (1) when WCA on the surface is low, a uniform water film will be formed and fogging will not occur, (2) when WCA is higher than 40°, water droplets will be formed on the surface and fogging will occur and reduce the light transmission since the droplets diffract light. In recent years, various studies have been conducted to develop anti-fogging coatings in order to improve the effectiveness of the optical surfaces,^{10, 20-23} such as multilayer nanoporous-silicate thin films,²⁰⁻²² TiO₂-based nanoparticle coatings²³ and solvent-sensitive stimuli-responsive polymer brush coated surfaces.¹⁰ All of these anti-fogging surfaces are hydrophilic and water is highly wettable on these surfaces.

Unfortunately, these surfaces are easily “damaged” by hydrocarbon contaminants in the ambient environment:¹¹ the adsorbed airborne hydrocarbons on the surface would lower the surface energy and thus render water to bead on such a “oil-coated” surface, which makes the surface no longer anti-fogging.⁹⁻¹¹ Therefore, in order to achieve an excellent long-term anti-fogging performance, the simultaneously oleophobic/hydrophilic surfaces which allow water to easily wet the surface while preventing oil from depositing are highly desirable.

1.1.2.3 Mechanism of ultraviolet (UV) bonding of PFPEs

In 1990, Saperstein and Lin²⁴ first published an article to indicate that far-UV treatment of a surface with a thin film of PFPEs can improve the adhesion and lower the surface free energy.²⁴ The possible mechanisms of the bonding of PFPE lubricants to the Si wafer substrate under UV irradiation had been discussed a few years later.²⁴⁻⁴³ Vurens et al. hypothesized that the bonding between the PFPE polymers and substrate is attributed to the photoelectrons which are excited by the UV from the substrate.²⁵⁻²⁶ However, Guo and Waltman challenged this mechanism based on the fact that the amount of photoelectrons generated by UV is not enough for the bonding between substrate and PFPEs.³⁵⁻³⁶ According to their calculation, the photoelectron mechanism contributes, at most, ~6% to the overall UV bonding.³⁵⁻³⁶ Guo and Waltman proposed a different mechanism that UV irradiation could be directly attributed to the photo-dissociation of PFPE polymer molecules.³⁵⁻³⁶ As shown in Figure 1, Nakakawaji³⁷ summarized that both the excitation of the substrate and the excitation of the adsorbate are contributed to the bonding between PFPEs and substrates under UV. It is suggested that bonding of lubricant layer to the substrate surfaces was caused not only by photoelectrons emitted from the substrate but also by the direct photo-dissociation of the PFPE chains by the UV treatment.³⁷ The reaction between PFPE polymers and Si wafer substrates are complex and one possible reaction occurred during UV irradiation is shown in Figure 2.

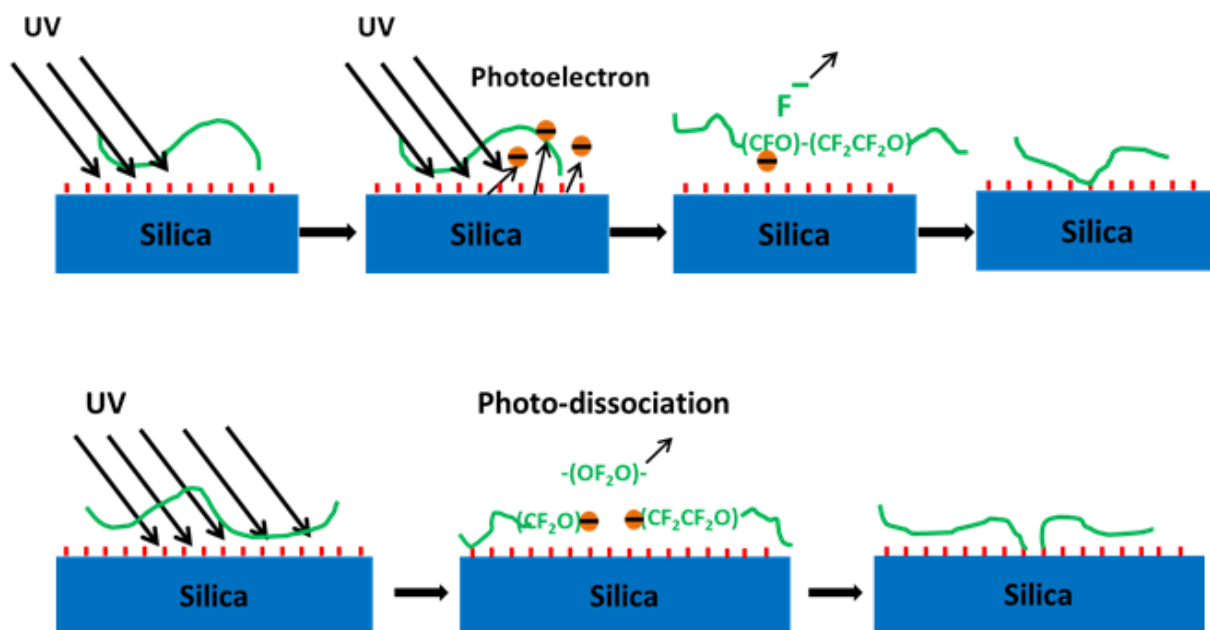


Figure 1. The schematic diagrams of the presumed bonding mechanisms.

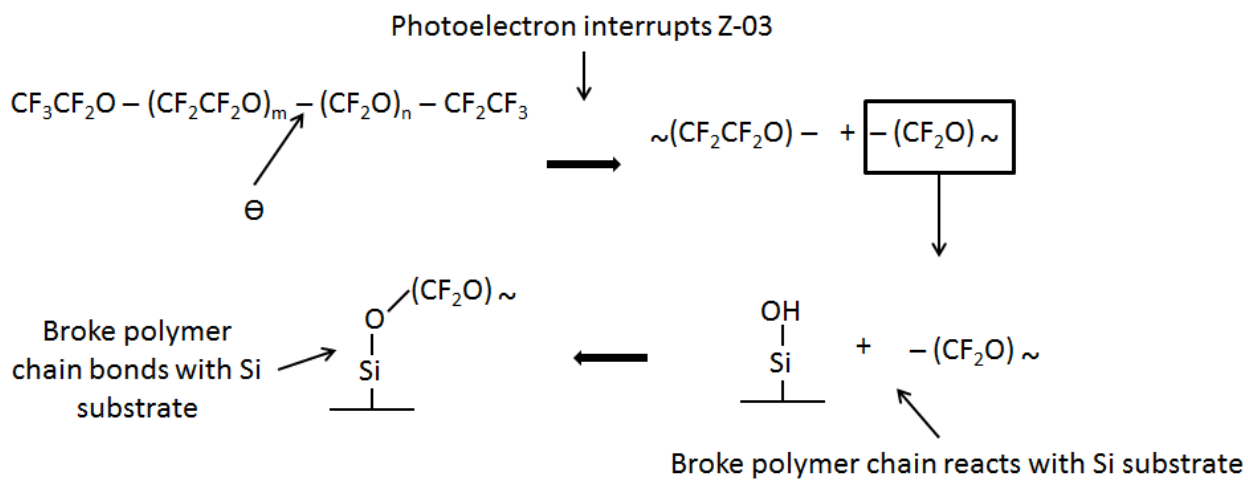


Figure 2 One possible bonding reaction between PFPEs and Si substrates

1.2 EXPERIMENTS

1.2.1 Materials and chemicals

Si wafer (purchased from Silicon Quest International, Inc.) with 2 nm native oxide (P/B <100> 1-10 OHM-CM, $279 \pm 25 \mu\text{m}$) and plain glass microscope slides (25*7*51 mm, Fisherbrand) were used as the substrates. Three PFPE polymers, commercially known as ZDOL, Z-03 and Z-tetraol, which were obtained from Solvay Solexis Inc., were used and the chemical structures of PFPE polymers are shown in Figure 3.

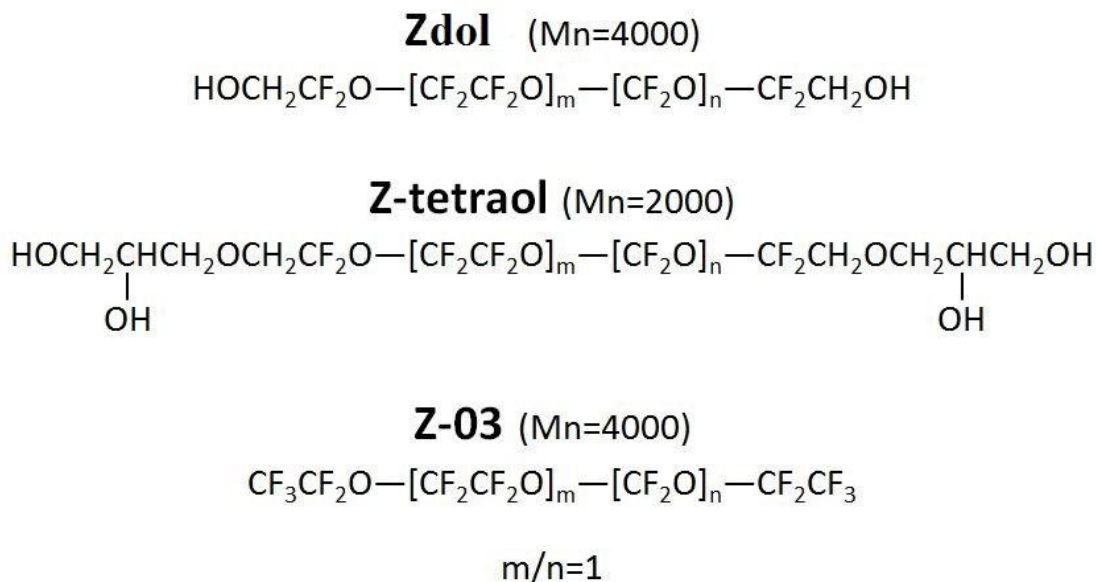


Figure 3. The Chemical Structures of PFPE polymers

As shown here, both ZDOL and Z-tetraol have polar hydroxyl end-groups while Z-03 has nonpolar CF_3 end-groups. 2,3-Dihydrodecafluoropentane, a good solvent for PFPEs, was

purchased from Miller Stephenson Chemical Co.. Deionized (DI) water was produced from a Millipore Academic A10 system with total organic carbon below 40 ppb. Hexadecane (anhydrous, $\geq 99\%$) was obtained from Sigma-Aldrich. All of these chemicals were utilized as received.

1.2.2 Fabrication of nanometer-thick films

The interactions between PFPE polymers and polar solid surfaces have been extensively studied.⁴⁴⁻⁴⁸ ZDOL and Z-tetraol can form hydrogen bonds with the polar surfaces via hydroxyl end-groups, and their backbones only have weak interaction with the polar surfaces.⁴⁴⁻⁴⁸ Z-03 cannot form hydrogen bonds with the polar surface at all because its end-groups are nonpolar. Moreover, Z-tetraol has two hydroxyl end-groups at each chain end while ZDOL only has one.⁴⁹ As a result, Z-tetraol has stronger attraction to the polar substrate than ZDOL⁵⁰. The very different interactions between these PFPEs and the polar surfaces are evidenced by the fact that all of the Z-03 polymers can be completely washed off the polar surface with a good solvent, e.g., 2,3-dihydrodecafluoropentane, while only part of the ZDOL and Z-tetraol polymers can be washed off the polar surfaces.⁴⁴⁻⁴⁸ The polymer molecules that form hydrogen bonds with the substrates and cannot be washed off the surface with 2,3-dihydrodecafluoropentane are defined as bonded polymers. The polymer molecules that do not form hydrogen bonds and can be washed off the substrates are defined as mobile polymers.⁴⁴⁻⁴⁸ Nanometer-thick films were coated on silicon wafer and glass slides by dip-coating with 2,3-dihydrodecafluoropentane as the solvent on the basis of a previously established “dip-withdraw” procedure. ZDOL and Z-tetraol films coated via the normal dip-withdraw procedure contain both bonded and mobile molecules.⁴⁶⁻⁴⁸ The dip-coating procedure is done with the dip-coater as shown in Figure 4.

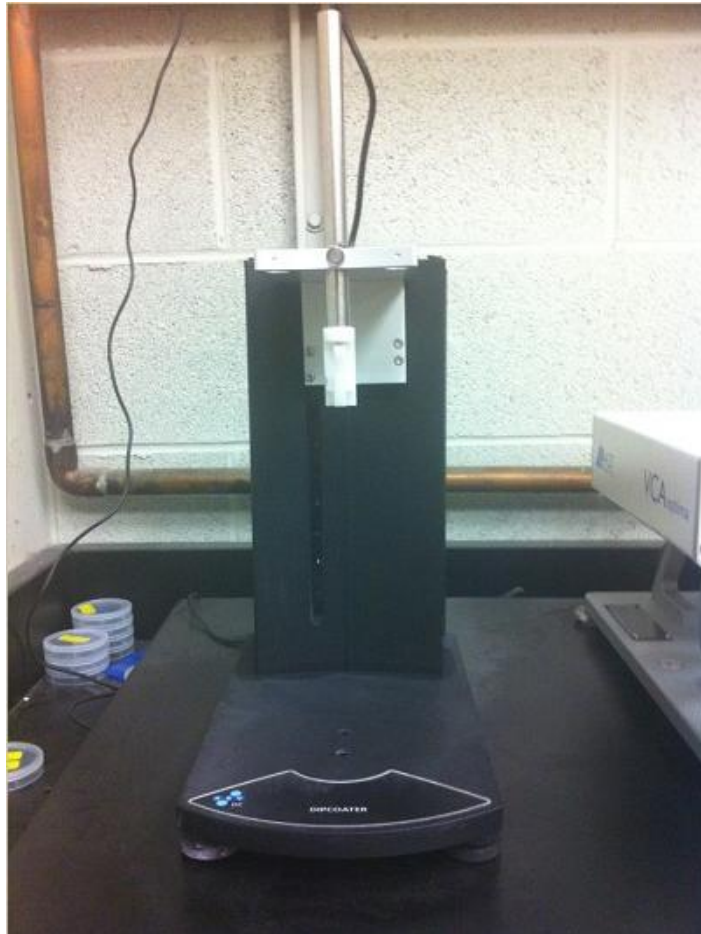


Figure 4. Dip-coating instrument

The formation mechanism of ZDOL polymers on the polar surface during dip-coating is shown in Figure 5. The image b is the solution adsorption in which ZDOL molecules form hydrogen bonds with the polar sites on the surface in solution and become bonded when the solid substrate is immersed into the solution during the dip-coating. The image c is the “viscous flow” mechanism in which a layer of ZDOL solution is forced to go with the solid substrate when the substrate is pulled out of the solution (note that the bonded molecules are already on the surface at this time), simply because the viscosity of the solution is not zero. Via this mechanism, ZDOL

molecules become the mobile portion after the solvent evaporates rapidly. Therefore, the mobile molecules are “forced” to stay on the solid surface. Although it has not been extensively studied, this phenomenon has been reported for polymer nanofilms fabricated by both dip-coating and spin-coating.^{46, 48, 51}

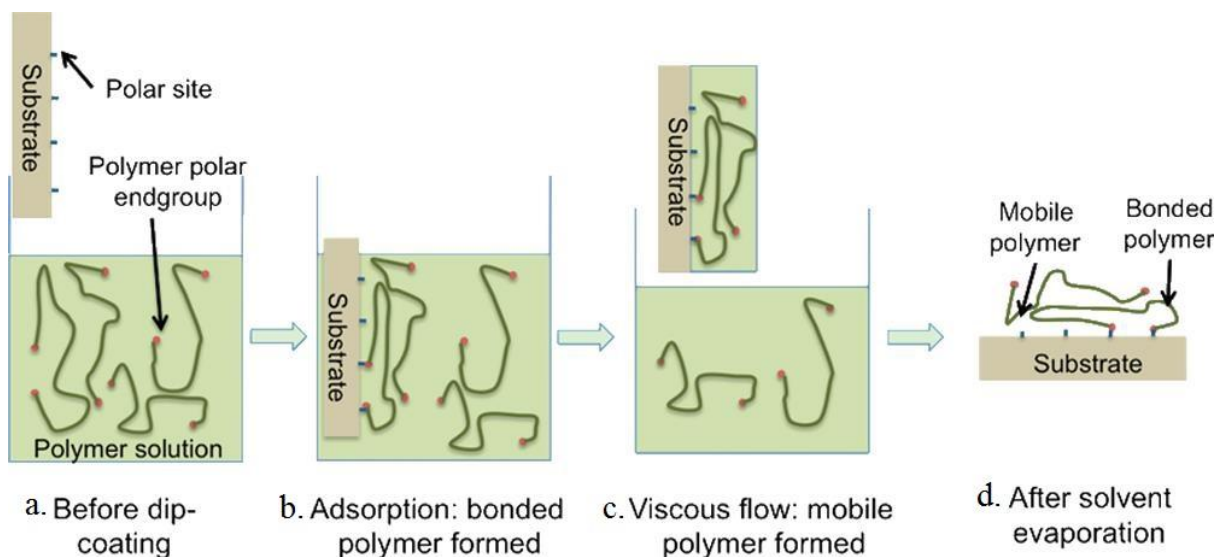
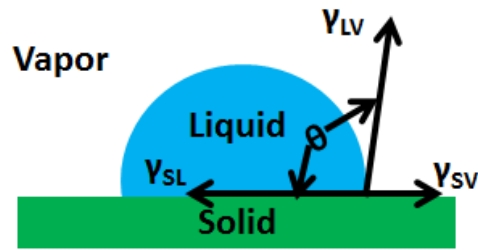


Figure 5. Formation mechanism of ZDOL polymers on the polar surface during dip-coating (Schematic not shown to scale)

1.2.3 Characterization

1.2.3.1 Contact angle measurement

Contact angle measurement has been conducted to study the surface wettability in this thesis. When a liquid droplet is deposited on a solid surface, the angle formed between the solid/liquid interface and the liquid/vapor interface is referred to as contact angle (as shown in Figure 6).³ The contact angle is related to solid–vapor (γ_{sv}) and solid–liquid (γ_{sl}) interfacial tensions which are of importance in surface and interface science.⁵²⁻⁵⁸



Young's Equation: $\gamma_{SV} = \gamma_{SL} + \gamma_{LV} \cos\theta$

θ is the contact angle

γ_{SV} is the solid surface free energy

γ_{SL} is the solid/liquid interfacial free energy

γ_{LV} is the liquid surface free energy

Figure 6. Schematic of a sessile-drop contact angle system.⁵³

In this work, the contact angle was studied by a VCA optima XE video contact angle system as shown in Figure 7 from AST Production Inc. Two types of contact angle measurements (static and dynamic contact angle) are measured in this thesis. For the static contact angle test, a 2 μ l liquid droplet was deposited on the sample surface and the image of this liquid droplet on the surface was immediately taken with a charge-coupled device (CCD) camera and then the contact angle was determined by the VCA software automatically.



Figure 7. VCA optima XE video contact angle system

The time-dependent static contact angle tests were conducted in two ways:

1. First, the contact angle was measured with the change of aging time for the same droplet on the same spot. Only ONE droplet was placed on the surface in this method. The contact angles were measured at different time (up to 24 hours) after this droplet was deposited on the surface. This method was intended to characterize the penetration process of the test liquid, e.g. water and hexadecane, within the nanofilm.
2. Second, the contact angle was measured with respect to the aging time for different droplets on different spots. This method was conducted right after the sample was fabricated and measured up to 10 days. In each measurement, a NEW droplet was deposited on an untested spot on the sample. This method was intended to capture the relaxation process of polymer nanofilm on the substrate.

For the dynamic contact angle, (e.g. advancing contact angle (ACA) and receding contact angle (RCA)), an initial droplet was formed by syringe on the substrate with a volume of 2 μ L for

ACA measurement and 5 μ L for RCA measurement. Then the droplet was dispensed or withdrew while images were captured in 5 seconds. The software featured high speed image capture capability for dynamic contact angle analysis (i.e., 30 images per second in our measurement). Last, all the contact angle images were analyzed and the advancing/receding contact angle were determined. The diameter of liquid droplet kept constant and the increased during the dispensing process and the CA in the last image before the diameter increased was taken as the ACA. The diameter of liquid droplet kept constant and then decreased during the withdrawing process and the CA in the last image before the diameter decreased was taken as the RCA. (shown in Figure 8) In other words, a range of contact angle values were collected during dispensing (withdrawing) the liquid droplet on the sample surface. And the largest (smallest) contact angle value was taken as ACA (RCA).

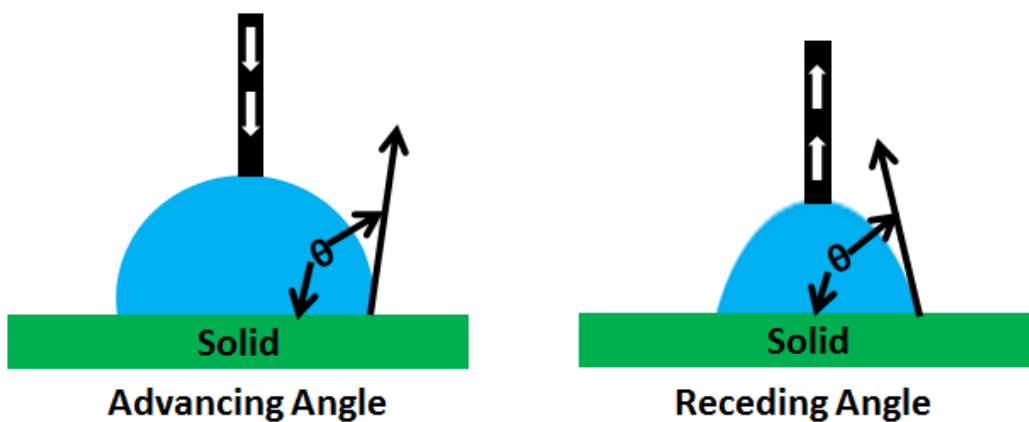


Figure 8. The measurement of advancing and receding contact angle

1.2.3.2 X-ray Photoelectron Spectroscopy (XPS)

XPS is one of the most powerful spectroscopic techniques that identifies the elemental composition of a surface on the atomic scale.⁵⁹⁻⁶⁰ As shown in Figure 9, XPS works by exciting electrons from the irradiated material with a beam of X-rays into higher energy states and the XPS spectra can be detected. Then, the kinetic energy and number of electrons escaping from the top 1-10 nm of the material surface will be analyzed.⁶¹ XPS measurement can identify the quantitative information about the elemental composition and chemical specificity of the surface.⁶² Typically, XPS spectra are plotted by the binding energy of the detected electrons versus the number of detected electrons. Each element can be identified according to their own related characteristic binding energy values.

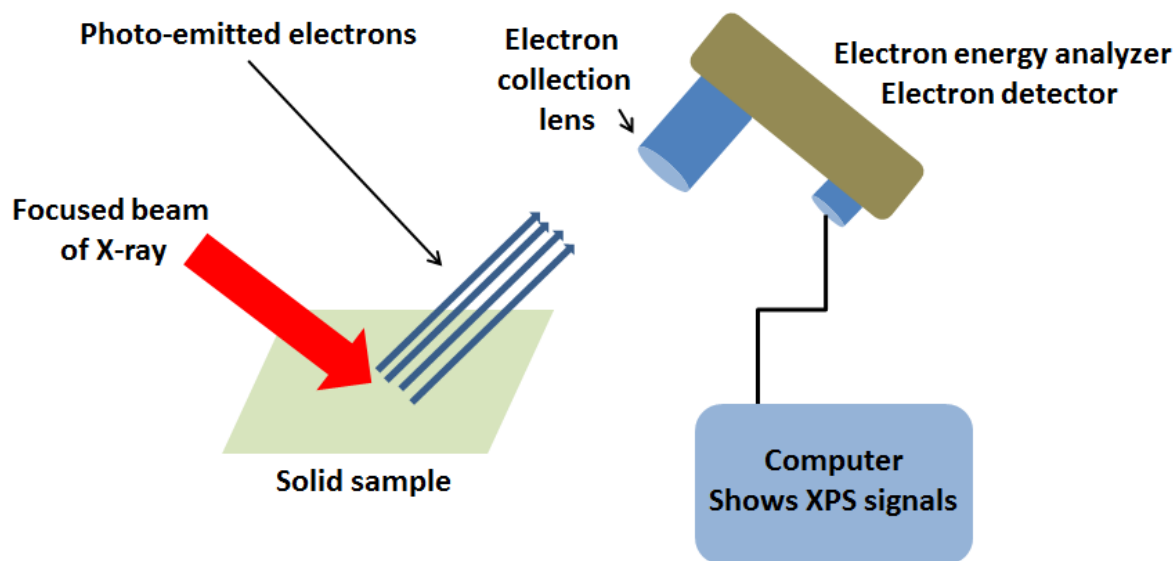


Figure 9. Basic components of a monochromatic XPS system.

In our experiment, the MCL- ESCALAB 250 XI Thermo Scientific XPS system with a monochromated Al K α source as shown in Figure 10 was used to characterize the chemical

structure of the polymers. A spot size of 400 μm was used for all experiments, and the charge compensation in the system was provided by a low-energy electron source and Ar^+ ions. An initial survey spectrum consisting of one scan was collected on each sample, using a pass energy of 200 eV. High-resolution scans around the C1s peak were collected using 20 scans and a pass energy of 50 eV. For high-resolution scans, only the low-energy electron source was used for charge compensation.



Figure 10. X-ray photoelectron spectroscopy

1.2.3.3 Scanning Probe Microscope (SPM)

SPM is a branch of microscopy that scans across the object surface to generate an image using a physical probe. Atomic force microscopy (AFM), which is used in our experiments, is the most common scanning probe techniques. It is typically used to measure the roughness of a sample surface at a high resolution. As shown in Figure 11, the tip is fastened to a cantilever

spring that has a lower spring constant than the effective spring between two atoms. With sufficient sensitivity in the spring deflection sensor, the tip can reveal surface profiles with atomic resolution.⁶³ The results will be collected and detected by the position-sensitive photodetector, which records the angle of reflection from a laser beam focused on the top of the cantilever as shown in Figure 12.⁶³

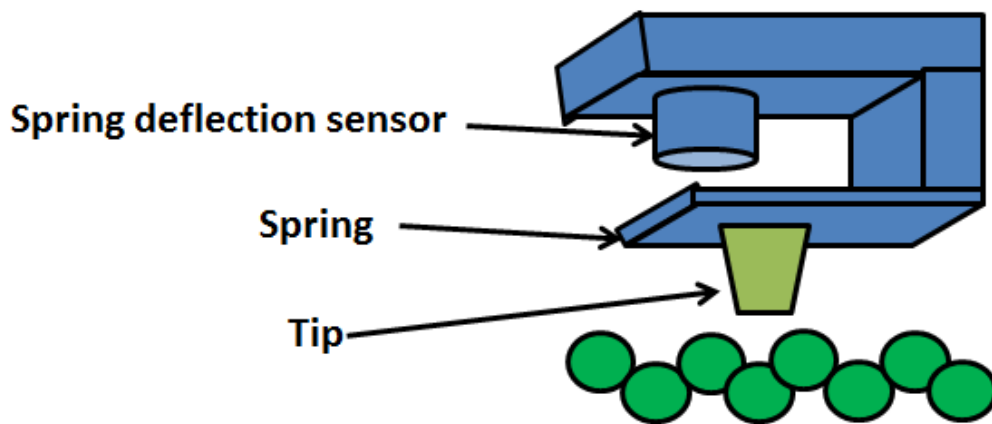


Figure 11. Scheme for an atomic force microscope.

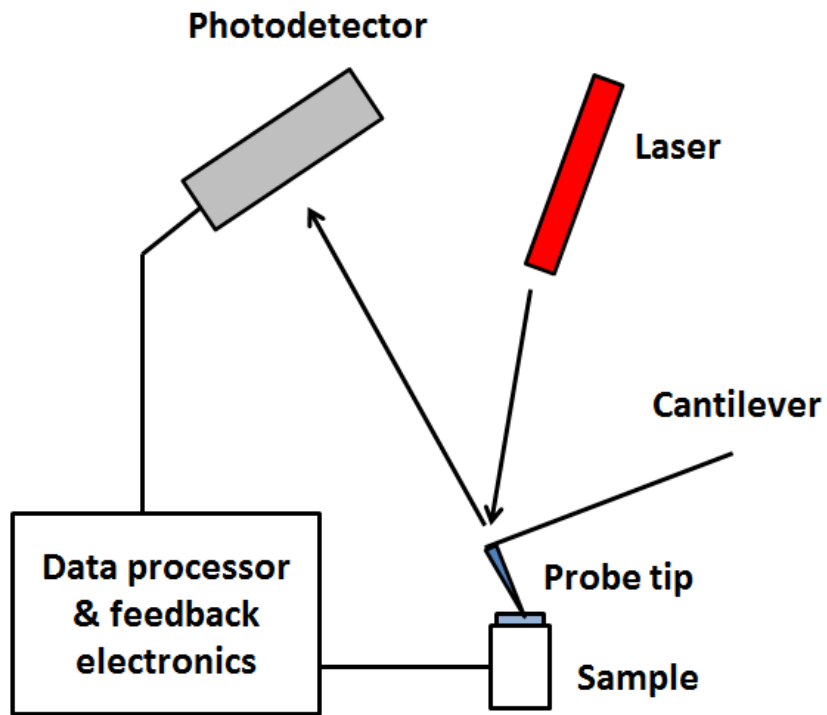


Figure 12. Block diagram of atomic-force microscope.

In our experiment, the topography and the roughness (R_a) of the polymer nanofilms were characterized using a Veeco MultiMode V SPM and AFM system as shown in Figure 13. All the experiments are under a tapping mode with a scanning area of $2\mu\text{m} \times 2\mu\text{m}$, the results are calculated by taking the average of four repeated measurements at different locations.

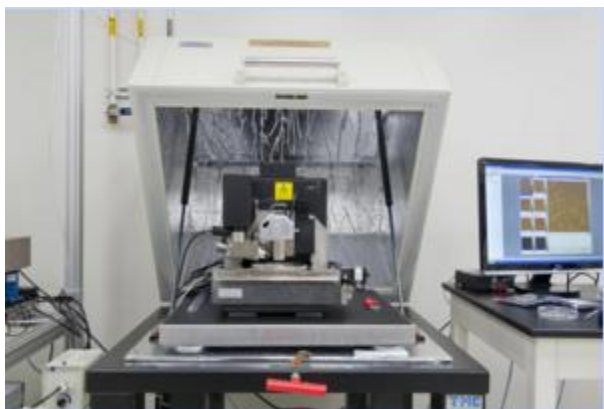


Figure 13. Atomic force microscopy

1.2.3.4 Spectroscopic ellipsometry

Spectroscopic ellipsometry is typically used to determine the optical constants and thickness of surface adsorbed thin films. It is based on the polarization state change of light upon reflection from a sample surface. In our experiment, the thickness of the polymer nanofilm was measured using a J. A. Woollam alpha-SETM ellipsometer as shown in Figure 15, which is a model-based technique. Two quantities that the ellipsometer directly measures are change in amplitude (Ψ) and change in amplitude (Δ), which represent the change in polarized light. A suitable optical model can be fit to these experimental raw data points to obtain the information about the sample and the schematic image of the working mechanism of ellipsometry is shown in Figure 14.

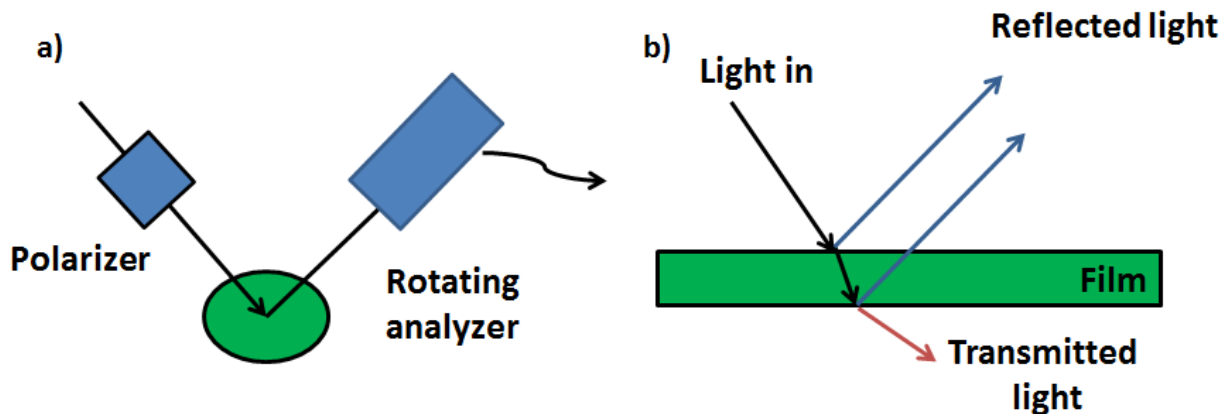


Figure 14 Schematic of ellipsometer configuration with a polarizer to define the incoming polarization and a rotating analyzer after light reflection. Reprinted with permission⁶⁴

For all the experiments, the bare silica surface was first measured to determine the thickness of native oxides,⁶⁵ and the thickness of the nanofilm which was coated on the bare silica surface was determined by curve-fitting using Cauchy model. To avoid thickness and index correlation between the very thin polymer films,⁶⁶ we fixed their optical constants using a Cauchy dispersion equation:

$$n(\lambda) = 1.30 + \frac{0.00250}{\lambda^2}$$



Figure 15. Alpha-SE ellipsometer

A typical ellipsometry fitting result of PFPE nanofilm on the silica surface is shown in Figure 16. The Mean Squared Error (MSE) value of the nanofilm calculated by ellipsometer was 1.784, indicating a good fitting result. The thicknesses of PFPE nanofilms, which is the mean of three repeated measurements at different locations.

Fit Results	Optical Model
MSE = 1.784 Thickness # 2 = 18.47 ± 0.109 Å	- Layer # 2 = <u>Cauchy</u> Thickness # 2 = <u>18.47 Å</u> (fit) A = <u>1.300</u> B = <u>0.00250</u> C = <u>0.00000</u> k Amplitude = <u>0.00000</u> Exponent = <u>1.500</u> Band Edge = <u>400.0 nm</u>
	Layer # 1 = <u>NTVE_JAW</u> Native Oxide = <u>13.99 Å</u>
	Substrate = <u>SI_JAW</u>

Experimental and Model Generated Data Fits

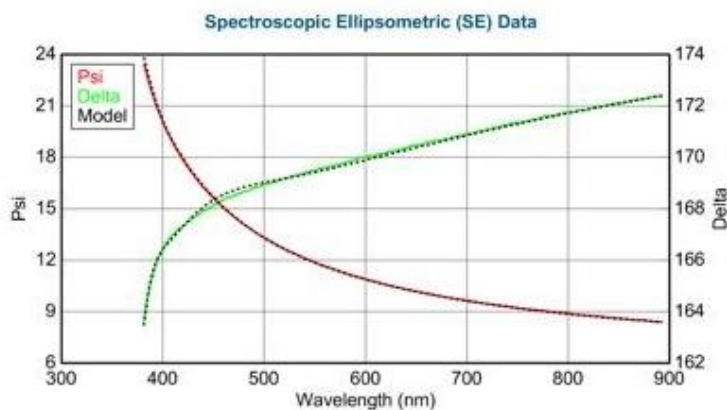


Figure 16. Typical fitting result of PFPE nanofilm on the silica surface

1.2.3.5 Thermogravimetric analysis (TGA)

TGA is a thermal analysis method by measuring the change of both chemical and physical properties versus the increase of temperature or the change of time.⁶⁷ Lots of chemical and physical properties can be determined by TGA such as vaporization, sublimation, absorption, adsorption, desorption, chemisorptions, desolvation (especially dehydration), decomposition, and solid-gas reactions.⁶⁷ In our experiment, SII Seiko Instruments SSC/5200 TGA as shown in Figure 17 was used to measure the mass change of hexadecane liquid as a function of time with a constant temperature, which is in order to check whether hexadecane liquid could be evaporated in the room temperature.



Figure 17. Thermogravimetric analysis.

2.0 WHY CAN A NANOMETER-THICK POLYMER COATED SURFACE BE MORE WETTABLE TO WATER THAN TO OIL

2.1 CHAPTER PREFACE

Materials contained in this chapter were published as a research article in *J. Mater. Chem.*; figures used in this chapter have been reprinted with permission from: *J. Mater. Chem.*, **2012**, *22*, 16719-16722 (listed as reference 18 in the bibliography section). Copyright © 2012 The Royal Society of Chemistry.

List of Authors: Lei Li, Yongjin Wang, Cassandra Gallaschun, Timothy Risch and Jianing Sun

Author Contributions: Y.W., and L.L. designed and directed the experiments. Y.W., C.G., T. R., and J.S. conducted the experiments. All authors discussed the results. L.L. wrote the manuscript with input from all authors.

2.2 INTRODUCTION

A surface more wettable to water than to oil is highly desirable in many important applications.⁸⁻
^{13, 15} For example, such a surface can be cleaned with just water (no detergent is needed) because water can easily replace the oil-type contaminant at the liquid–solid interface and flushes the oil away from the surface.⁸⁻¹¹ This “detergent-free” surface will largely reduce the consumption of detergents which will protect the environment from the detergent-related pollution and conserve the valuable energy resource, petroleum, that is the raw material for detergents. Moreover, this type of surface has excellent long-term anti-fogging performance,^{10-11, 15} which is critical to glasses, goggles, automobiles and greenhouse windows, analytical and medical instruments and solar energy devices. If the surface of an oil– water separating membrane is more wettable to water than to oil, the separation efficiency will be enhanced since the water permeability will increase relative to the oil permeability.¹²⁻¹³ This improved water–oil separation efficiency will benefit oil, metal and food processing industries.¹²⁻¹³ While a surface more wettable to water than to oil is highly desirable, can we fabricate such a surface? When a drop of liquid is placed on a solid surface, the equilibrium contact angle (θ) is related to liquid surface tension (γ_l), solid surface tension (γ_s) and solid–liquid interface tension (γ_{sl}) as described by Young’s equation.¹⁸

$$\gamma_l \cos\theta + \gamma_{sl} = \gamma_s$$

Since only θ and γ_l can be determined experimentally and how γ_{sl} is dependent on γ_l and γ_s is still a matter of debate, there are two unknowns in the Young’s equation. As a result, a

theoretical model unambiguously correlating θ to γ_1 and γ_s is not available at present.³⁻⁵ However, experimentally it was found^{7, 68} that, in general, θ increases with γ_1 and decreases with γ_s . Since γ_1 of oil, e.g. hexadecane is much lower than that of water, the hexadecane contact angle (HCA) is always lower than the water contact angle (WCA) on the same solid surface, which has been proven to be true experimentally for many solid surfaces.^{7, 68} (Two examples are shown in Fig. 1(a) and (b).) Since the contact angle is an inverse measure of wettability,⁶⁸ a solid surface is expected to be more wettable to oil than to water. In other words, a surface more wettable to water than to oil is not expected. However, a couple of recent studies⁸⁻¹¹ showed surprising results. Badyal *et al.*⁸⁻⁹ coated a monolayer of cationic amphiphilic fluoropolymers on plasma polymer substrates and found that the HCA is significantly higher than the WCA on this surface. Youngblood and Howarter¹⁰⁻¹¹ covalently bonded a nanometer-thick perfluorinated amphiphilic polymer with a polyethylene glycol (PEG) headgroup to an isocyanate-modified silica surface and also found that the HCA is significantly higher than the WCA. These results suggest that it is possible to fabricate a surface more wettable to water than to oil though the mechanism behind the peculiar wetting behavior remains unclear. Both authors proposed⁸⁻¹¹ that the amphiphilic polymer molecule takes a conformation that the per-fluorinated segments stay on the very top of the monolayer surface repelling hexadecane, which results in a higher HCA. They also speculated⁸⁻¹¹ that water molecules, attracted to the subsurface with high surface tension, penetrate the perfluorinated layer, which results in a lower WCA. The implication is that hexadecane and water selectively “see” two different molecular moieties at the same macroscopic surface. However, a given macroscopic surface should have only one fixed surface tension value no matter how complicated the molecular-level structure is. Therefore, more

research is needed to uncover the mechanism, which is the key to fabricating surfaces more wettable to water than to oil.

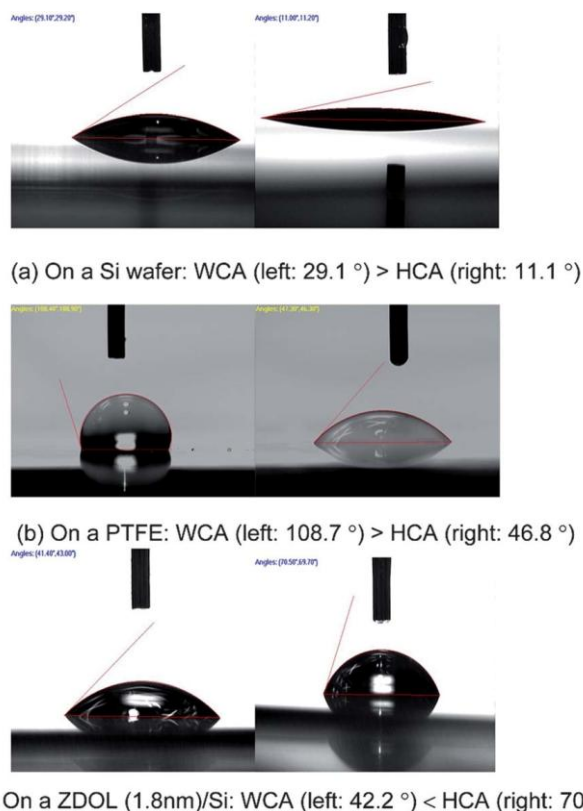


Figure 18. Images of contact angles of water and hexadecane.

If water can penetrate the polymer layer due to the attraction between water and the subsurface (with high surface tension), hexadecane should have the same tendency as well because hexadecane “likes” the substrate (of high surface tension) much better than perfluorinated moieties. This is supported by the fact that the HCA is much lower on silica than on poly (tetrafluoroethylene) (PTFE), as shown in Figure 18. In previous studies,⁸⁻¹¹ the HCA, which was measured within a relatively short time duration, *e.g.* minutes, has been considered as an equilibrium value. The possibility that the HCA could change with time, especially a long

time period, has not been investigated. Since the hexadecane molecule is much bigger than the water molecule,⁶⁹ the penetrating process, if occurring, could be much slower. In the current thesis, the time-dependence of the HCA on a nanometer-thick amphiphilic perfluoro-polymer coated surface, showing the HCA higher than the WCA, has been investigated. The effect of the structure of both substrate and nanofilms on the peculiar wetting behavior has also been studied to uncover the mechanism.

2.3 EXPERIMENTAL SECTION

2.3.1 Materials

Two perfluoropolyether (PFPE) polymers, commercially known as ZDOL and Z-03, with identical backbone and different end-groups and the chemical structures are shown in Figure 19. ZDOL has polar hydroxyl end-groups and is an amphiphilic polymer while Z-03 has non-polar CF_3 end-groups.

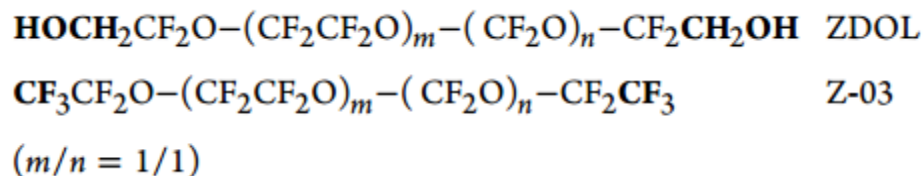


Figure 19. The Chemical Structures of ZDOL and Z-03 polymers

ZDOL and Z-03 were purchased from Solvay Solexis Inc. and utilized as received. 2,3-dihydrodecafluoropentane, a good solvent for PFPEs, was purchased from Miller Stephenson Chemical Co. and used as received. The Si <100> wafers covered with 2nm native oxides (P/B <100> 1-10 OHM-CM; $279 \pm 25\mu\text{m}$) were purchased from Silicon Quest International, Inc. and rinsed with 2,3-dihydrodecafluoropentane thoroughly before usage. DI water was produced from a Millipore Academic A10 system in house with total organic carbon below 40 ppb. Hexadecane (anhydrous; 99%) was purchased from Sigma-Aldrich and use as received. The PTFE sheet with

a thickness of 0.03'' was purchased from eplastics.com and rinsed with 2,3-dihydrodecafluoropentane thoroughly before usage.

2.3.2 Fabrication of nanometer-thick films

All the nanometer-thick films were deposited using A KSV-DCX2 dip-coater, equipped with a Kinetic Systems vibration free platform. ZDOL and Z-03 films were coated on Si wafer by dip-coating with 2,3-dihydrodecafluoropentane as the solvent at a pullout velocity of 1 mm/s. The ZDOL solution with the concentration of 0.5 g/L and 1.5 g/L were utilized to produce the films with different thicknesses on the Si wafer. The Z-03 solution with the concentration of 2.0 g/L was used to produce the film on the Si wafer. For ZDOL coated PTFE sheet, the solution with the concentration of 1.5 g/L was used.

2.3.3 Characterizations

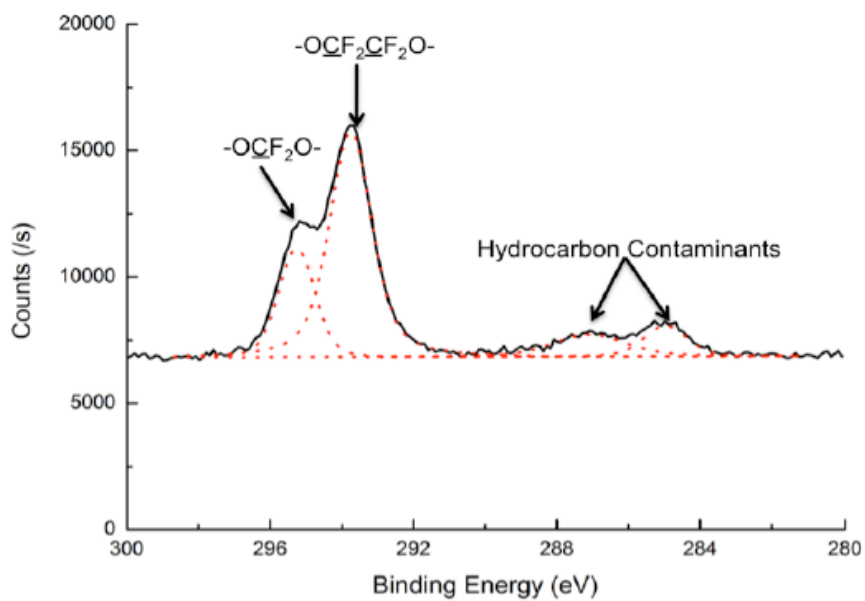
2.3.3.1 PFPE thin films characterization

The roughness of the PFPE-coated samples was determined by AFM and the thickness of the thin films was determined by ellipsometer, the results are as shown in Table 1.

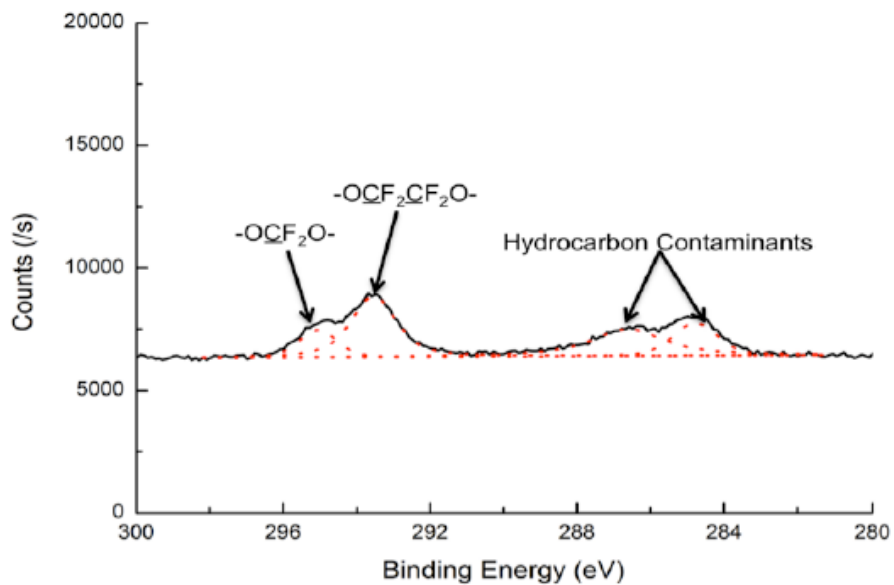
Table 1. Roughness (Ra) and PFPE thickness on Si Wafers

Sample Name	Solution concentration (g/L)	Ra (nm)	PFPE Total Thickness (nm)
Z-03 1.7 nm	2.0	0.18	1.7
ZDOL 0.9 nm	0.5	0.19	0.9
ZDOL 1.8 nm	1.5	0.17	1.8

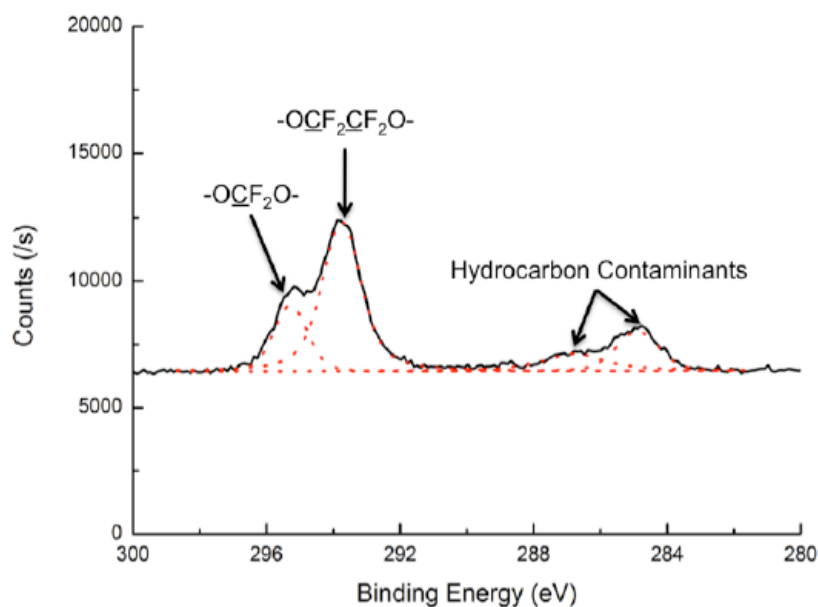
The chemical structure of the PFPE thin films was characterized by X-ray Photoelectron Spectroscopy (XPS). The XPS experimental procedure was described in the section 1.2.3.2.¹⁶ The XPS C1s spectra of all three PFPE samples are similar and the raw data, along with the curve-fitting results, are shown in Figure 20. For all three samples, the peaks centered around 295 eV and 294 eV are assigned to -OCF₂O- and -OCF₂CF₂O-, respectively.⁷⁰ The smaller peaks centered around 287 eV and 285 eV of all three samples are assigned to the contaminants, which is consistent with previous reports.⁷⁰



1.8 nm ZDOL/Si



0.9 nm ZDOL/Si



1.7 nm Z-03/Si

Figure 20. XPS C1s spectra and curve-fitting results

2.3.3.2 Water contact angle characterization

The contact angle measurement procedure was described in detail in section 1.2.3.1.¹⁶ To study the time dependence of the hexadecane contact angle, a hexadecane droplet was left on the sample surface and the contact angles were measured at different times for up to three days. To minimize the possible interruption caused by the sample movement and airflow, the sample was left on the stage of the goniometer during the entire testing period and covered all the time except when the contact angle measurement was conducted.

2.4 RESULTS

As shown in Table 2, for bare Si wafer and PTFE, the WCA is higher than the HCA as expected. When nanometer-thick ZDOLs are coated on the Si wafer, the WCA is lower than the HCA, as shown in Figure 18 (c). The values of the WCA and the HCA are comparable to previous reports.⁸⁻¹¹

Table 2. Static water and hexadecane contact angles

	DI Water	Hexadecane
Si control	28.7(\pm 1.9)	10.3(\pm 1.4)
PTFE	110.4(\pm 3.8)	47.4(\pm 0.6)
Z03 1.7 nm/Si	35.4(\pm 2.4)	20.2(\pm 2.0)
ZDOL 0.9 nm/Si	33.2(\pm 2.3)	55.5(\pm 3.5)
ZDOL 1.8 nm/Si	41.9(\pm 1.8)	70.7(\pm 1.7)
ZDOL 1.3 nm/PTFE	120.7(\pm 1.4)	52.4(\pm 0.9)

The time-dependence of the HCA on ZDOL/Si is shown in Figure 21 and Figure 22. For both 0.9 nm and 1.8 nm ZDOL, $\cos\theta$ increases (θ decreases) significantly with time during the three-day test period. Since the evaporation does not occur to the hexadecane, as shown by thermogravimetric analysis (TGA) (Figure 23), the change in the HCA cannot be attributed to evaporation as reported before.⁷¹⁻⁷²



Figure 21. Change in hexadecane contact angles with time on ZDOL (0.9 nm)/Si (From left to right: 5 min, 300 min and 1440 min).

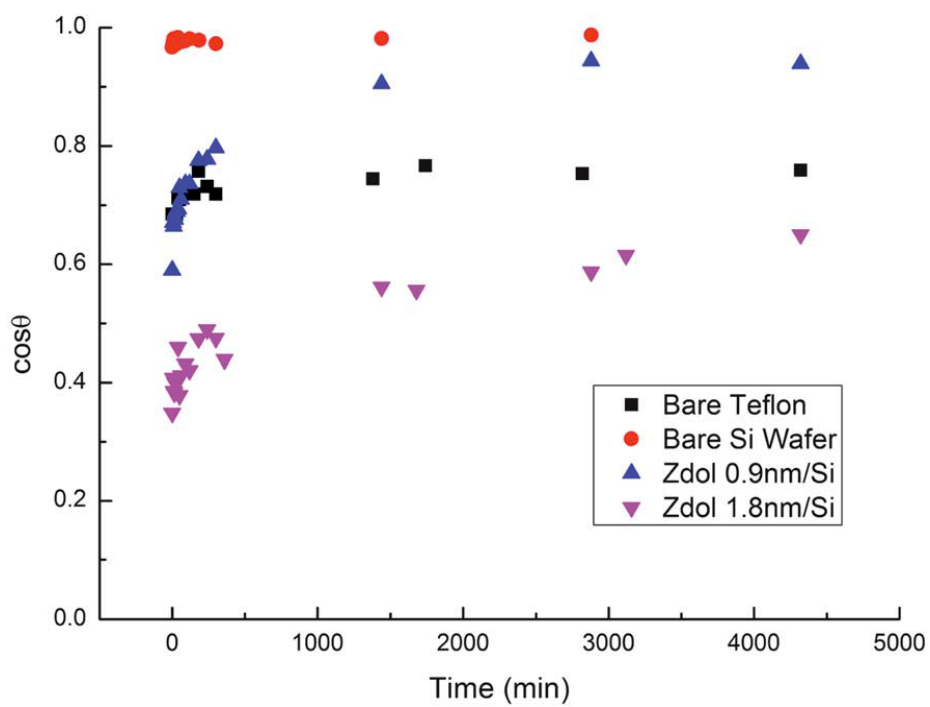


Figure 22. Time dependence of $\cos \theta$ of hexadecane on various surfaces.

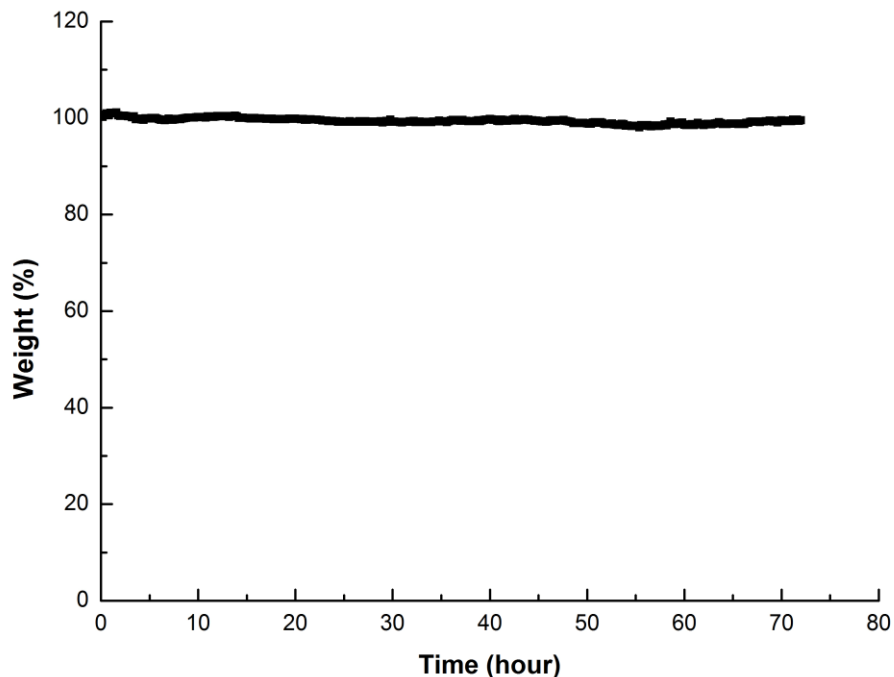
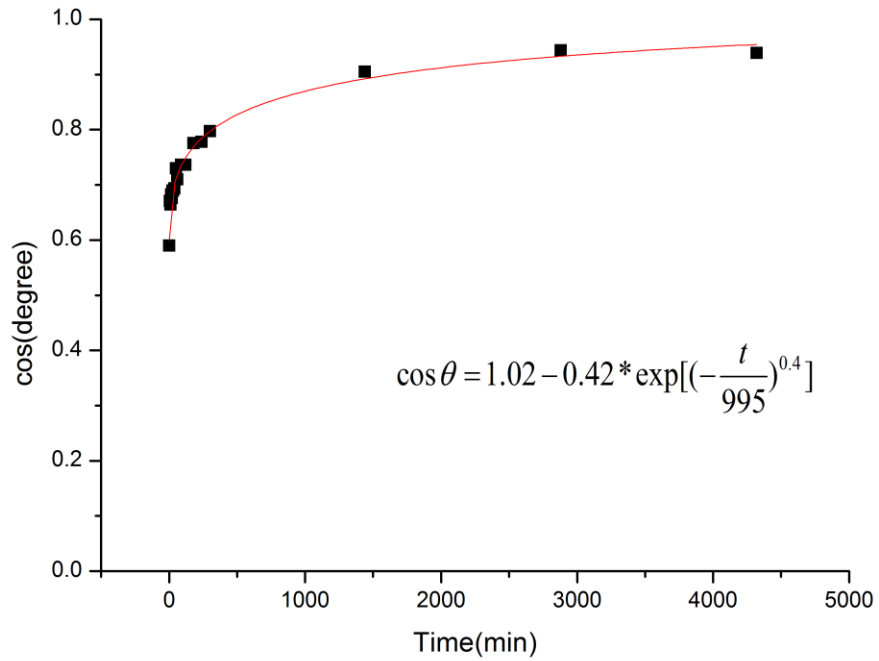


Figure 23. TGA results of hexadecane (room temperature in air)

To further confirm that this time dependence of the hexadecane contact angle is caused by the ZDOL/Si surface, the control experiments were conducted on a bare Si wafer and a PTFE surface, respectively, and the results are also shown in Figure 22. For bare Si wafer, there is no detectable change in θ . For PTFE, the change in θ is only 4 degrees for up to three days. The $\cos\theta$ - t plots of two ZDOL/Si samples can be fitted with a modified Kohlrausch–Williams–Watts (Equation is shown in below) function as shown in Figure 24. The curve-fitting results show that the change of the HCA on the thicker ZDOL is almost forty times slower than that of the thinner ZDOL.

$$\cos\theta(t) = \cos\theta_e + (\cos\theta_0 - \cos\theta_e) * \exp\left[-\left(\frac{t}{\tau}\right)^\beta\right]$$

Here t is the aging time, $\cos\theta_e$ is the equilibrium contact angle, $\cos\theta_0$ is the initial contact angle, τ is the relaxation time constant indicating how fast the system approaches equilibrium and β is the stretch factor characterizing the nonlinearity of the relaxation process.



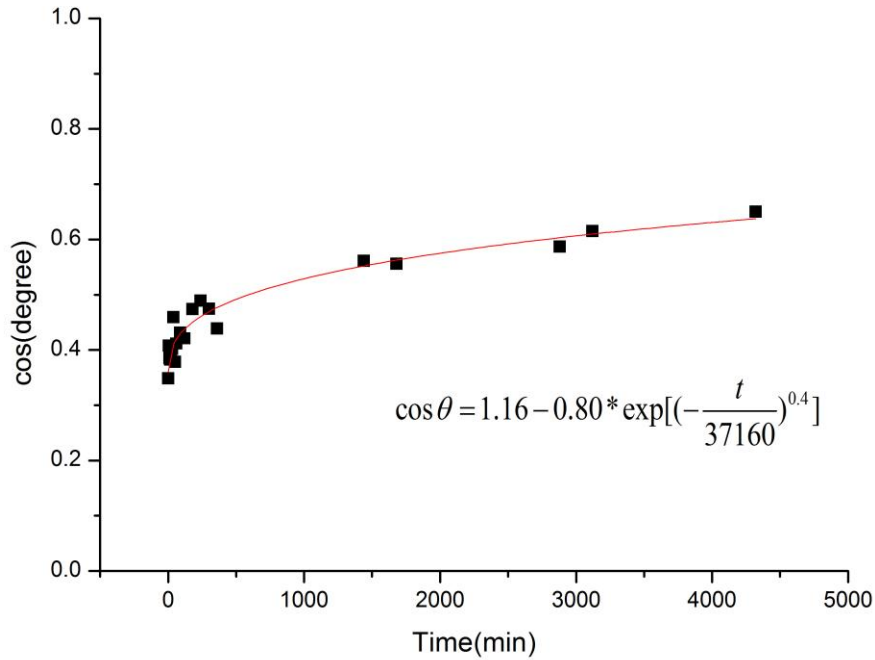


Figure 24. KWW Fitting results of $\cos\theta$ of hexadecane on ZDOL (0.9 nm)/Si (top) and ZDOL (1.8 nm)/Si (bottom)

Previously, Wu and Mate⁷³ also reported that the HCA on a ZDOL/Si sample decreases with time, which is consistent with our finding here, though the WCA was not reported in that work. The observed time dependence of the HCA on a ZDOL/Si surface indicates that the static HCA measured within a short time period is not the equilibrium value. Therefore, the observed higher HCA (higher than the WCA) is kinetic in nature. This is clearly shown in the case of a ZDOL 0.9 nm/Si sample. After three days, the HCA drops from 54 degrees to 20 degrees, this is already lower than the WCA (28 degrees) on the bare Si wafer. Since the equilibrium static WCA on a ZDOL/Si surface should be higher than that of a bare Si surface due to the fluorinated chain structure of ZDOL, the WCA must be higher than the HCA under the true equilibrium state. (Since the τ for the penetration of hexadecane through the nanofilm is in the same order

with the τ for the nanofilm polymer relaxation, so the penetration is related to the nanofilm polymer relaxation. See section 5.0)

2.5 DISCUSSION

Why does the HCA change with time? Is it possible that the molecular segments reorganize, e.g. “flip-flop”, with time and the fluorinated segments on the top surface are replaced? Previous study¹⁶ showed that for ZDOL/Si, the fluorinated segments stay on the polymer–air interface and the hydroxyl end-groups stay on the polymer/Si interface to minimize the overall interfacial energy. After a hexadecane droplet is placed on the ZDOL/Si surface, the reorganization of the polymer segments/end-groups is highly unlikely since the hydroxyl end-groups are attracted to the silica rather than hexadecane.

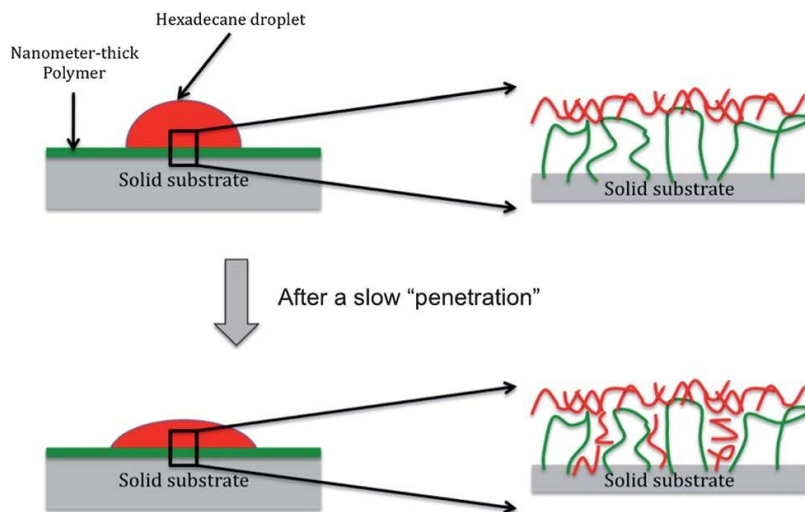


Figure 25. Schematic show of the “penetration” mechanism (not to scale).

An alternative mechanism is the slow penetration of hexadecane towards the ZDOL/Si interface. On the surface of thick fluorinated polymer coatings, it has been reported^{68, 74-75} that the penetration of the alkane liquids into the polymer coatings occurs. In the current study, the fluorinated polymer film is nanometer thick and the hexadecane is attracted to the substrate (with high surface tension) thermodynamically, which renders the penetration very likely. As is schematically shown in Figure 25, initially hexadecane “sees” a fluorinated surface and shows the high contact angle. With time, the penetration occurs and the contact angle drops gradually. This hypothesis is supported by the fact that the HCA decreases much more slowly with the increase of ZDOL thickness. Since the water molecule is much smaller than the hexadecane molecules, the penetration should be much faster.⁶⁸ As a result, in a given short time period, the measured static WCA is close to the equilibrium value where the HCA is much higher than the equilibrium value. Therefore, the observed higher HCA (higher than the WCA) is kinetically controlled rather than thermodynamically determined.

To date, the reported peculiar wetting behavior was only found when a nanometer-thick amphiphilic perfluoropolymer was coated on a hydrophilic substrate. To fully understand the effect of both the polymer and substrate and thus uncover the mechanism, the contact angles on Z-03/Si and ZDOL/PTFE were also measured. Interestingly, as shown in Table 2, both surfaces show “normal” behavior: the WCA is higher than the HCA. Since the only difference between Z-03 and ZDOL is the end-group, the fact that Z-03/Si shows normal wetting behavior indicates that the polar hydroxyl end-group plays an important role in the peculiar wetting behavior. However, since ZDOL/PTFE also shows normal wetting behavior, the end-group by itself cannot result in the observed peculiar wetting behavior. On the basis of all these experimental results, it is suggested that the ZDOL–Si interaction is the key. Since the slow penetration of hexadecane

results in the short-term higher HCA, the size of the intermolecular “hole” in the nanometer-thick polymer layer is critical. For a nanometer-thick polymer film, the full coverage on a substrate is not always guaranteed.⁴⁷ The polymer–substrate interaction, which affects the packing density and dynamics, is the key here.^{16, 45-47} When there is attractive interaction, the polymers pack more orderly and have lower mobility, which results in a smaller “hole” size. Previous studies^{16, 45-47} showed that ZDOL can form hydrogen bonds with the polar surface via hydroxyl end-groups while Z-03/Si and ZDOL/PTFE cannot. As a result, it has been proposed⁴⁷ that this attractive interaction between ZDOL and a solid substrate renders a more ordered packing of ZDOL molecules. Meanwhile, the dynamics of ZDOL molecules on Si is much slower.¹⁶ Therefore, the “hole” size in ZDOL/Si should be much smaller than in Z-03/Si and ZDOL/PTFE. When the “hole” size is big, both water and hexadecane can penetrate the polymer layer quickly, which results in the normal thermodynamically determined wetting behavior. When the “hole” size is appropriately small, water penetrates quickly while hexadecane penetrates much slower, which results in the kinetically controlled peculiar wetting behavior. (At a given “hole” size, the thickness of the polymer layer also plays a role. When the polymer layer is thicker, the penetration is slower and thus the relaxation time constant is longer, as is supported by the curve-fitting results in Figure 24) When the “hole” size is too small, both water and hexadecane cannot penetrate (or the penetration is very slow), which again results in normal wetting behavior. The latter case has been reported extensively^{16, 76-77} for highly ordered self-assembly monolayers (SAMs), which show normal wetting behavior though both WCA and HCA are high. Further research is required to determine the exact “hole” size for the peculiar wetting behavior. On the basis of the size of water and hexadecane,⁶⁹ it is estimated to be on the order of 100 \AA^3 . With the new mechanism proposed here, the design criteria to surfaces more

wettable to water than to oil could also be established for a nanometer-thick polymer coated substrate. First, the substrate must have high surface tension, so that there is a driving force for the liquid, either water or oil, to penetrate the polymer layer and migrate towards the substrate. Second, the polymer film must have a perfluorinated segment to provide a high initial oil contact angle. Third, the polymer–substrate interaction must be appropriate such that the intermolecular “hole” serves as a “filter” to “separate” the fast penetration of small water molecules and the slow penetration of large oil molecules. From the design viewpoint, the polymer–substrate system that maximizes the difference in the penetration rates of water and oil will provide the most robust peculiar wetting behavior.

2.6 CONCLUSIONS

In conclusion, it was found experimentally that the HCA on a nanometer-thick amphiphilic perfluoropolyether (PFPE) coated Si wafer, which is more wettable to water than to oil, decreases with time significantly. The results suggest that the previously reported surprising behaviors of some surfaces, which show higher HCA than WCA, are kinetically controlled. By comparing the PFPEs and substrates with different structures, we have proposed that the interaction between the nanometer-thick polymer and the substrate is the key to the appropriate size of the intermolecular “hole” in the polymer layer, which in turn determines the kinetics of the penetration of water and hexadecane. Only when the “hole” size is appropriate, so that the penetration rate of hexadecane is much slower than that of water, the peculiar wetting performance is observed. On the basis of these findings, the design criteria to fabricating surfaces more wettable to water than to oil have also been proposed.

3.0 EFFECT OF END-GROUP ON SIMULTANEOUS OLEOPHOBICITY/HYDROPHILICITY AND ANTI-FOGGING PERFORMANCE OF NANOMETER-THICK PERFLUOROPOLYETHERS (PFPEs)

3.1 CHAPTER PREFACE

Materials contained in this chapter were published as a research article in *RSC Advances*; figures used in this chapter have been reprinted with permission from: *RSC Adv.*, **2015**, 5, 30570-30576 (listed as reference 91 in the bibliography section). Copyright © 2015 The Royal Society of Chemistry.

List of Authors: Yongjin Wang, James Knapp, Aleigh Legere, Jacob Raney and Lei Li

Author Contributions: Y.W., and L.L. designed and directed the experiments. Y.W., J.K., A.L., and J.R. conducted the experiments. All authors discussed the results. Y.W., and L.L. wrote the manuscript with input from all authors.

3.2 INTRODUCTION

Simultaneously oleophobic/hydrophilic coatings are highly desirable in many important applications, *e.g.*, anti-fogging. Fogging, which often occurs on the surface of glasses, goggles, camera lenses and automobile windows, reduces the light transmission and could degrade the device performance dramatically.¹⁵ To understand the fogging mechanism, Briscoe¹⁵ studied the condensation of water vapor on the surfaces of polyethylene and glass and found that when the water contact angle (WCA) on a solid surface is low, a uniform water film will be formed and fogging will not occur. When WCA is higher than a critical value, water droplets will be formed on the solid surface and fogging will occur and reduce the light transmission. In recent years, different anti-fogging coatings have been developed in order to improve the effectiveness of the optical devices,^{10, 20-23} including multilayer nanoporous-silicate,²⁰⁻²² TiO₂-based nanoparticle coatings²³ and solvent-sensitive stimuli responsive polymer brush coatings.¹⁰ All of these anti-fogging coatings are designed to be hydrophilic and it is expected that water will form a uniform film on the coated surface and, as a result, fogging will not occur. Indeed, this is the case in the short term. Unfortunately, in long-term applications these hydrophilic coatings, which have high surface energy, are easily contaminated by airborne hydrocarbons in the ambient environment.¹⁰ The adsorbed airborne hydrocarbons on the surface will lower the surface energy and thus render the surface more hydrophobic. As a result, water forms droplets on such an “oil coated” surface, which makes the surface no longer antifogging.⁹⁻¹¹ A promising approach to address this issue is to develop simultaneously oleophobic/hydrophilic coatings, which are expected to allow water to easily wet the surface due to their “hydrophilicity” and reduce the hydrocarbon contamination due to their “oleophobicity”. Unfortunately, WCA is usually higher than oil contact angle (OCA) on the same solid surface according to previous theoretical and experimental studies.⁶⁻⁷ The

lower OCA indicates that a solid is expected to be more wettable to oil than to water. In other words, if a solid surface is hydrophilic, it cannot be oleophobic. However, a few recent reports indicated that it is possible to achieve simultaneous oleophobicity/hydrophilicity with some nanometer-thick amphiphilic coatings on some hydrophilic substrates.⁸⁻¹¹ For example, polyelectrolyte plasma polymer substrates, coated with ionic amphiphilic fluoro-surfactants, were reported to be more wettable to water than to oil.⁸⁻⁹ Moreover, a reactive isocyanate-silane modified silica substrate, covalently grafted with perfluorinated polyethylene glycol oligomers (f-PEG) layers, was reported to have significantly lower WCA than hexadecane contact angle (HCA).¹⁰⁻¹¹ The possible mechanisms of simultaneous oleophobicity/hydrophilicity have been discussed previously.⁸⁻¹¹ Howarter and Youngblood¹⁰⁻¹¹ proposed that the PEG segments, which is hydrophilic, stay on the bottom of the polymer layer and the perfluorinated segments, which is hydrophobic, stay on the top of the layer. Water would swell the PEG constituents while hexadecane would not as it is not a good solvent for PEG. Therefore, water would “see” the hydrophilic PEG segments, resulting in a small WCA, and hexadecane would “see” the hydrophobic perfluorinated segments, resulting in a larger HCA. In other words, they proposed that water and hexadecane “see” two different “surface energies” on the same surface. However, a given solid surface should have only one fixed surface energy. Clearly, further research is required to uncover the underlying mechanisms of the simultaneously oleophobic/hydrophilic coatings.

In the current paper, based on our recent finding¹⁷ that a nanometer-thick PFPE with hydroxyl end-groups shows simultaneous oleophobicity/hydrophilicity on a silica substrate, we have investigated the mechanisms of simultaneous oleophobicity/hydrophilicity by systematically varying the end-groups of PFPEs. The static and time-dependent WCA and HCA

results suggested that the simultaneous oleophobicity/hydrophilicity can be achieved only when the end-groups of PFPEs have the appropriate interaction with the substrate so that the inter-chain distance of PFPE in the nanofilm is appropriately small. In this case, water penetrates the polymer nanofilm quickly while oil penetrates the nanofilm much more slowly. As a result, the coating shows simultaneous oleophobicity/hydrophilicity. More interestingly, X-ray photoelectron spectroscopy (XPS) and anti-fogging testing results showed that the simultaneously oleophobic/hydrophilic coating is indeed more resistant to airborne hydrocarbon contamination, leading to improved long-term anti-fogging performance.

3.3 EXPERIMENTAL SECTION

Si wafer (purchased from Silicon Quest International, Inc.) with 2 nm native oxide (P/B <100> 1–10 ohm cm, $279 \pm 25 \mu\text{m}$) and plain glass microscope slides (25 x 7 x 51 mm, Fisherbrand) were used as the substrates for contact angle and anti-fogging tests, respectively. The substrates were coated with three PFPE polymers, commercially known as ZDOL, Z-03 and Z-tetraol, which were obtained from Solvay Solexis Inc. The chemical structures of PFPEs are shown in Figure 26.

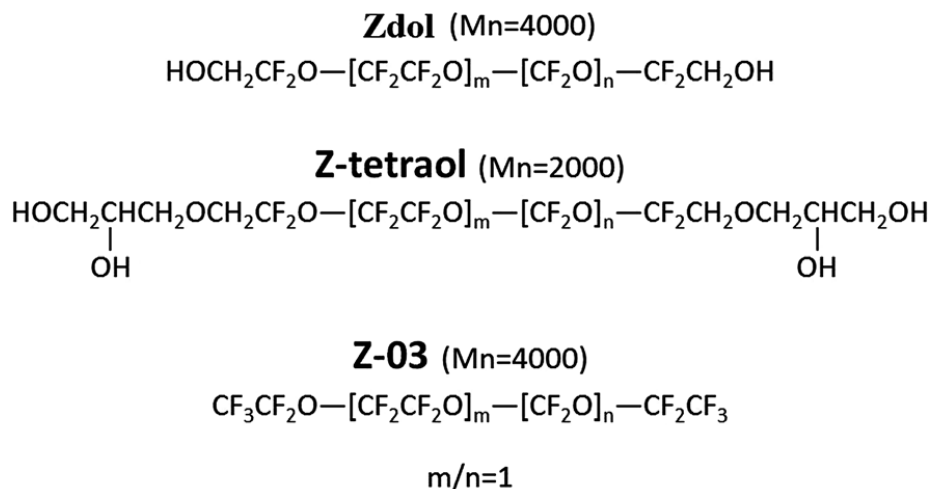


Figure 26. The chemical structures of PFPE polymers.

These three PFPEs have the same backbone but different end-groups, which result in the different interactions with silica surfaces.⁴⁴⁻⁴⁶ The nanofilms were coated on silica wafer by dip-coating¹⁷ with 2,3-dihydrodecafluoropentane as the solvent, which was obtained from Miller Stephenson Chemical Corporation. Deionized (DI) water, produced from a Millipore Academic

A10 system with total organic carbon below 40 ppb, and hexadecane (anhydrous, \$99%, Sigma-Aldrich) were used as the testing liquids for contact angle measurements. All of the chemicals were utilized as received.

The chemical structure of PFPE nanofilms was characterized using ESCALAB 250 XI (Thermo Scientific) X-ray photoelectron spectroscopy (XPS) system. The spectra were collected using a monochromatic Al K α X-ray source with a spot size of 200 μm . An electron flood gun was used to neutralize charge on the nonconductive samples. For each experiment, the sample was inserted into the analysis chamber where a vacuum was maintained at $\sim 10 \times 10^{-10}$ mBar by magnetic manipulator. Then a survey spectrum (5 scans, 150 eV pass energy, 1 eV step) and a high-resolution C1s scan (20 scans, 50 eV pass energy, 0.1 eV step) were collected. The spectra analysis was performed using Thermo Advantage software.

The WCA and HCA on the PFPE-coated Si wafers were measured using a VCA optima XE (AST Production Inc.) video contact angle system. For the static contact angle test, a 2 μL liquid droplet was deposited on the sample surface and then the image of this liquid droplet on the surface was taken with a charge-coupled device (CCD) camera and eventually the contact angle was determined by the VCA software automatically. To minimize the possible interruption caused by the evaporation of the liquid, the time-dependent WCA test was done in a sealed system and the sample was left on the stage of the goniometer during the entire testing period. The sealed system is shown in Figure 27: a 4.5 cm x 1 cm x 1 cm section of sponge was placed in a round glass cuvette. The sponge was soaked with the testing liquid, *e.g.* water. An open-top septum cap with a rubber seal was utilized for the cuvette and the parafilm was used to further seal the system. Since the needle of VCA instrument penetrates the rubber septum easily, testing liquids can be introduced on the sample without opening the cuvette. After placing the droplet of

the testing liquid on each sample, contact angles of the same droplet were monitored in the following 24 hours.

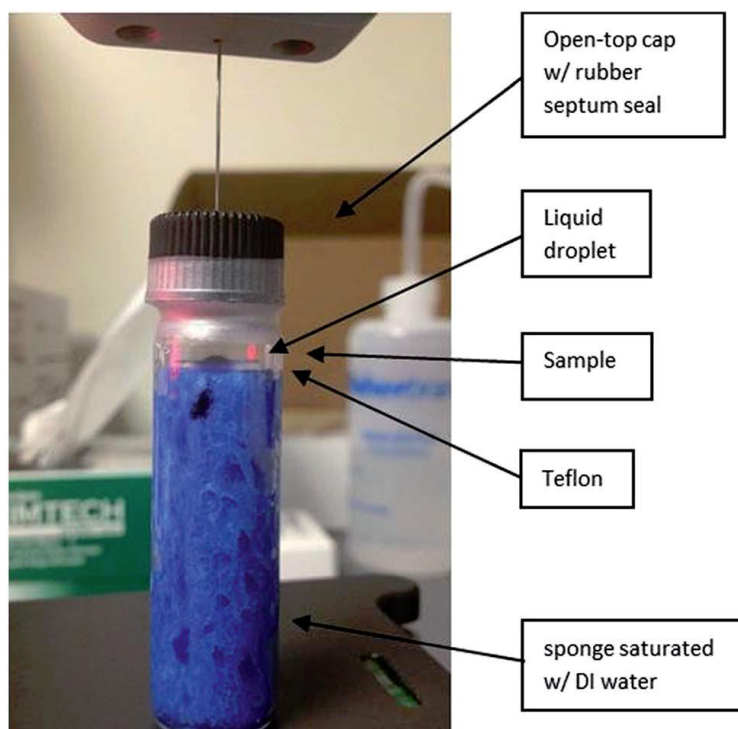


Figure 27. Sealed cuvette with needle piercing rubber septum.

To characterize the anti-fogging performance of the nanometer-thick polymer coatings, the PFPE-coated glass slides were held over the boiling water for five seconds and then removed and photographed.¹¹

3.4 RESULTS

3.4.1 Thickness of PFPE nanofilms

The thickness of PFPE nanofilms was measured using a J.A. Woollam alpha-SETM Ellipsometer and the detailed procedure was described elsewhere.¹⁶ The average thickness based on three repeats at different samples, are 1.6 ± 0.2 nm, 1.7 ± 0.2 nm and 2.0 ± 0.2 nm for Z-03, ZDOL and Z-tetraol, respectively, as shown in Table 3.

Table 3. The thickness of PFPE nanofilms on silica surfaces

PFPE nanofilm	Concentration of solution for dip-coating (g/L)	Thickness (nm)
Z-03	2.0	1.6 ± 0.2
Zdol	1.5	1.7 ± 0.2
Z-tetraol	0.4	2.0 ± 0.2

3.4.2 Topography of PFPE nanofilms

Atomic force microscopy (AFM) images of PFPE nanofilms were obtained with a Veeco MultiMode V scanning probe microscopy (SPM) and the images are shown in Figure 28. The surface roughness (Ra) is 0.134 nm, 0.126 nm and 0.184 nm for ZDOL/Si, Z-03/Si and Z-tetraol/Si, respectively. These results show that these PFPE nanofilms have similar topography and are all very smooth.

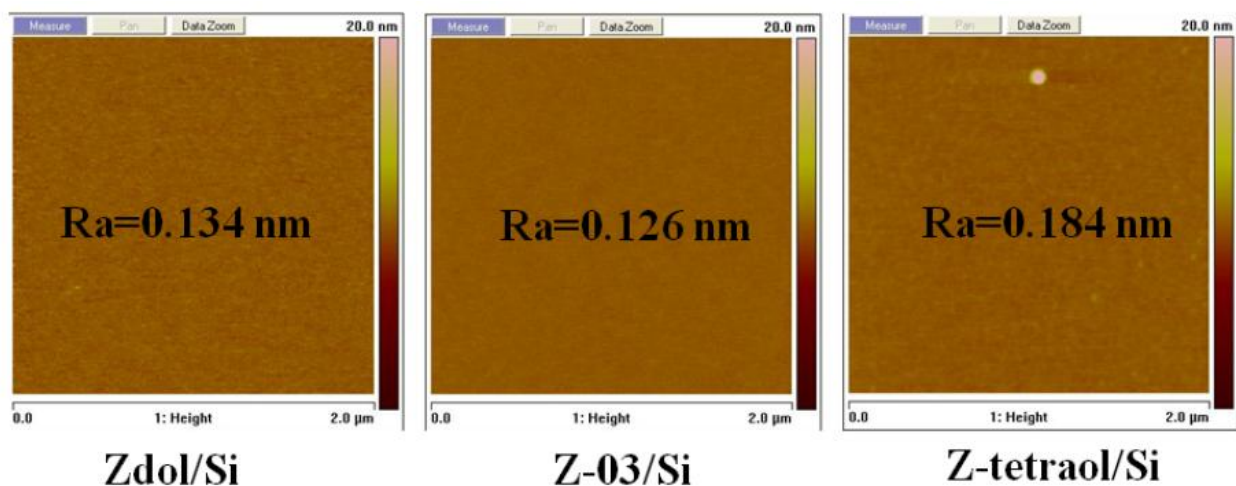


Figure 28. AFM images of PFPE nanofilms on silica surfaces.

3.4.3 Static and time-dependent contact angle tests

The static WCA and HCA on three PFPE-coated Si wafers are shown in Table 4, which indicate totally different wetting behavior. The WCA on Z-03/Si is 43.4° , which is larger than the HCA (32.6°), and thus Z-03/Si still shows “normal” wetting behavior: WCA is larger than HCA. On the contrary, ZDOL/Si is simultaneously oleophobic/hydrophilic as WCA (46.5°) is lower than HCA (70.1°). Interestingly, for Z-tetraol/Si, both WCA (66.2°) and HCA (68.8°) are relatively large and they have similar values.

Table 4. Static water and hexadecane contact angle on different surfaces.

	DI Water	Hexadecane
Z-03/Si	43.4 ± 0.8	32.6 ± 0.5
Zdol/Si	46.5 ± 0.9	70.1 ± 0.9
Z-tetraol/Si	66.2 ± 1.2	68.8 ± 1.2

The time-dependent HCA and WCA on three PFPE-coated Si wafers are shown in Figure 29a and b, respectively. As shown in Figure 29a, HCA does not change with time up to 1500 min for both Z-tetraol/Si and Z-03/Si. However, for ZDOL/Si, $\cos\theta$ (HCA) changes from 0.39 (66.8°) to 0.63 (50.8°) during the same time period. This is consistent with previous^{17, 73} reports that the HCA on ZDOL/Si decreases with time. Since hexadecane does not evaporate during the experiment,¹⁷ the change in HCA cannot be attributed to the evaporation as reported before.⁷¹ Instead, the results indicate the “penetration” of hexadecane through the ZDOL nanofilms⁷. As shown in Figure 29b, all three samples show similar trend of time-dependent WCA: $\cos\theta$ doesn't change significantly during 24 hours.

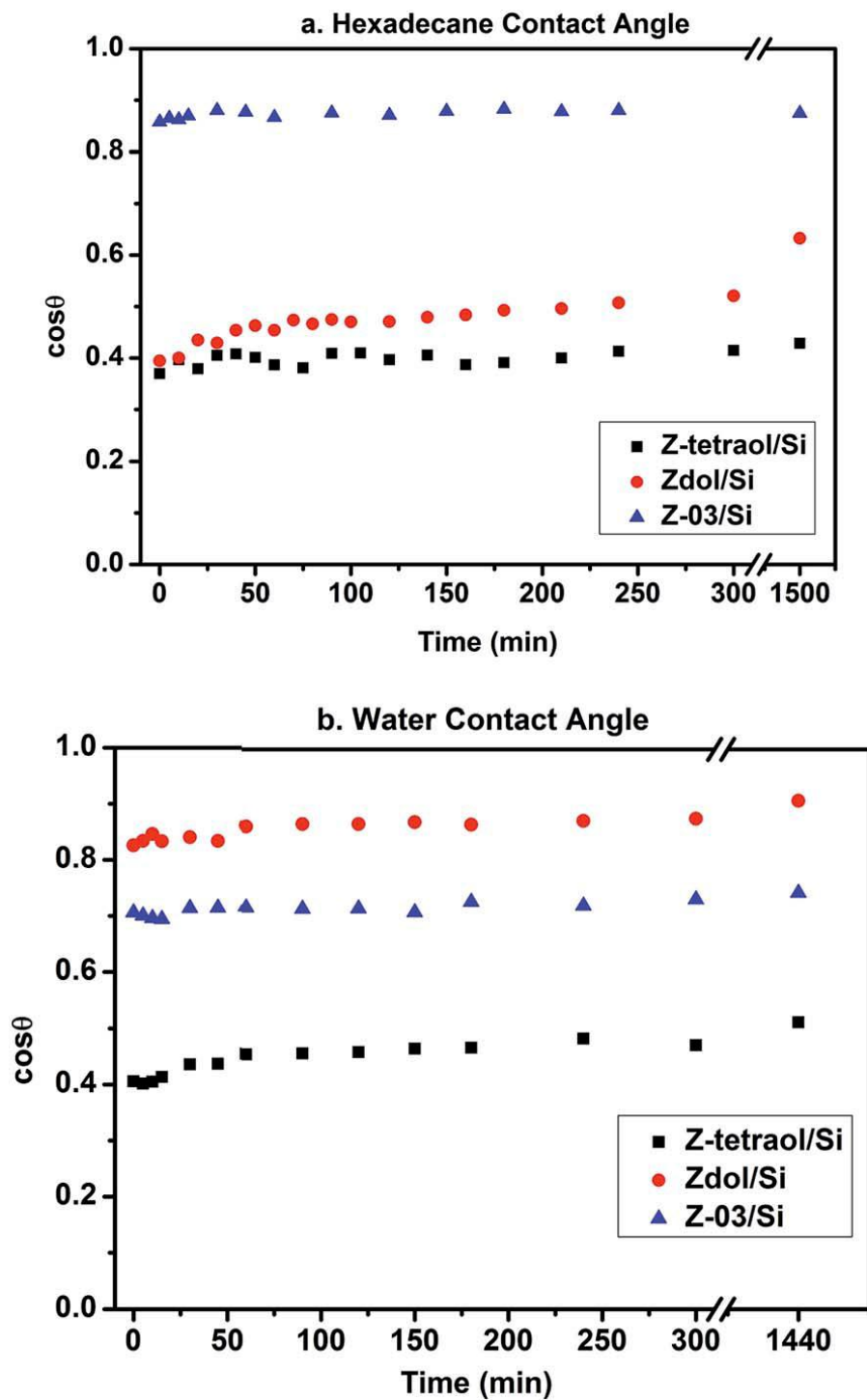


Figure 29. $\cos \theta$ ((a) hexadecane, (b) water) vs. time on different PFPE nanofilms.

3.4.4 Evaporation effect on time-dependent contact angles (CA)

Although time-dependent contact angle tests were conducted in a “sealed” system, it did not completely stop the evaporation. Bourges-Monnier has showed that, during the evaporation of a liquid droplet, the diameter of the droplet decreases with time.⁷¹ As shown in Table 5 the diameter of water droplet decreased a little bit during 24 hours in the time-dependent water contact angle (WCA) experiments, indicating that there has been slight evaporation. On the contrary, the hexadecane droplet does not evaporate as shown previously by thermogravimetric analysis (TGA).¹⁷ More interestingly, the diameter of hexadecane droplet on ZDOL 1.8nm/Si actually increased by 0.35 mm after 24 hours as shown in Table 5, indicating that the change of hexadecane contact angle (HCA) is due to the “penetrating” instead of evaporation of hexadecane.

Table 5. The decrease of diameter of water and hexadecane droplet.

	Droplet Diameter Decrease (mm)	
	Water	Hexadecane
Z-03 1.7nm/Si	0.06	0.00
Zdol 1.8nm/Si	0.08	-0.35
Z-tetraol 2.2nm/Si	0.03	0.00

3.4.5 Advancing contact angle (ACA) and receding contact angle (RCA)

The dynamic contact angle was measured with a VCA optima XE instrument, the process of adding (advancing) or withdrawing (receding) test liquid to and from an existing test liquid

droplet was recorded by a CCD camera (30 images per second). The ACA and RCA were determined by measuring the tangent of the test liquid droplet at the intersection of the air/drop surface while adding (advancing) and withdrawing (receding). The results of dynamic WCA and HCA are shown in Table 6.

Table 6. Dynamic contact angles of PFPEs coated on silica surfaces.

	Water_ACA	Water_RCA	Hexadecane_ACA	Hexadecane_RCA
Z-03	51.3 ± 1.5	12.8 ± 0.4	43.0 ± 1.5	7.5 ± 0.2
ZDOL	47.5 ± 1.4	21.1 ± 1.9	67.7 ± 1.6	32.3 ± 1.7
Z-tetraol	63.3 ± 2.2	33.6 ± 1.5	75.6 ± 3.5	59.9 ± 0.7

3.4.6 Effect of molecular weight (MW) on contact angle results

The WCA and HCA of ZDOL/Si, with the MW of ZDOL as 2610g/mol, 4000g/mol and 8778g/mol, respectively, are shown in Table S5. The results show that there is no significant change in both WCA and HCA, which suggests that the molecular weight has little effect on the wetting behavior.

Table 7. WCA and HCA on different ZDOL nanofilms with different molecular weights

	Zdol 2610	Zdol 4000	Zdol 8778
WCA	46.9 ± 0.6	46.0 ± 0.9	47.8 ± 0.6
HCA	66.5 ± 0.4	67.0 ± 0.7	67.1 ± 0.4

3.4.7 XPS and anti-fogging tests

3.4.7.1 Anti-fogging tests

The anti-fogging test results of PFPE-coated glass slides are shown in Figure 30. The tests were conducted on the 1st day and the 14th day after the samples were fabricated. Z-tetraol showed the worst anti-fogging performance on both days and this can be attributed to the fact that it is the most hydrophobic one with the highest WCA among three PFPEs. ZDOL and Z-03 showed similarly good anti-fogging performance on the 1st day. However, with the increase of aging time, the anti-fogging performance of Z-03 degraded significantly while there was much less change for ZDOL. As a result, on the 14th day, ZDOL showed significantly better anti-fogging performance than Z-03.

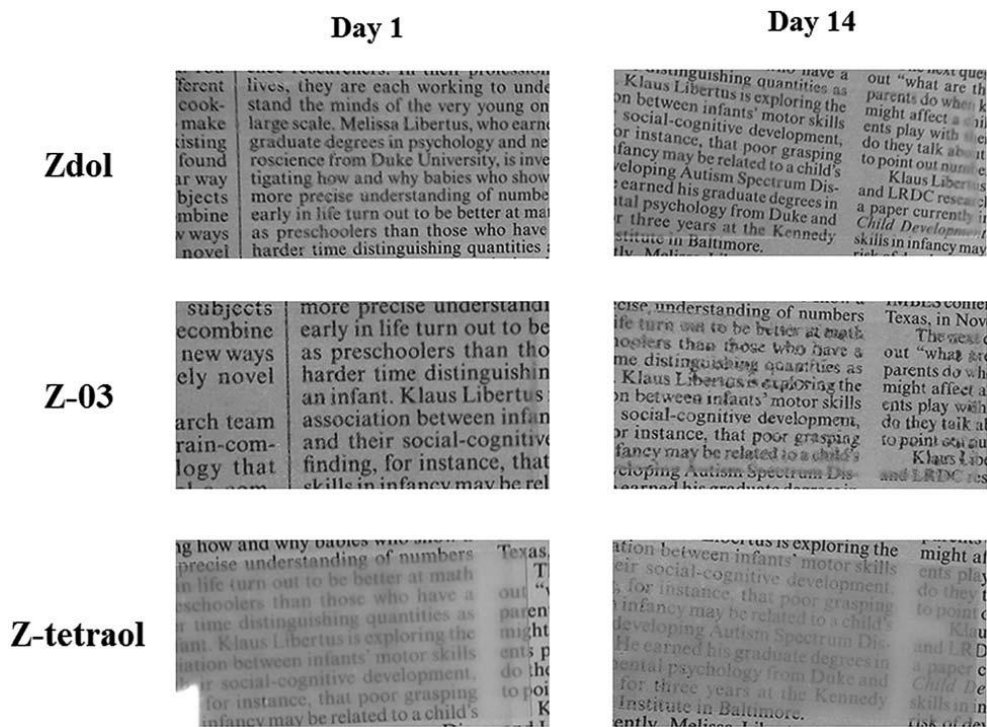


Figure 30. Anti-fogging testing results of PFPE-coated glass slides.

3.4.7.2 XPS results

To understand the relationship between airborne hydrocarbon contamination and the long-term antifogging performance, the XPS C1s spectra of ZDOL, Z-tetraol and Z-03 coated glass slides have been collected and are shown in Figure 31. To synchronize with anti-fogging tests, the XPS experiments were also conducted on the 1st day and the 14th day after the samples were fabricated, respectively. The peaks at 295.12 eV and 293.03 eV are assigned to fluorocarbon constituents and the peaks between 282.00 to 290.00 eV are assigned to hydrocarbon constituents based on previous literature.⁷⁰

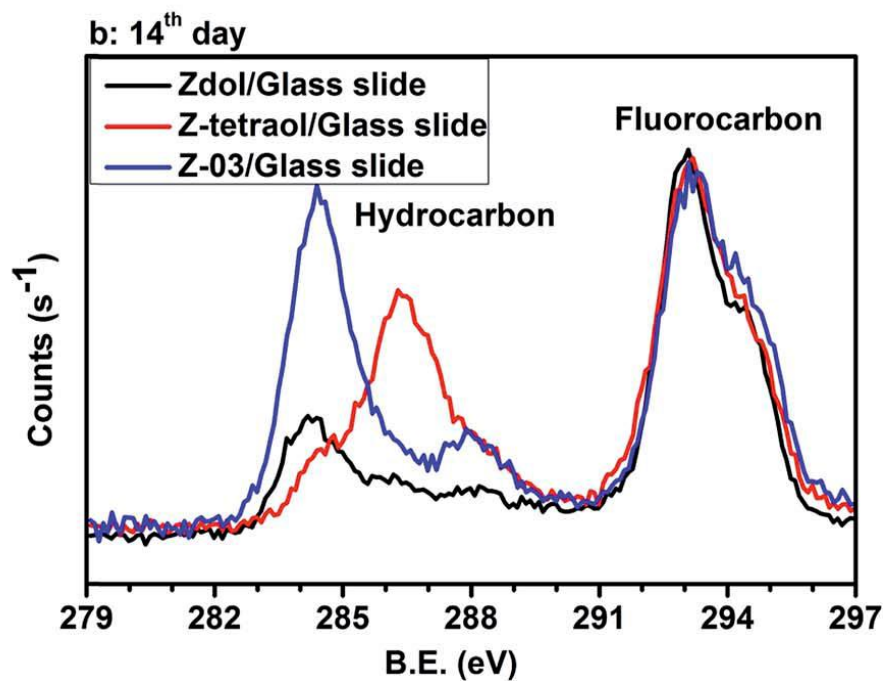
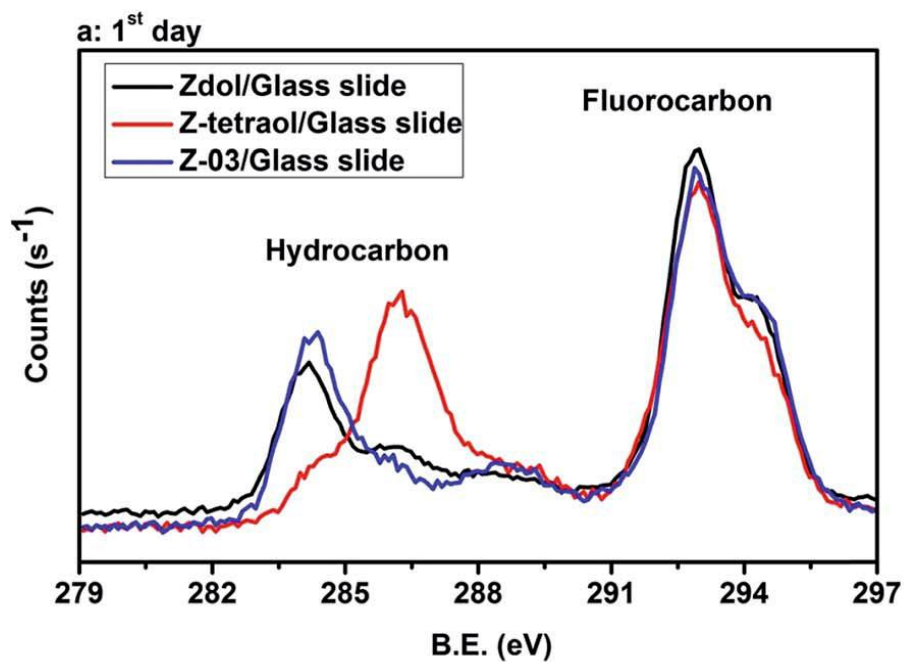


Figure 31. XPS C1s spectra of PFPE-coated glass.

3.4.7.3 XPS peaks assignments

Since there is no hydrocarbon moiety in Z-03 molecule, all the hydrocarbon peaks are attributed to the airborne hydrocarbon contaminants for Z-03 sample. Because both ZDOL and Z-tetraol polymers contain hydrocarbon moiety in their end-groups, the hydrocarbon peaks are attributed to both airborne hydrocarbon contaminants and the end-groups of polymers. The XPS peaks assignments are shown in Figure 32 and Figure 33.

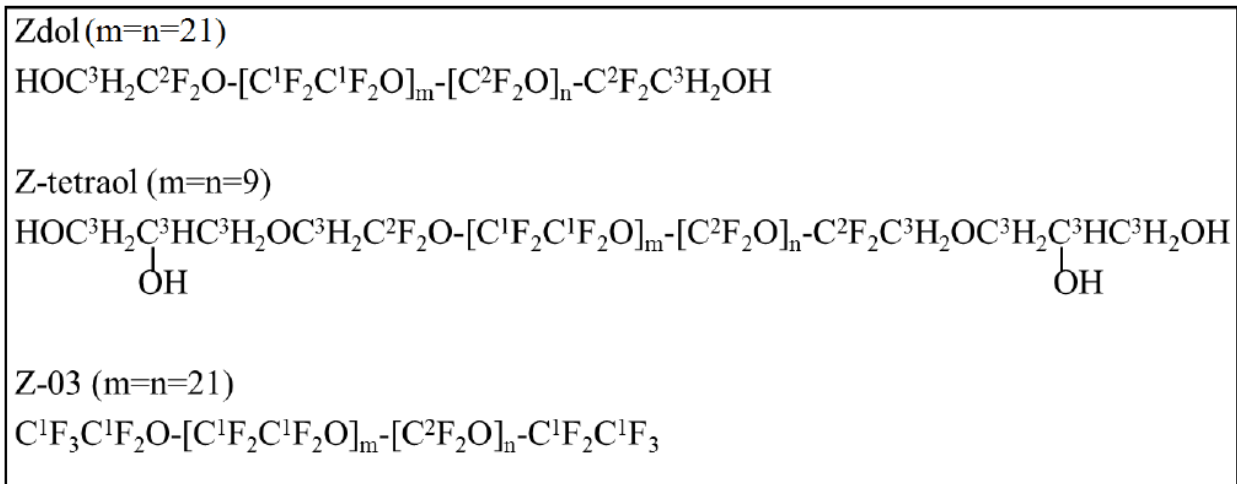
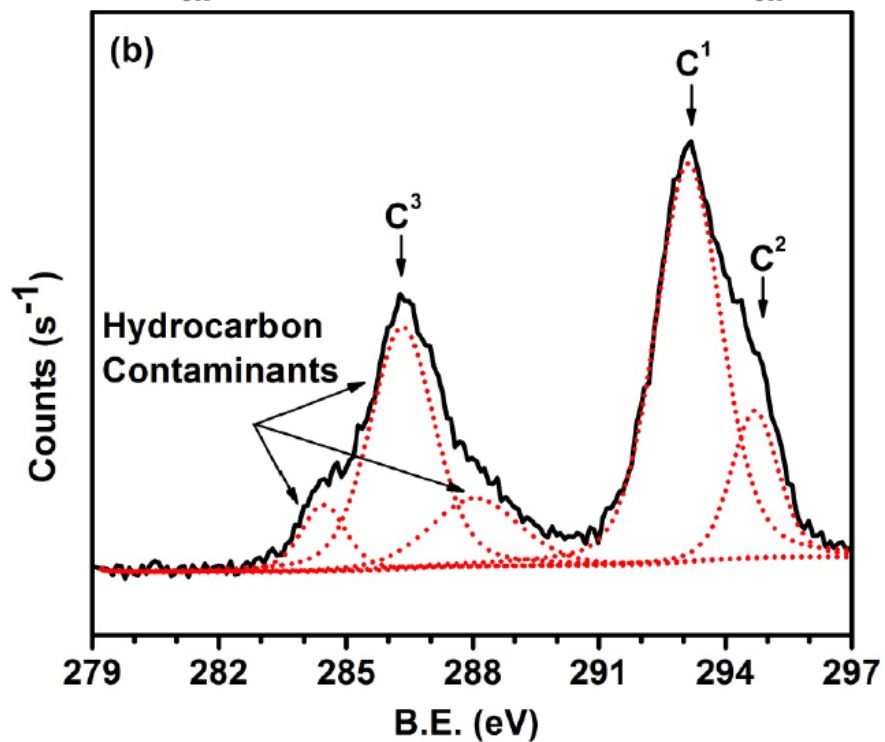
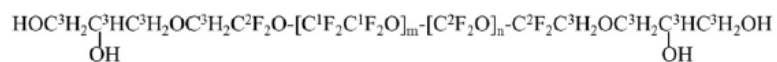
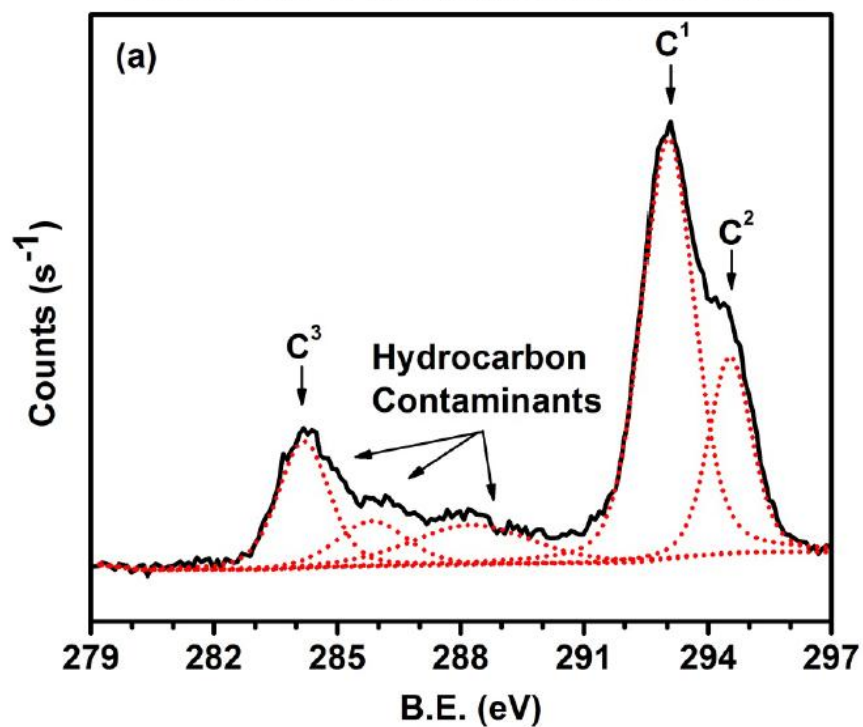


Figure 32. Molecular formula of PFPEs.

Note: Not all the C³ in Z-tetraol are exactly the same. However, these carbons have very similar binding energy and are labeled as the “same” carbon here.



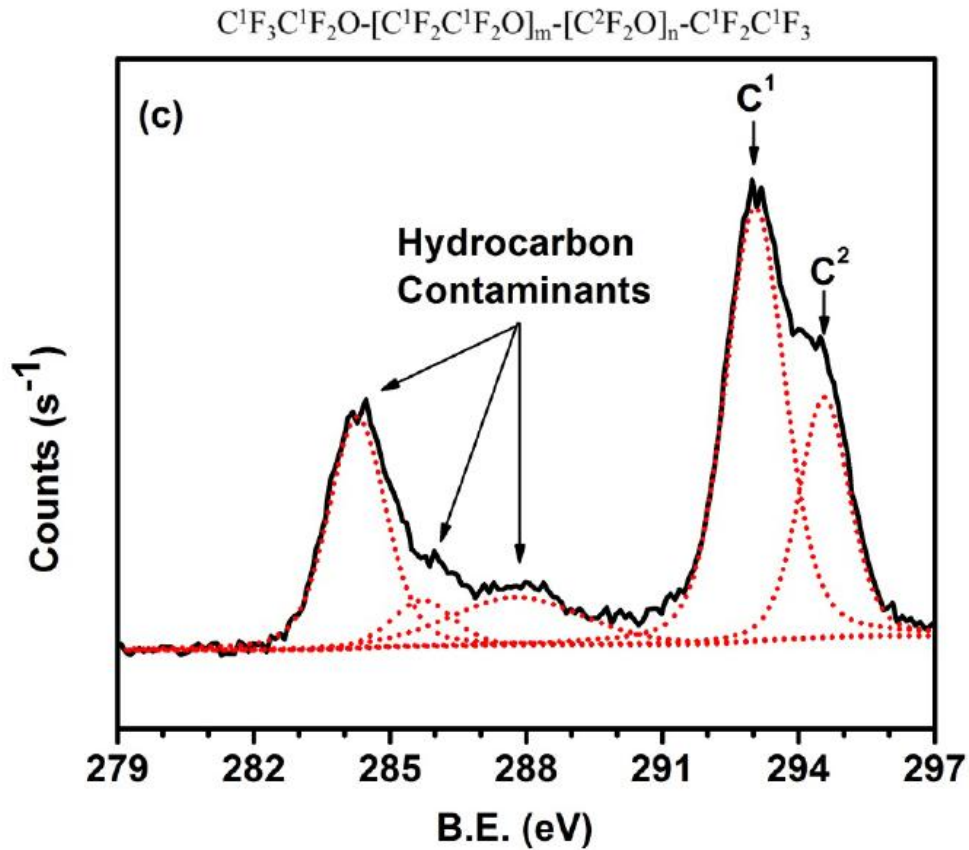


Figure 33. XPS C1s spectra and curve-fitting results (a) ZDOL, (b) Z-tetraol, (c) Z-03

3.4.7.4 Calculation of the amount (%) of airborne hydrocarbon contaminants

Based on XPS results and the molecular formula of PFPEs, the fluorocarbon% and total hydrocarbon%, including the hydrocarbons from both PFPE end-groups and airborne contaminants, were determined first. Then the airborne hydrocarbon contaminants% is determined by subtracting the hydrocarbon% in end-groups, which is calculated according to the molecular formula of PFPEs and fluorocarbon%, from the total hydrocarbon%. The area% of different C1s peaks (mean value of the three repeats) of PFPEs on different days is shown in Table 8.

Table 8. XPS C1s curve fitting results for different PFPEs coated glass slides on the 1st day (a) and the 14th day (b) after the samples were fabricated

a. 1st day

Peak	Zdol	Z-tetraol	Z-03
Fluorocarbon (%)	74.25 ± 7.53	59.54 ± 2.27	63.63 ± 3.24
Hydrocarbon (%)	25.75 ± 7.53	40.46 ± 2.27	36.68 ± 3.24
Hydrocarbon from end-group (%)	2.19	15.9	0
Hydrocarbon contaminants (%)	23.56 ± 7.53	24.56 ± 2.27	36.68 ± 3.24

b. 14th day

Peak	Zdol	Z-tetraol	Z-03
Fluorocarbon (%)	70.92 ± 1.04	57.64 ± 0.72	49.12 ± 3.74
Hydrocarbon (%)	29.08 ± 1.04	42.36 ± 0.72	50.88 ± 3.74
Hydrocarbon from end-group (%)	2.19	15.9	0
Hydrocarbon contaminants (%)	26.89 ± 1.04	26.46 ± 0.72	50.88 ± 3.74

The amount of airborne hydrocarbon contaminants (in atomic% of total carbon; mean value of the three repeats) at day1 and day 14 are shown in Figure 31. On the 1st day after the samples were fabricated, the amount of airborne hydrocarbon contaminants was 23.56%, 24.56% and 36.68% for ZDOL, Z-tetraol and Z-03, respectively. And on the 14th day, the amount of airborne hydrocarbon contaminants was 26.89%, 26.46% and 50.88% for ZDOL, Z-tetraol and Z-03, respectively. Between the 1st day and the 14th day, the amount of airborne hydrocarbon contaminants increased by 14.2%, 2.9% and 1.9% for Z-03, ZDOL and Z-tetraol, respectively. Clearly, Z-03 is the most easily contaminated by the airborne hydrocarbons.

3.5 DISCUSSIONS

3.5.1 Underlying mechanisms of simultaneous oleophobicity/hydrophilicity

As shown in Table 4, three PFPE-coated silica surfaces show different wetting behaviors: ZDOL/Si shows a characteristic of simultaneous oleophobicity/hydrophilicity; Z-tetraol/Si is both “hydrophobic” and “oleophobic” while Z-03/Si shows the “normal” wetting behavior with WCA higher than HCA. Since the only differences among three PFPEs are molecular weights and end-groups and the molecular weight has little effect on the wetting behavior as shown in Table 7. Therefore, the endgroups are the key to the simultaneous oleophobicity/hydrophilicity. Chen et al.⁴⁷ studied the interaction between PFPE polymers and hydrophilic substrates and suggested that ZDOL molecules form hydrogen bonding with hydrophilic substrates via the hydroxyl end-groups, leading to an ordered packing structure of polymer chains. If this is true, Z-03 molecules should have a disordered packing structure on the silicon wafer since Z-03 doesn't have hydroxyl end-groups and thus cannot form hydrogen bonds with hydrophilic substrates. Moreover, since Z-tetraol has more hydroxyls end-groups than ZDOL,⁴⁹ Z-tetraol molecules are expected to have stronger attraction to the silicon wafer, resulting in a highly ordered packing structure.⁵⁰ According to the discussion above, a proposed “bonding” model for PFPE polymers and hydrophilic substrates is schematically shown in Figure 34. Both ZDOL and Z-tetraol form hydrogen bonds with silica surfaces and Z-tetraol has a more ordered packing structure than ZDOL. Z-03 doesn't form hydrogen bonds with silica surface, leading to a disordered packing structure.

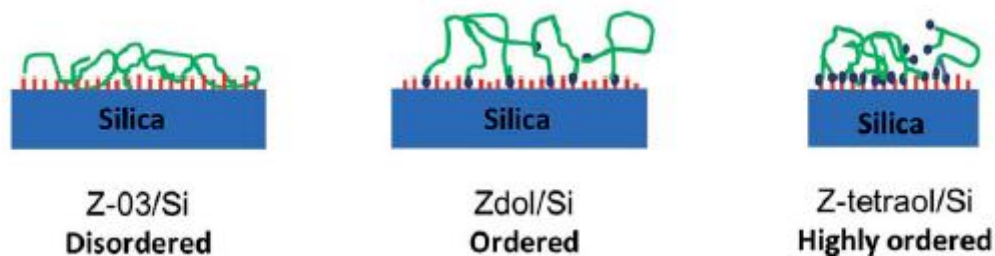


Figure 34. Schematic bonding models of PFPE polymers on silica surfaces (not shown to scale).

Based on this model, different packing structure will lead to different inter-chain distances, i.e., the size of the intermolecular “holes”. The highly ordered Z-tetraol nanofilm should have the smallest intermolecular “holes”, *i.e.*, inter-chain distance, and the disordered Z-03 nanofilm should have the largest intermolecular “holes”. When a liquid is placed on PFPE-coated silica surface, it has the tendency to penetrate the nanofilm to “see” the substrate instead of fluorinated surface since the substrate has higher surface energy.^{5, 17, 74} The penetration rate is dependent on both the molecular size of the liquid and the size of the intermolecular “holes” within the polymer nanofilm. If the molecular size of the liquid is smaller than the size of the “holes”, it will penetrate the nanofilm quickly and reach an equilibrium contact angle value on the substrate in a short time period. If the molecular size of the liquid is much larger than the size of the “holes”, it will penetrate the nanofilm much more slowly. For Z-03, the size of the intermolecular “holes” is large so that both water and hexadecane penetrate the nanofilm quickly, resulting in a normal wetting behavior with WCA larger than HCA. For Z-tetraol, the size of the intermolecular “holes” is so small that both water and hexadecane cannot penetrate the nano film. As a result, both HCA and WCA are relatively high. For ZDOL, the size of the intermolecular “holes” is appropriately small so that water molecules penetrate the nanofilm quickly while

hexadecane molecules penetrate the nanofilm much more slowly, which renders HCA higher than WCA.

The above-mentioned mechanisms are further supported by the time-dependent contact angle results. As shown in Figure 29, the HCA significantly decreases with time only for ZDOL/Si and doesn't change with time for Z-03/Si and Z-tetraol/Si. The time dependent HCA on ZDOL/Si cannot be explained by the rearrangement of the polymer segments. Thermodynamically, the fluorinated backbone of ZDOL polymer will stay on the top of the nanofilms and the hydroxyl end-groups will stay on the bottom of the nanofilms to minimize the overall interfacial energy for ZDOL/Si sample.¹⁷ After a drop of hexadecane is placed on the surface, the only possible segmental rearrangement is that the hydroxyl end-groups move to the top of the nanofilms. However, since the hydroxyl end-groups “like” the hydrophilic silica substrate more than the hexadecane, there is no driving force for this segmental rearrangement to occur. Moreover, if this segmental rearrangement indeed occurred, we should have observed similar time-dependent HCA for Z-tetraol/Si because Z-tetraol also has hydroxyl end-groups. However, experimental results show that HCA on Z-tetraol/Si does not change with time. Therefore, the observed time-dependent HCA on ZDOL/Si cannot be attributed to the segmental rearrangement. Instead, this can be reasonably explained by the different packing orders and the resulting inter-chain distances of three PFPEs. The inter-chain distance in Z-03 is large so that the “penetration” of hexadecane occurs instantaneously. As a result, no time dependence of HCA was observed for Z-03 sample. For Z-tetraol, the inter-chain distance is so small that no “penetration” can occur and thus no time-dependence of HCA was observed for Z-tetraol sample, either. For ZDOL, the inter-chain distance is appropriately small so that hexadecane molecules penetrate the nanofilm slowly and show clear time-dependence. In contrast, there is no time

dependence in WCA for all three samples as shown in Figure 29. This can be attributed to the fact that the “penetration” of water molecule occurs instantaneously for ZDOL and Z-03 coatings while no “penetration” of water molecule occurs for Z-tetraol coating.

To summarize, as shown in Figure 35, a model has been proposed to describe the “penetration” mechanisms of hexadecane and water at the ZDOL/Si interface, which results in the observed simultaneous oleophobicity/hydrophilicity. After a drop of hexadecane is placed on the ZDOL/Si surface, initially hexadecane molecules “see” a fluorinated surface and therefore show a high HCA in a short time period. Gradually, HCA decreases as the “penetration” proceeds. On the contrary, smaller water penetrates the nanofilm very quickly and reaches the equilibrium value on the substrate almost immediately after a drop of water is placed on the ZDOL/Si surface. As a result, immediately after the contact angle measurement, the static WCA is close to the equilibrium value while the HCA is much higher than the equilibrium value. Therefore, the observed higher HCA (than WCA) is kinetically controlled rather than thermodynamically determined.

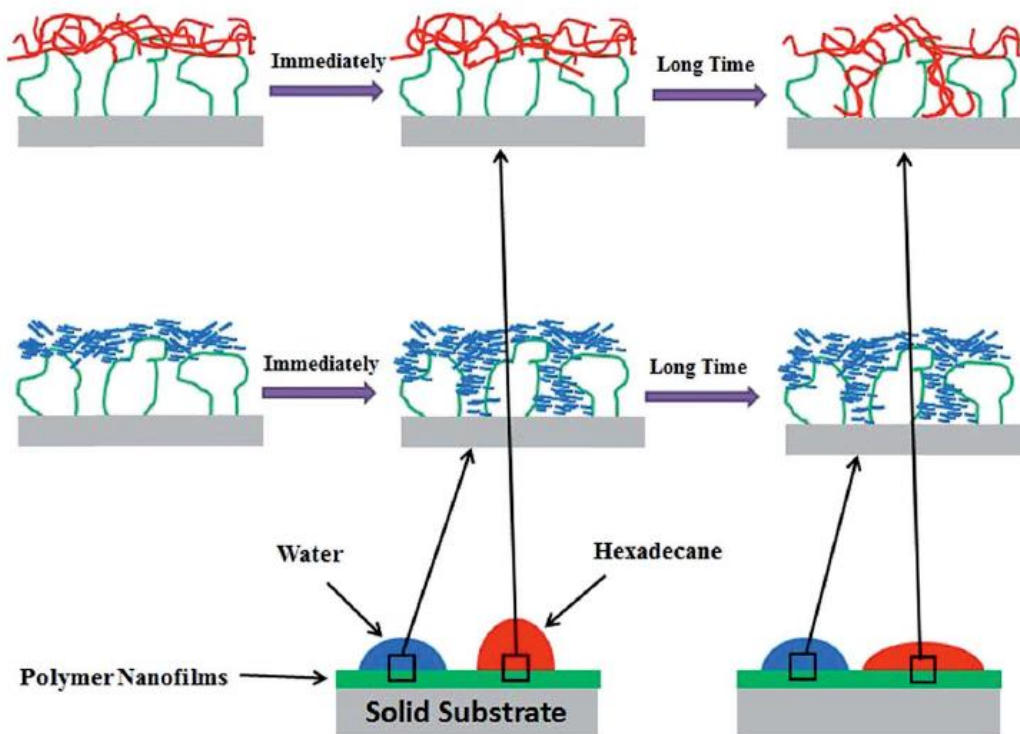


Figure 35. Schematic show of the “penetration” mechanism of water and hexadecane on ZDOL/Si (not shown to scale).

3.5.2 Airborne hydrocarbon contamination and anti-fogging performance

When a cold glass slide meets humid air, water will condense on the glass surface, which could reduce the transmittance of the glass slide.⁷⁸ If the surface is hydrophilic, a water film will be formed on the surface and fogging will not occur. If the surface is hydrophobic, water droplets will be formed on the surface and fogging will occur.¹⁵ For the three PFPE samples, Z-tetraol is the most hydrophobic one and thus it exhibits the worst antifogging performance, regardless of aging time, as shown in Figure 30. On the contrary, the anti-fogging performance of Z-03 and ZDOL samples is good right after sample fabrication and degrades with the aging time. Rangel *et al.* reported that a solid surface exposed to the ambient environment could be contaminated due

to the adsorption of the airborne hydrocarbons.⁷⁹⁻⁸⁰ For the surface with “normal” wetting behavior, OCA is lower than WCA and thus the hydrocarbon contamination will occur easily. As a result, the originally hydrophilic surface becomes more hydrophobic and not anti-fogging anymore. However, for the surfaces with simultaneously oleophobic/hydrophilic behavior, hydrocarbon contamination is expected to be reduced due to the oleophobicity and the long-term antifogging performance should be improved. Indeed, Youngblood and Howarter showed that simultaneously oleophobic/hydrophilic f-PEG is promising for anti-fogging coating.¹¹ More recently, Badyal and *et al.* reported that the solvent-cast copolymer–fluorosurfactant complexes, which show simultaneously oleophobic/hydrophilic behavior, also have excellent antifogging performance.¹⁹ However, there has not been reported whether or not the anti-fogging performance will change with the aging time. Moreover, the relationship between hydrocarbon contamination and the anti-fogging performance has not yet been experimentally demonstrated. The anti-fogging testing and XPS results shown in Figure 30 and Figure 31, respectively, shed the new light to these questions. On the 1st day, both ZDOL and Z-03 have the least airborne hydrocarbon contaminants and show good anti-fogging performance. On the 14th day, Z-03 has significantly more airborne hydrocarbon contaminants than ZDOL and also shows significantly worse anti-fogging performance than ZDOL, which is simultaneously oleophobic/hydrophilic. These results indicate that the simultaneously oleophobic/hydrophilic surfaces do slow down the airborne hydrocarbon contamination and therefore have improved longterm anti-fogging performance (Figure 30 and Figure 31 show that ZDOL and Z-03 have similarly good anti-fogging performance while Z-03 has more airborne hydrocarbon contaminants than ZDOL at day 1. This can be attributed to the fact that the anti-fogging experiments were performed immediately after the samples were fabricated, where both ZDOL and Z-03 were rarely polluted

by the airborne hydrocarbon contaminants. However, the XPS experiments were conducted several hours after the samples were fabricated and it is likely that more airborne hydrocarbon contaminants were adsorbed on Z-03 than on ZDOL during the time period). Moreover, since PFPE ZDOL is an excellent lubricant, which has been utilized in hard disk drive industry and aerospace application,⁸¹ and has very good high-temperature stability,⁸¹ it will provide outstanding long-term reliability in the real-life anti-fogging applications.

3.6 CONCLUSIONS

Both static and time-dependent WCA and HCA results suggested that PFPE polymers with different end-groups interact with the hydrophilic substrates in very different ways, leading to different packing order of polymer chains and thus different inter-chain distances, *i.e.*, the size of the intermolecular “holes”. Only when the size of the intermolecular “holes” is appropriately small, the large oil molecules penetrate the polymer layer slowly while the small water molecules penetrate the polymer layer quickly, resulting in a larger OCA than WCA in a short time period, *i.e.*, simultaneous oleophobicity/hydrophilicity. The XPS and anti-fogging test results demonstrated that simultaneously oleophobic/hydrophilic surfaces effectively reduce the airborne hydrocarbon contamination and therefore have an improved long-term anti-fogging performance.

4.0 FABRICATING NANOMETER-THICK SIMULTANEOUSLY OLEOPHOBIC/HYDROPHILIC COATINGS VIA A COST-EFFECTIVE PHOTOCHEMICAL APPROACH

4.1 CHAPTER PREFACE

Materials contained in this chapter will be submitted as a research article.

List of Authors: Yongjin Wang, Michael Dugan, Brian Urbaniak and Lei Li

Author Contributions: Y.W., and L.L. designed and directed the experiments. Y.W., M.D., and B.U., conducted the experiments. All authors discussed the results. Y.W., and L.L. wrote the manuscript with input from all authors.

4.2 INTRODUCTION

The simultaneously “oleophobic/hydrophilic” coatings, which is less wettable to oil than to water are highly desirable for applications in anti-fogging,^{10-11, 19, 82-83} detergent-free cleaning,^{10-11, 19, 82, 84} water and oil separating^{19, 83} and anti-fouling.⁸⁵⁻⁸⁶ However, this type of coating was rarely reported since most surfaces are more wettable to oil than to water, *i.e.*, water contact angle (WCA) is larger than oil contact angle (OCA), according to previous theoretical and experimental studies.^{6, 18} Our previous studies suggested that the simultaneous oleophobicity/hydrophilicity can be achieved by coating nanometer-thick polymers with perfluorinated backbone and polar end-groups, *e.g.* diolic-perfluoro-poly (oxyethylene-ran-oxymethylene) commercially known as ZDOL, on a hydrophilic substrate.^{17, 87} Based on the experimental results, we proposed that the peculiar wetting behavior results from the attractive interaction between hydroxyl end-groups of ZDOL and polar sites on the hydrophilic substrate, which leads to a nanometer-thick polymer network with the appropriately small intermolecular “holes”, *i.e.*, inter-chain distance. Both water and oil molecules tend to penetrate the network to approach the equilibrium state since the hydrophilic substrate has high surface energy. Water molecules penetrate the nanometer-thick network quickly while oil molecules penetrate the nanometer-thick network very slowly since water molecules are much smaller than oil molecules. As a result, the measured WCA is lower than OCA and therefore the surface shows simultaneous oleophobicity/hydrophilicity.^{17, 87} The proposed model is supported by the fact that all previously reported simultaneously oleophobic/hydrophilic polymer coatings^{8-11, 17} are nanometer-thick perfluorinated polymers with polar end-groups and the substrates utilized accordingly are

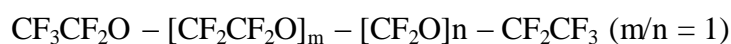
hydrophilic. However these type of polymers are not feasible for real-life applications since it is very expensive to synthesize the polymers with perfluorinated backbone and polar end-groups. The perfluorinated polymers without polar end-groups, *e.g.*, perfluoro-poly(oxyethylene-ran-oxymethylene) commercially known as Z-03, are much more cost-effective. However this type of polymer coating doesn't show the desired simultaneous oleophobicity/hydrophilicity since there is no polar end-groups and therefore no attractive interaction between the polymer and hydrophilic substrates as shown in our previous work.^{17, 87}

In the current paper, we report a UV-induced photochemical approach to fabricate the simultaneously oleophobic/hydrophilic coatings using perfluoropolyethers without polar end-groups, as evidenced by the contact angle testing results. The ellipsometry and X-ray photoelectron spectroscopy (XPS) results indicated that UV irradiation results in the covalent bonding between the polymer backbone and the substrate, which renders the formation of the nanometer-thick polymer network with the appropriately small "holes" and thus makes the coating simultaneously oleophobic/hydrophilic. Moreover, the anti-fogging testing and XPS results showed that such coatings reduce the airborne hydrocarbon contamination and thus have improved long-term anti-fogging performance. Such coatings also had higher detergent-free cleaning capability.

4.3 EXPERIMENTAL SECTION

4.3.1 Materials and sample fabrication

The PFPE polymer with nonpolar CF₃ endgroups, which is commercially known as Z-03 (M_n= 4000 g/mol), was obtained from Solvay Solexis Inc.. The molecular structure of Z-03 is shown below:



2,3-Dihydrodecafluoropentane, which was purchased from Miller Stephenson Chemical Co., was used as a good solvent for Z-03 polymer.^{16-17, 87} All the chemicals were utilized as received. The substrates used in the experiment were silicon wafer with 2 nm native oxide (P/B <100> 1-10 OHM-CM, 279 ± 25 μm), which was obtained from Silicon Quest International, Inc., and 25 x 7 x 51 mm plain glass microscope slides obtained from Fisher Scientific. The nanometer-thick polymer films were fabricated by dip-coating and the detailed procedure was described elsewhere.^{50, 63, 76}

4.3.2 UV treatment

UV treatment was conducted with a BioForce Nanosciences UV/Ozone Procleaner. This cleaner emits a high-intensity UV light with the wavelengths of both 185 nm and 254 nm. All the UV treatment are conducted under near-constant temperature (~ 24°C) and humidity (~ 48%) conditions in ambient air for a desired time period, *i.e.*, 0.5, 1, 2.5, 5, 7.5 and 10 minutes.

4.3.3 Characterizations

4.3.3.1 Contact angle tests

The contact angle tests on various samples were measured using a VCA optima XE (AST Production Inc.) video contact angle system in the ambient environment. Two liquids were used in the contact angle tests: 1) Deionized (DI) water, produced from a Millipore Academic A10 system with total organic carbon below 40 ppb; 2) Hexadecane (anhydrous, $\geq 99\%$), purchased from Sigma-Aldrich. The static contact angle tests were measured immediately after the liquid droplet was deposited and the reported results are the average of three repeats at different locations on the same sample. The time-dependent hexadecane contact angles were measured for the same droplet on the same spot.

4.3.3.2 Ellipsometry

The thickness of nanometer-thick polymer was measured using a J.A. Woollam alpha-SETM Ellipsometer. In the measurement, the bare silica surface was first measured to determine the thickness of native oxides and then the thickness of the PFPE nanofilm was determined by curve-fitting using Cauchy model fitting.^{50, 63, 76}

4.3.3.3 XPS

The chemical structure of the nanometer-thick Z-03 film was characterized using ESCALAB 250 XI (Thermo Scientific) X-ray photoelectron spectroscopy (XPS) system. The monochromatic Al Ka x-ray with a spot size of 200 μm was used as the source to generate spectra in the XPS system. For all the measurement on the non-conductive samples, an electron flood gun was used to neutralize charge. A survey spectrum (5 scans, 150 eV pass energy, 1 eV

step) followed with a high-resolution C1s scan from 270 to 298 binding energy (eV) (20 scans, 50 eV pass energy, 0.1 eV step) were collected for each experiment and the results were analyzed by Thermo Advantage software.

4.3.3.4 Anti-fogging tests

Anti-fogging tests for Z-03/glass samples were conducted by holding the coated glass slides over the boiling water for five seconds and then removed and photographed.^{11, 87}

4.3.3.5 Detergent-free cleaning

Detergent-free cleaning capability was tested by dispensing hexadecane droplets onto Z-03 coated glass slide followed by rinsing with DI water. Oil Red O (Dye content, $\geq 75\%$) purchased from Sigma-Aldrich was added in hexadecane liquid to improve the visual contrast for detergent-free cleaning.¹⁹

4.3.3.6 Mechanical wipe test

The mechanical robustness of Z-03/Silica samples were tested under different wiping conditions: 1) no wiping, 2) light wiping (wipe once and light) and 3) hard wiping (wipe several times and hard). Kimwipes™ Delicate Task Wipers purchased from Fisher Scientific (Catalog No. S47299) were utilized in the mechanical testing. Before and after the tests, the thickness and the chemical compositions of the sample were characterized by ellipsometry and XPS, respectively.

4.4 RESULTS AND DISCUSSIONS

4.4.1 Simultaneous oleophobicity/hydrophilicity:

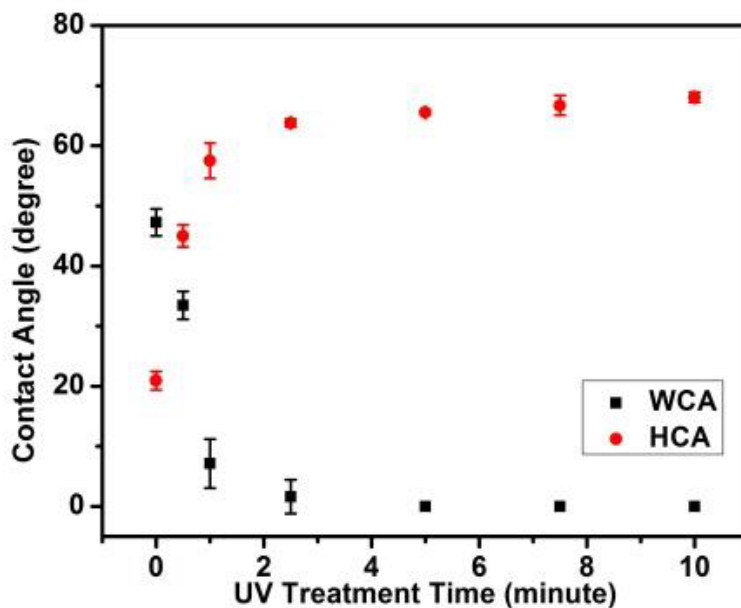
Static hexadecane contact angle (HCA) and WCA for freshly made Z-03 coated silica substrates (Z-03/Silica) with different UV-treatment times are shown in Figure 36a. Z-03/Silica without UV treatment shows a normal wetting behavior: WCA is 47.3° that is higher than HCA (20.9°). On the UV irradiated Z-03/Silica, WCA gradually decreases while HCA gradually increases with the UV time. When the UV time is larger than 5 minutes, both WCA and HCA level off and HCA ($\sim 68^\circ$) is significantly higher than WCA ($\sim 0^\circ$), i.e., the UV irradiation makes the Z-03/Silica coating simultaneously oleophobic/hydrophilic. Model oils other than hexadecane show the similar oleophobic/hydrophilic behavior on the UV-irradiated Z-03/silica samples. (See Table 9)

Table 9. Contact angles on the Z-03/Silica

	Non-treated	10 min-UV treated
Hexadecane	22.7 ± 0.8	66.3 ± 0.1
Dodecane	10.3 ± 1.1	59.2 ± 0.8
Hexane	0	48.9 ± 1.1
Water	38.6 ± 0.8	0

To uncover the underlying mechanisms behind the UV irradiation, the thickness of Z-03 after the solvent washing, which is defined as the bonded thickness^{50, 63, 76}, was measured by ellipsometry. For Z-03/Silica without UV treatment, it is well known that all of the Z-03

molecules can be washed off the silica substrate, *i.e.*, the bonded thickness is ~ 0 nm since Z-03 does not have polar end-groups and thus there is no attractive interaction between the polymer and the substrate.^{50, 63, 76} As shown in Figure 36b, here we also observed that the bonded thickness of Z-03 without any UV irradiation was close to 0 nm. However, the bonded thickness increased with the UV time and became 0.73 nm after 10 minutes' UV treatment, which suggests that the UV irradiation induces the bonding between the polymer and the substrate. As shown in Figure 36c, XPS results also showed that the percentage of fluorine element of the bonded Z-03/Silica (after solvent wash) increases with the UV time, which is consistent with ellipsometry results on the bonded thickness.



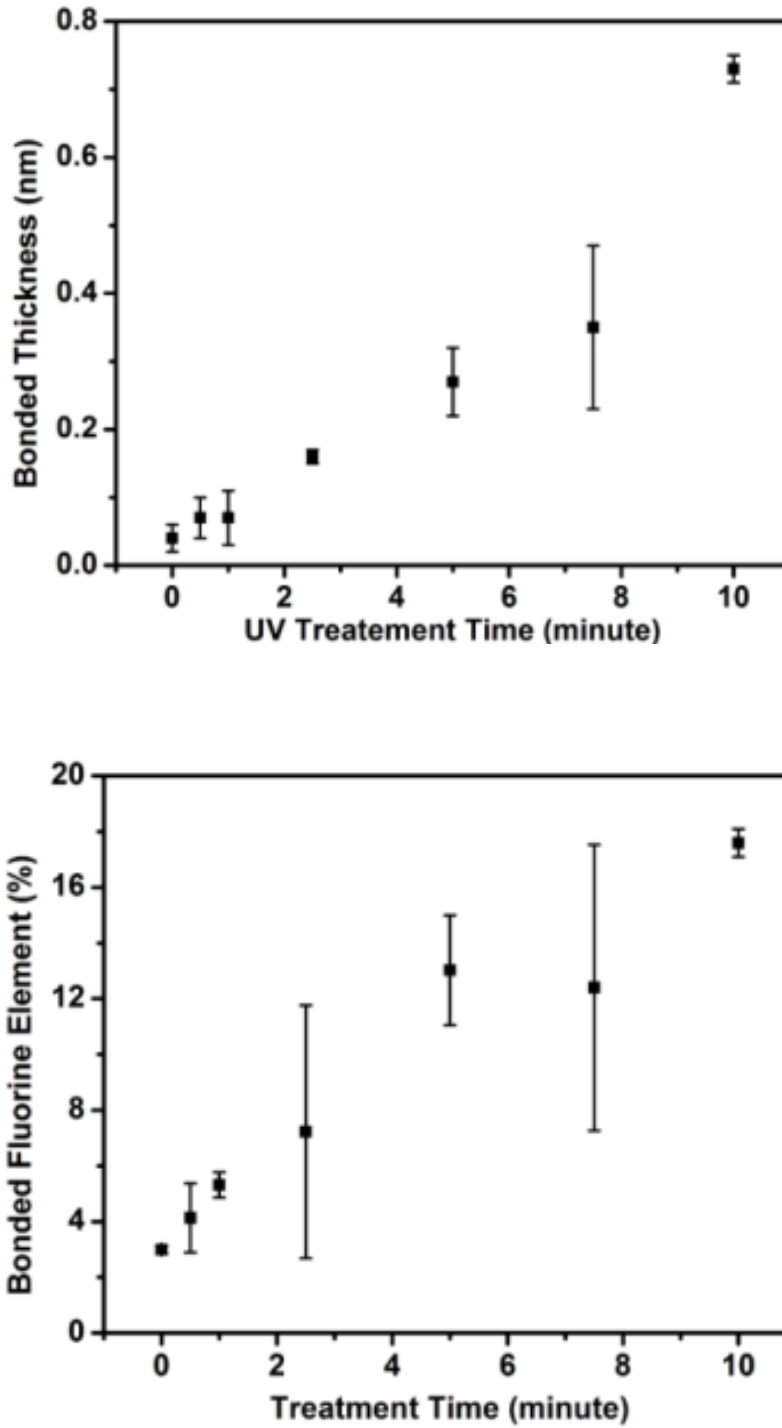


Figure 36. (a) (top) HCA and WCA on Z-03/Silica as a function of UV treatment time. (b) (middle) Bonded thickness as a function of UV time. (c) (bottom) Fluorine element percentage of Z-03/Silica (bonded) as a function of UV exposure time.

Why does the covalently bonding between Z-03 polymer and the silica substrate render the surface simultaneously oleophobic/hydrophilic? As proposed in our previous study,^{17, 87} the simultaneous oleophobicity/hydrophilicity results from the appropriate size of the “holes”, *i.e.*, inter-chain distance, which results from the attractive interaction between the polymer nanofilm and the substrate and thus the ordered packing of polymer chains. The peculiar wetting behavior is kinetic in nature: larger oil molecules are unable to penetrate through the nanometer-thick polymer as quickly as smaller water molecules, which makes oil molecules stay on top of the perfluorinated backbone of polymers while water molecules stay on the hydrophilic substrate. As shown in previous studies,^{17, 87} the attractive interaction can be realized by the hydrogen bonding between the hydroxyl end-groups and the polar sites on the hydrophilic substrate. Therefore, for Z-03 that does not have the polar end-groups, the simultaneous oleophobicity/hydrophilicity was not observed. As shown in Figure 37, UV irradiation created the covalent bonding between Z-03 and the substrate and therefore results in a more ordered packing structure of polymer segments on the silica substrate, leading to smaller inter-chain distance within the polymer network. As a result, water molecules can go through the PFPE nanofilm quickly while hexadecane molecules go through it very slowly, *i.e.*, HCA is much higher than WCA and the simultaneous oleophobicity/hydrophilicity is observed.

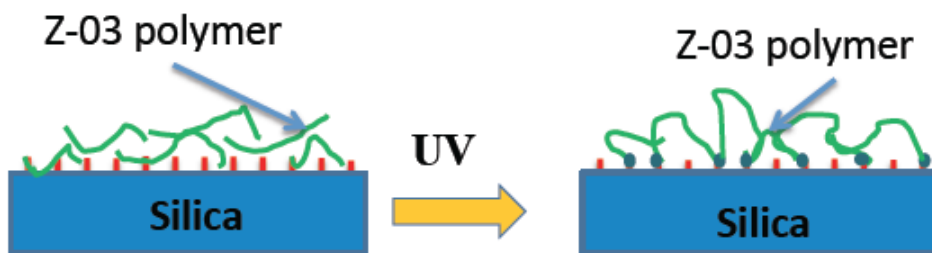


Figure 37. Schematic bonding models of Z-03 polymers on silica substrate during UV irradiation (not shown to scale)

Our CA, ellipsometry and XPS results suggested that UV irradiation created covalent bonding between Z-03 and the substrate and therefore results in a more ordered packing structure of polymer segments on the silica substrate, leading to smaller inter-chain distance within the polymer network. As a result, water molecules can penetrate the PFPE nanofilm quickly while hexadecane molecules penetrate it very slowly, *i.e.*, the simultaneous oleophobic/hydrophilic is observed. If the hypothesis is true, it is expected that the HCA will decrease with time for the same drop of hexadecane deposited on the UV-treated Z-03/Silica sample while HCA will stay the same for the non-treated Z-03/Silica samples. Indeed, as shown in Figure 38, HCA didn't change with time up to 400 minutes for non-treated Z-03/Silica while HCA decreased from 68.2° to 34.8° during the same time period for UV-treated sample. Since hexadecane doesn't evaporate during the experiment,⁸²⁻⁸³ the decrease of HCA is attributed to the penetration of hexadecane through UV-treated Z-03 nanofilms, as described in our hypothesis.

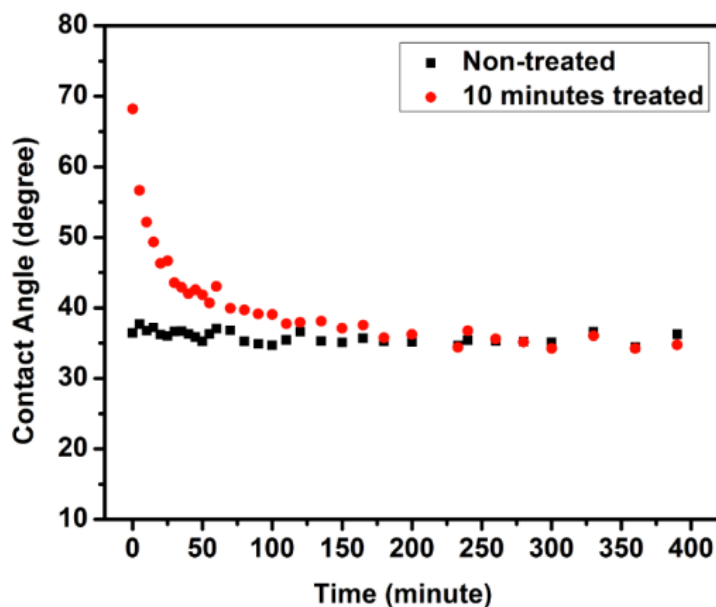
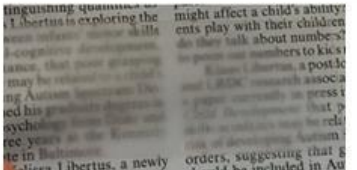


Figure 38. HCA change with time on Z-03/Silica wafer without UV treatment and with 10 minutes' UV treatment.

4.4.2 Anti-fogging:

Currently, the state-of-the-art anti-fogging coatings are hydrophilic since it is believed that no fogging will occur if water forms a uniform transparent film on the surface, *i.e.*, water wets the surface well.¹⁵ However, this type of anti-fogging surface can be easily “damaged” when exposed to the ambient due to the airborne hydrocarbon contaminations, which makes the surface hydrophobic and no longer anti-fogging.⁸⁰ Since the simultaneously oleophobic/hydrophilic coatings allow water to easily wet the surface due to their “hydrophilicity” and are expected to reduce the hydrocarbon contamination due to their “oleophobicity”, they are expected to have better long-term anti-fogging performance.¹¹ To test the anti-fogging performance of UV-treated Z-03/Silica, the anti-fogging tests were conducted on 10-minute UV treated Z-03/glass with non-treated Z-03/glass as control. As shown in Figure 39a right after sample fabrication, both non-treated and UV-treated sample showed similarly good anti-fogging performance. However, after 14 days’ exposure to the ambient environment, UV-treated Z-03/glass sample showed a better anti-fogging performance than non-treated sample.

	Non treated	10-minute treated
Fresh		
Aged		

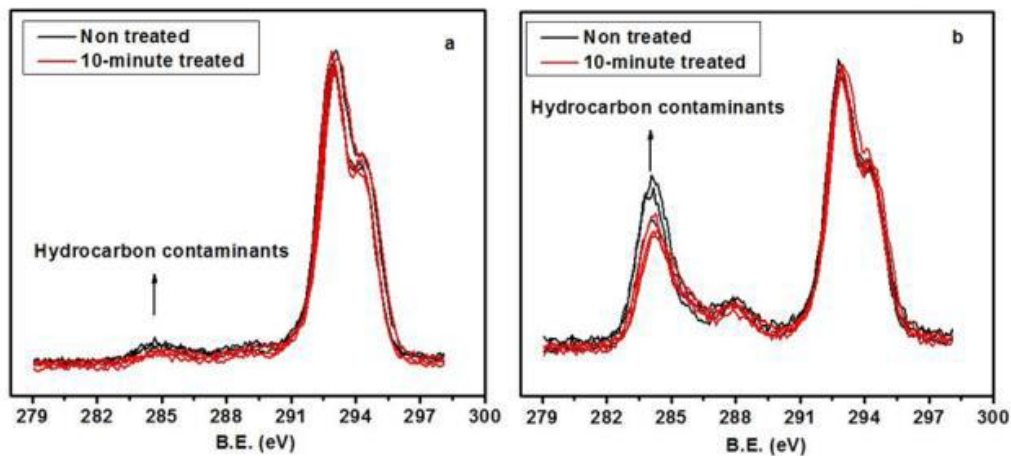


Figure 39. (a) (top) Anti-fogging testing results of Z-03 polymer coated glass slides without and with 10-minutes UV irradiation. (b) (bottom) XPS C1s spectra of Z-03 polymer coated glass slides without and with 10-minutes UV irradiation: Fresh (left) and Aged (right). (The time period between the fresh and aged samples is 14 days)

To uncover the underlying mechanisms governing the improved anti-fogging performance of UV-treated Z-03/glass after aging, the XPS C1s spectra (three repeats) has been collected for both UV-treated and non-treated Z-03/glass samples and are shown in Figure 39b. In the XPS spectra, the peaks between 282 to 290 eV are assigned to hydrocarbon constituents, which are attributed to airborne hydrocarbon contamination, and the peaks at 295 eV and 293 eV are assigned to fluorocarbon constituents, which are attributed to Z-03 polymers according to previous reports.⁷⁰ As shown in Figure 39b, the fresh non-treated and UV-treated samples have similarly small amount of hydrocarbon contamination while the amount of hydrocarbon contaminants increased after 14-day exposure to the ambient for both samples. However, there is clearly much more hydrocarbon contaminants on the non-treated sample than on UV-treated sample. The results suggested that UV-induced simultaneous oleophobicity/hydrophilicity slows down the airborne hydrocarbon contaminating and therefore improves the long-term anti-fogging performance.

4.4.3 Detergent-free cleaning:

Moreover, it is expected that the simultaneously oleophobic/hydrophilic surface can be cleaned with just water, *i.e.*, no detergent is needed because the surface is more wettable to water than to oil and therefore water can easily replace the oil-type contaminants at the liquid-solid interface and flushes the oil away from the surface.¹⁰⁻¹¹ This type of surface will largely reduce the consumption of detergents which will protect the environment from the detergent-related pollution and conserve the valuable energy resource, e. g. petroleum that is the raw material of detergent. Here we testified the hypothesis on UV-treated Z-03/glass sample and the results are shown in Figure 40. Our results show that the hexadecane droplets, which are dyed with Oil Red O to enhance the contrast, deposited on 10-minute UV-treated Z-03/glass sample can be washed away simply by water rinsing. However, for non-treated Z-03/glass sample, the same hexadecane droplets cannot be removed from the surface by water rinsing.

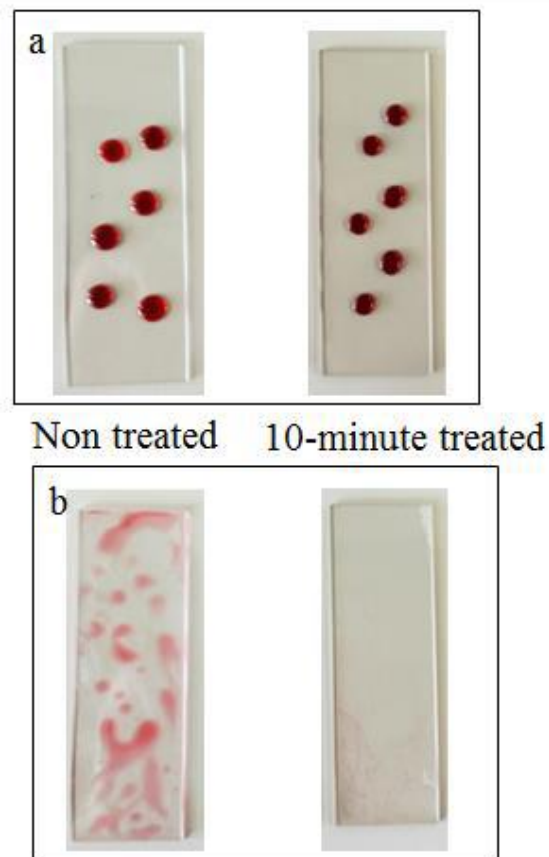


Figure 40. Detergent-free cleaning testing results of Z-03 polymer coated glass slides without and with 10-minutes UV irradiation: (a) with hexadecane on the surfaces. (b) after rinse with DI water

4.4.4 Mechanical robustness:

The nanometer-thick PFPE is transparent and the previous study also showed that PFPE is an excellent lubricant with good thermal stability⁴⁶. To investigate the mechanical robustness of Z-03/Silica, the samples were tested under different conditions. As shown in Figure 41 a and b, there is no detectable change in both thickness and chemical composition of Z-03 before and after wiping, indicating that Z-03 will provide excellent long-term reliability in many real-life applications.

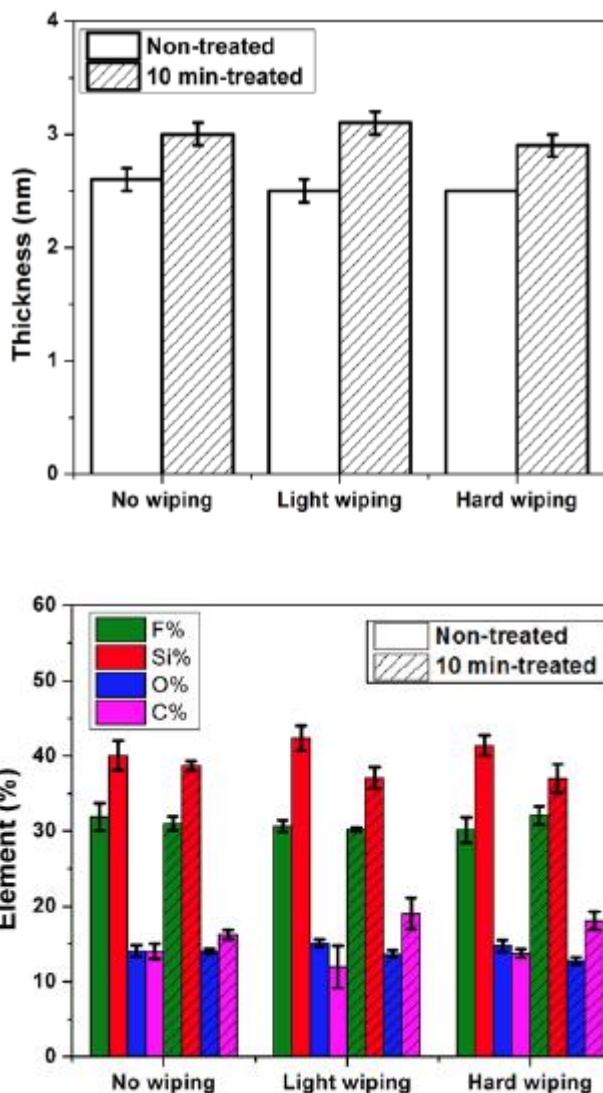


Figure 41. (a) (top) Thickness of Z-03 before and after wiping. (b) (bottom) XPS results of Z-03 before and after wiping.

4.5 CONCLUSIONS

In conclusion, we have developed an UV-based photochemical approach to fabricate nanometer-thick simultaneously oleophobic/hydrophilic coatings using cost-effective perfluoropolyethers

(PFPEs) without polar end-groups. The contact angle, ellipsometry and XPS results indicated that the UV irradiation results in the covalent bonding between the polymer and the substrate, which renders more ordered packing of polymer chains and thus the appropriately small inter-chain distance. As a result, the small water molecules penetrate the polymer network much more quickly than large oil molecules, *i.e.*, the coating shows the simultaneous oleophobicity/hydrophilicity. Moreover, we also demonstrated that this nanometer-thick simultaneously oleophobic/hydrophilic coating has improved long-term anti-fogging performance and detergent-free cleaning capability and is mechanically robust. The photochemical approach established here potentially can be applied on many other polymers and greatly accelerate the development and application of simultaneously oleophobic/hydrophilic coatings.

5.0 THE ROLE OF THE INTERFACIAL INTERACTION IN THE SLOW RELAXATION OF NANOMETER-THICK POLYMER MELTS

5.1 CHAPTER PREFACE

Materials contained in this chapter were published as a research article in *Langmuir*; figures used in this chapter have been reprinted with permission from: *Langmuir*, **2012**, 28.(14), 6151-6156 (listed as reference 17 in the bibliography section). Copyright © 2012 American Chemical Society.

List of Authors: Yongjin Wang, Jianing Sun, and Lei Li

Author Contributions: Y.W., and L.L. designed and directed the experiments. Y.W., and J.S. conducted the experiments. All authors discussed the results. L.L. wrote the manuscript with input from all authors.

5.2 INTRODUCTION

With the fast growth of nanotechnology, nanoscale polymers at interfaces have found many important applications, such as photoresist nanofilms for nanoimprint lithography (NIL), nanocomposites for biomaterials, sensors, batteries, and lubrication nanofilms for microelectromechanical systems (MEMSs)/nanoelectromechanical systems (NEMSs) and hard disk drives (HDDs).⁸⁸⁻⁹³ Because the fundamental interactions at the nanoscale and interfaces are different from those in the bulk, “bulk rules” may not hold anymore in these applications and “nanorules” need to be discovered. In bulk polymer glasses, the structural relaxation is slow because the large-scale molecular motion is frozen. This slow relaxation results in a change of certain properties with aging time and thus limits the lifetime of engineering plastics in many applications.⁹⁴⁻⁹⁵ In bulk polymer melts, the large-scale molecular motion is activated so that the relaxation of polymer chains is fast.⁹⁶ Therefore, the potential change of material properties with time due to the relaxation in a long run is not a concern.

However, for polymer melts in nanofilms on a substrate, the polymer–substrate interaction becomes more dominating with a decrease of the film thickness and the relaxation of polymer molecules could be very different from that in the bulk.⁸⁸ First, the thermodynamic driving force of the relaxation could be very different since the fundamental interaction changes.⁸⁹ Second, the kinetics of the relaxation at the polymer–solid interface could be much slower.^{89, 91, 97-100}

Van Alsten et al. reported that the apparent dynamic viscosity of polydimethylsiloxane (PDMS) melts confined between two mica surfaces is significantly higher than that in the bulk

and there is a liquid-to-solid transition, represented by a yielding stress, when the thickness is lower than a critical value.⁹⁷ They speculated that the solid like behavior results from a glass-like state, where chains are trapped in a non-equilibrium state, that of metastable liquid with a longer relaxation time than the experimental time scale, e.g., hours.⁹⁷ Luengo et al. also observed an effective viscosity enhancement in polybutadiene thin films confined between mica surfaces and a liquid-to-solid transition when the film is thinner than a critical value.⁸⁹ Cho et al. measured the dielectric response of cis-polyisoprene films “sandwiched” between mica surfaces and found that the relaxation becomes much slower than that in bulk liquids.⁹⁸ They attributed the slow relaxation to both spatial confinement and attractive polymer–substrate interaction (adsorption).⁹⁸ The two factors, spatial confinement and interfacial interaction, cannot be distinguished here due to the nature of the experimental setup. Meanwhile, molecular dynamic (MD) simulations have shown inconsistent results regarding the role of spatial confinement and interfacial interaction.^{91, 99-100} Aoyagi et al. found that the relaxation time of polymer melts near the solid wall increases drastically and attributed the slower relaxation to both spatial confinement and polymer–solid attraction.⁹⁹ Borodin et al. observed that the conformational and structural relaxations of poly(ethylene oxide) (PEO) are substantially slower and more heterogeneous near TiO₂ surfaces than those in the bulk and attributed the slowing to interfacial interaction rather than spatial confinement.¹⁰⁰ Later, Vogel showed that PEO exhibits substantially slower rotational and translational dynamics close to the TiO₂ solid interfaces and the substantial slowing is essentially restricted to the layer next to the solid interface, indicating that the changes in PEO dynamics are dominated by interfacial interaction rather than spatial confinement.⁹¹ The slow relaxation renders the property change of the polymer nanofilms with time a serious concern, similar to the structural relaxation of polymer glasses in the bulk. Indeed,

Zhang et al. reported¹⁰¹ that the frictional force of a 2 nm PFPE-coated substrate continues to increase with aging time and the change is up to 70% after 72 h, indicating the slow relaxation impacts the tribology properties significantly.

To be able to optimize the long-term performance of nanoscale polymer melts at interfaces, it is critical for us to understand the governing mechanism(s) of the relaxation. The polymer–solid interaction at the interface, which does not have a bulk counterpart, could play a key role.⁸⁸⁻⁸⁹ However, as discussed above, previous research did not demonstrate that the effect of the interfacial interaction unambiguously. Moreover, there has not been any work that illustrates how exactly the interfacial interaction will affect the thermodynamic driving force and the kinetics of the relaxation.

In the current paper, the relaxation of nanometer-thick perfluoropolyether melts on a silicon wafer has been investigated by water contact angle measurement. The polymer–substrate interactions have been systematically changed by tailoring the polymer structure to clarify the effect of the interfacial interaction. The experimental results show that: (1) when there is attractive interaction at the interface, some polymers are anchored to the substrate and others are free, (2) the attractive interfacial interaction drives the free polymers to relax at the interface, and (3) the relaxation is much slower than in the bulk, which has been attributed to the low mobility of the anchored polymer chains and the motional cooperativity between anchored and free polymer chains in the nanometer-thick films.

5.3 EXPERIMENTAL SECTION

5.3.1 Materials

Two PFPE liquids, commercially known as ZDOL ($M_n = 4000$ g/mol, radius of gyration (R_g) of 1.5 nm^{102}) and Z-03 ($M_n = 4000$ g/mol, $R_g = 1.5 \text{ nm}^{103}$), were purchased from Solvay Solexis Inc. and utilized as received. As shown in Figure 42, ZDOL has polar hydroxyl end groups while Z-03 has nonpolar CF_3 end groups and their backbones are identical

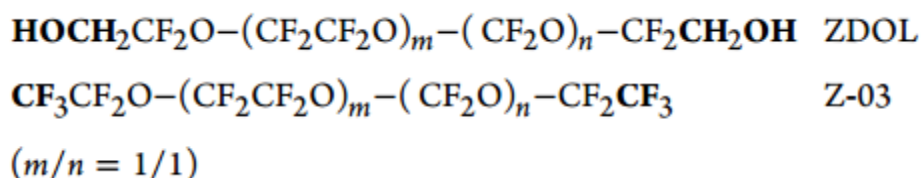


Figure 42. The Chemical Structures of ZDOL and Z-03 polymers

2,3-Dihydrodecafluoropentane, a good solvent for PFPEs, was purchased from Miller Stephenson Chemical Co. and used as received. Deionized (DI) water was produced from a Millipore Academic A10 system with total organic carbon below 40 ppb. The Si wafers covered with 2 nm native oxides (P/B 100 1-10 OHM-CM, $279 \pm 25 \mu\text{m}$, water contact angle $23.7 \pm 2.2^\circ$) were purchased from Silicon Quest International, Inc. and rinsed with 2,3-dihydrodecafluoropentane thoroughly before use. The interactions between PFPE polymers and polar solid surfaces have been extensively studied.⁴⁴⁻⁴⁸ ZDOL can form hydrogen bonds with the polar surface via hydroxyl end groups, and its backbone has no attractive interaction with the polar surface.⁴⁴⁻⁴⁷ Z-03 cannot form hydrogen bonds with the polar surface at all because their end groups are nonpolar. The very different interactions between the two PFPEs and the polar

surface are evidenced by the fact that all of the Z-03 polymers can be completely washed off the polar surface with a good solvent, e.g., 2,3-dihydrodecafluoropentane, while only part of the ZDOL polymers can be washed off the polar surface.⁴⁴⁻⁴⁸ On the silica surface, ZDOL and Z-03 are ideal model polymers for us to study the effect of interfacial interaction on the relaxation of polymer melts in nanofilms since they have similar chain structures while their interactions with the silica surface are very different.

5.3.2 Fabrication of nanometer-thick films

“ZDOL 1.2 nm” and “Z-03 1.3 nm” films were coated on Si wafers by dip-coating with 2,3-dihydrodecafluoropentane as the solvent on the basis of a previously established “dip–withdraw” procedure.⁴⁶⁻⁴⁸ The ZDOL molecules that form hydrogen bonds with the silica surface and cannot be washed off the surface with 2,3-dihydrodecafluoropentane are defined as bonded ZDOL. The ZDOL molecules that do not form hydrogen bonds and can be washed off the silica surface are defined as mobile ZDOLs.⁴⁴⁻⁴⁸ ZDOL 1.2 nm films coated via the normal dip–withdraw procedure⁴⁶⁻⁴⁸ contain both bonded and mobile molecules. For the “ZDOL100% bonded 0.8 nm” sample, a concentrated solution (3 wt %) was utilized and the Si wafer was kept in the solution for 1 h before it was pulled off the solution at a velocity of 1 mm/s. The sample was then washed twice with 2,3-dihydrodecafluoropentane immediately after the dip-coating. Thus, the ZDOLs remaining on the silica surface are the molecules that cannot be washed off, and they are 100% bonded by definition.

5.3.3 Characterization

5.3.3.1 Spectroscopic ellipsometer

The thickness of the polymer films was measured using a J.A. Woollam Co. M-2000 spectroscopic ellipsometer. The bare silicon substrate was first measured to determine the thickness of native oxides.⁶⁵ To avoid thickness and index correlation between the very thin polymer films,⁶⁶ we fixed their optical constants using a Cauchy dispersion equation:

$$n(\lambda) = 1.30 + \frac{0.00250}{\lambda^2}$$

Here n is the refractive index and λ is the wavelength in micrometers.

5.3.3.2 Scanning probe microscope (SPM)

The topography and the roughness (R_a) of the polymer films were characterized using a Veeco MultiMode V scanning probe microscope (SPM), under tapping mode with a scanning area of $2 \mu\text{m} \times 2 \mu\text{m}$, by taking the average of four repeated measurements at different locations.

5.3.3.3 XPS results

The chemical structure of the polymer thin film was characterized by X-ray photoelectron spectroscopy (XPS) analysis, which was performed using a Thermo Scientific K-Alpha XPS system with a monochromated Al $K\alpha$ source. A spot size of $400 \mu\text{m}$ was used for all experiments, and the charge compensation in the system was provided by a low-energy electron source and Ar^+ ions. An initial survey spectrum consisting of one scan was collected on each sample, using a pass energy of 200 eV. High-resolution scans around the C1s peak were collected using 25

scans and a pass energy of 50 eV. For high-resolution scans, only the low-energy electron source was used for charge compensation.

5.3.3.4 Water contact angle

The relaxation of polymer nanofilms on the silica surface was characterized by water contact angle measurement, a technique that has been rarely utilized⁴⁸ to study the relaxation of polymer thin films. While the polymer chains in the nanofilms undergo relaxation, e.g., the rearrangement of chain segments, the hydrophilic segments at the polymer–air interface migrate toward the polymer–substrate interface, and this will significantly impact the measured water contact angle.^{48, 104}

Previously, a study¹⁰⁴ on self-assembled alkanethiol monolayers containing mixtures of hydroxyl and methyl groups at their air/monolayer interface has indicated that the water contact angle testing is capable of capturing the rearrangement of the alkanethiol molecules in the monolayer. As shown before⁴⁸ and further supported in the current study, this relatively simple technique is very powerful in “capturing” the relaxation of polymer nanofilms when the migration of hydrophilic segments is involved in the relaxation process. The water contact angle (θ) measurement was conducted with a VCA optima XE video contact angle system at 24 °C and 48% relative humidity. A droplet with a volume of 2 μ L was formed at the end of the needle and then lowered carefully until it touched the sample surface. Afterward the needle was withdrawn immediately so that the droplet was left on the sample surface. Then the image of the droplet was taken with a charge-coupled device (CCD) camera right away, and the static contact angle was calculated automatically by the VCA software. It took about 45s to complete the whole measurement process. The measurement was conducted right after sample fabrication and

continued at different spots on the sample surface in the following two weeks to capture the relaxation process. Each single measurement was repeated three times.

5.4 RESULTS

As shown in Table 10, both the Ra values and the thicknesses of all three PFPE samples, ZDOL 1.2 nm, Z-03 1.3 nm, and ZDOL 100% bonded 0.8 nm, are comparable.

Table 10. Roughness and PFPE Thickness

sample name	Ra (nm)	PFPE total thickness (nm)	PFPE bonded thickness (nm)
Z-03 1.3 nm	0.18	1.3	0
ZDOL 1.2 nm	0.17	1.2	0.1 (right after fabrication) 0.5 (after two weeks of aging)
ZDOL 100% bonded 0.8 nm	0.17	0.8	0.8

Since different roughnesses of nanofilms could impact the coverage on the substrate and thus impact the water contact angle data, the similar Ra values exclude the possible contact angle changes resulting from the difference in roughness. The atomic force microscopy (AFM) image of the Z-03 1.3 nm sample is shown in Figure 43 as an example.

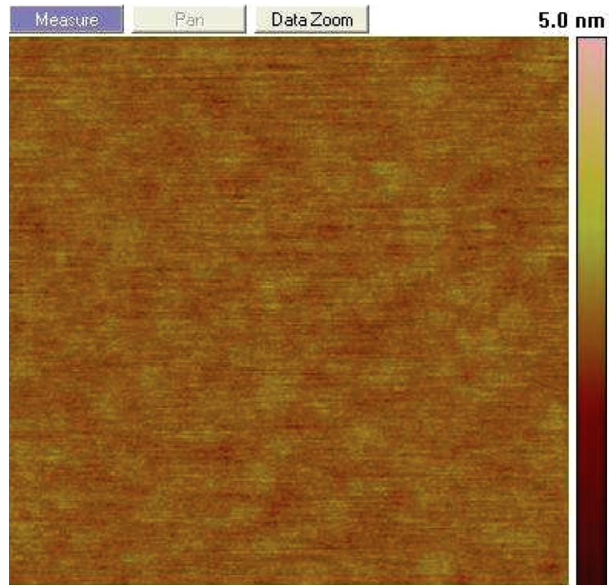


Figure 43. AFM image of the Z-03 1.3 nm/Si wafer.

The XPS C1s spectra of both ZDOL and Z-03 samples are similar. The result of a 1.8 nm ZDOL sample is shown in Figure 44, as an example. The peaks at 295.26 and 293.75 eV are assigned to $-\text{OCF}_2\text{O}-$ and $-\text{OCF}_2\text{CF}_2\text{O}-$, respectively.⁷⁰ The small peaks at 287.09 and 284.96 eV are assigned to the contaminants, which is consistent with previous reports.⁷⁰

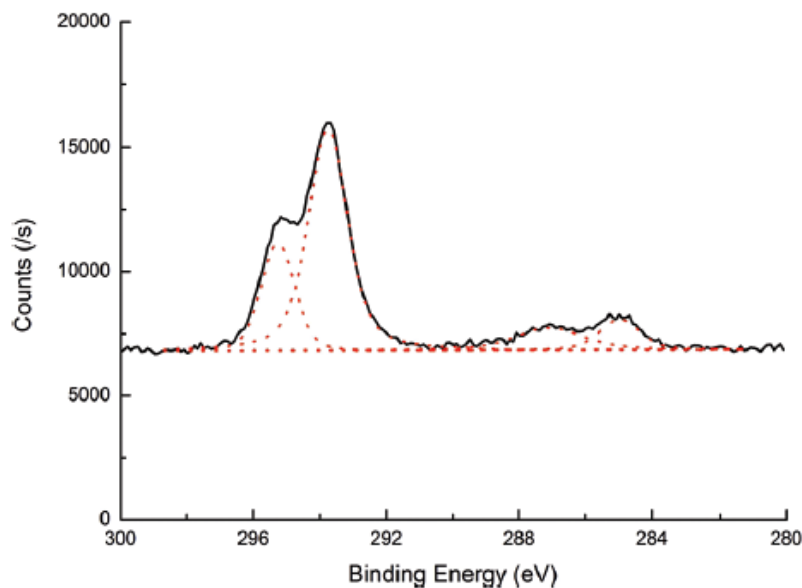


Figure 44. XPS C1s spectra (solid line) and curve-fitting (dotted line) results of a 1.8 nm ZDOL/Si samples.

As shown in Figure 45 $\cos \theta$ of the ZDOL 1.2 nm sample continues to decrease (relax) with aging time up to two weeks.

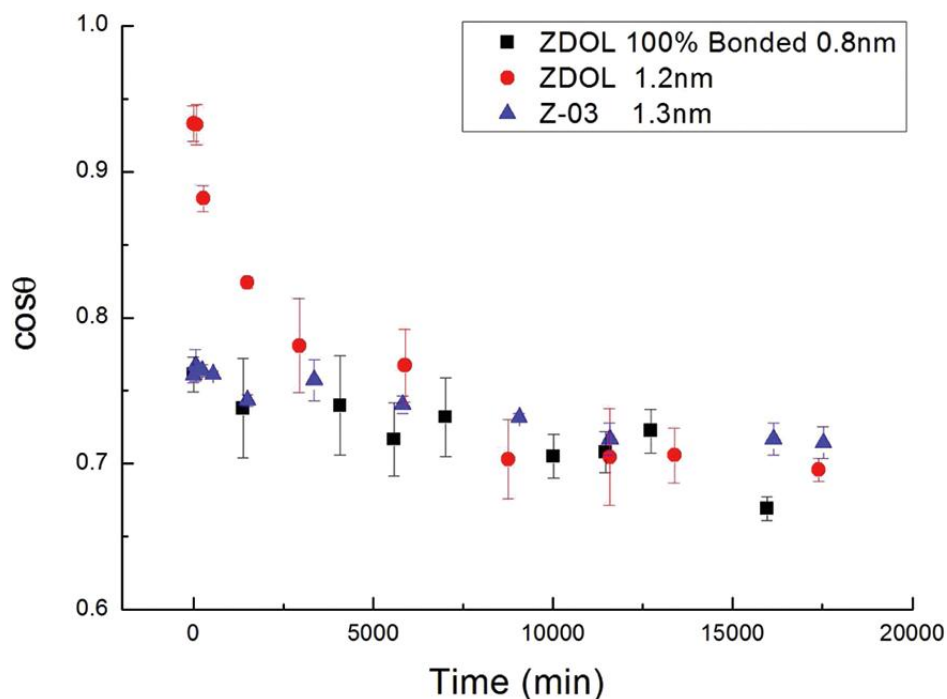


Figure 45. Water contact angle of PFPE-coated Si wafers vs aging time.

However, the $\cos \theta$ values of the Z-03 1.3 nm and ZDOL 100% bonded 0.8 nm samples show much smaller changes with the aging time. This small change in $\cos \theta$ for Z-03 and 100% bonded ZDOL is attributed to the adsorption of adventitious hydrocarbons. When a more hydrophobic silicon wafer (N/Sb 100 0.007–0.02 OHM-CM, $525 \pm 15 \mu\text{m}$, 285 nm wet thermal oxides, water contact angle $43.0 \pm 1.0^\circ$, purchased from MEMC), which is also more resistant to the contamination of adventitious hydrocarbons due to its lower surface energy, is utilized in the same experiment, the $\cos \theta$ values for both the Z-03 and 100% bonded ZDOL samples do not change with aging time, as shown in Figure 46 and Figure 47.

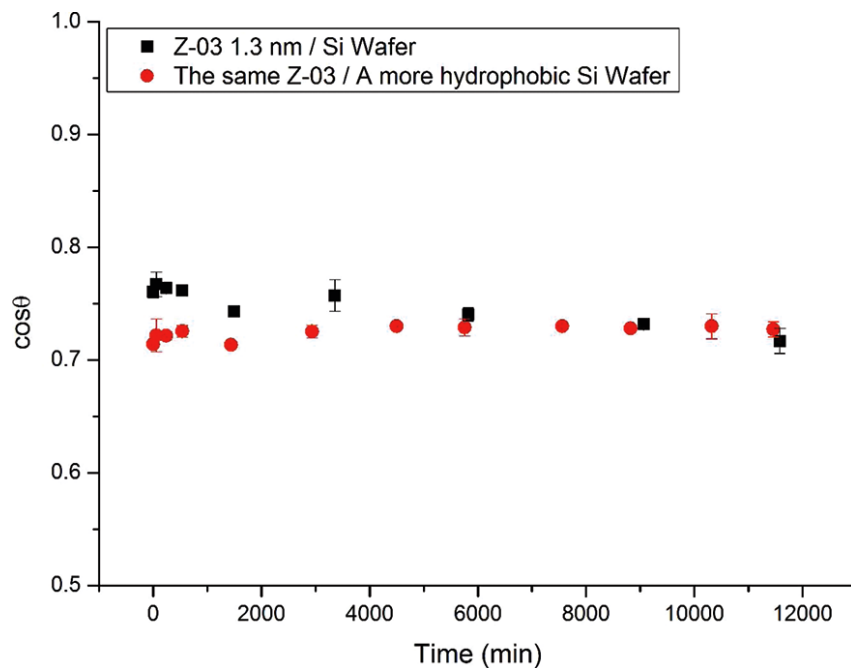


Figure 46. Water contact angle of Z-03 on different Si wafers.

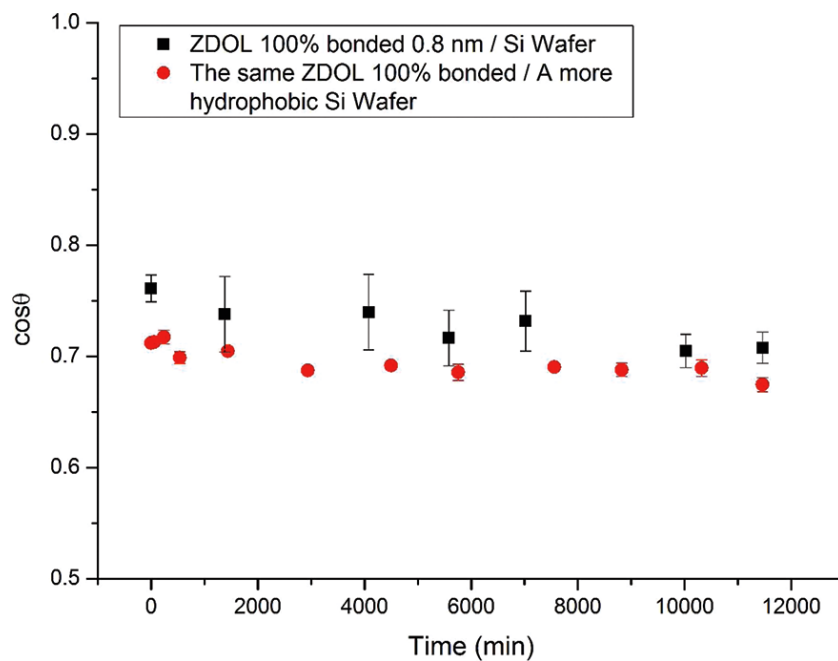


Figure 47. Water contact angle of 100% bonded ZDOL on different Si wafers.

Furthermore, as shown in Figure 50 the relaxation of ZDOL 1.2 nm can be fitted with a modified Kohlrausch–Williams–Watts (KWW) function⁴⁸ as follows:

$$\cos\theta(t) = \cos\theta_e + (\cos\theta_0 - \cos\theta_e) * \exp[-(\frac{t}{\tau})^\beta]$$

Here t is the aging time, $\cos\theta_e$ is the equilibrium water contact angle, $\cos\theta_0$ is the initial water contact angle, τ is the relaxation time constant indicating how fast the system approaches equilibrium, and β is the stretch factor characterizing the non-exponentially of the relaxation process.

As shown in Figure 48, the change in $\cos\theta$ of a bare Si wafer, which is attributed to the adsorption of adventitious hydrocarbons, shows very different time dependence from that of ZDOL/Si. For ZDOL/Si, the change can be fitted with a KWW function: bigger change initially and much smaller change in the later stage. While for bare Si wafer, the change is gradual and much less significant. This difference becomes more evident when the data taken in the first 24 hours is carefully checked. As shown in Figure 49. There is little change of $\cos\theta$ for bare Si while there is significant change for ZDOL/Si. Therefore, the observed change of $\cos\theta$ of ZDOL/Si is attributed to the relaxation of ZDOL molecules rather than the adsorption of adventitious hydrocarbons.

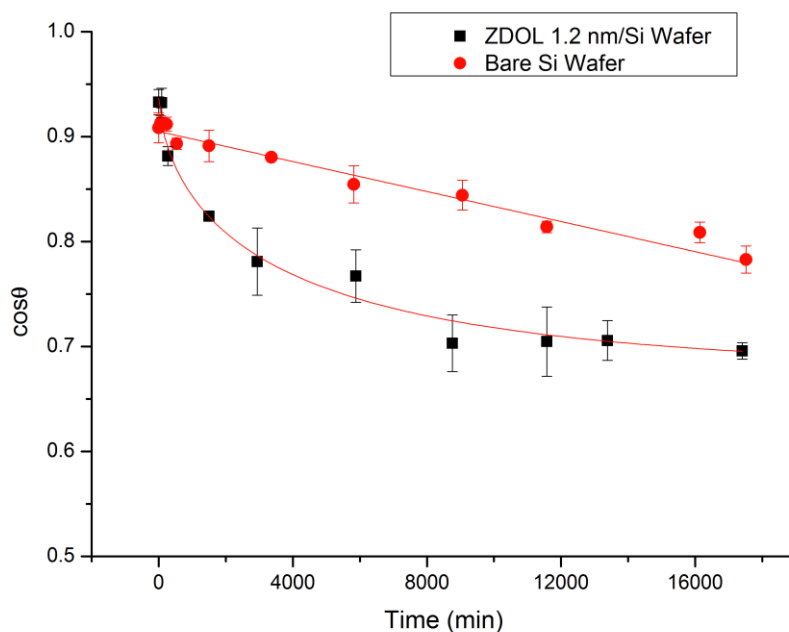


Figure 48. $\cos\theta$ (θ is water contact angle) of ZDOL/Si and bare Si with aging time.

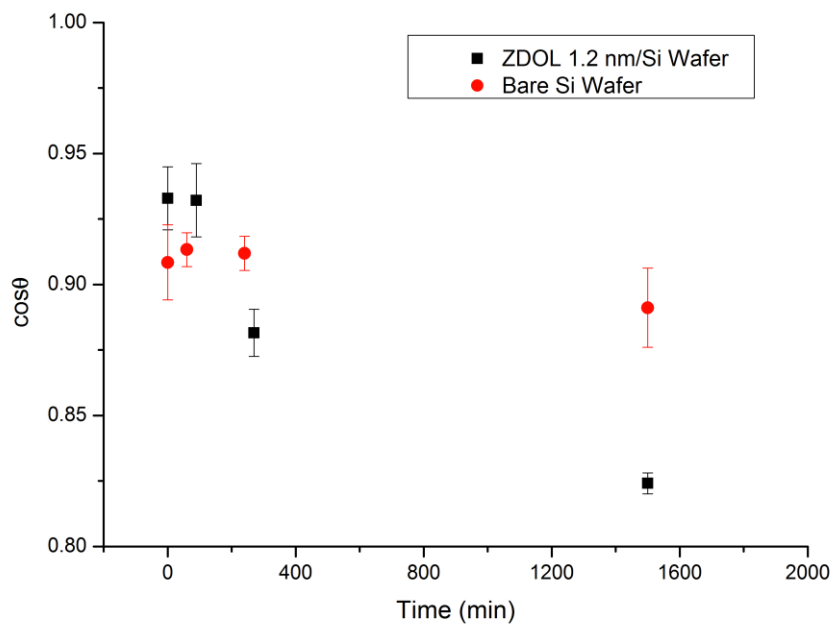


Figure 49. $\cos\theta$ (θ is water contact angle) of ZDOL/Si and bare Si with aging time (Zoom: initial 24 hours).

By comparing the change in $\cos \theta$ with time of ZDOL/Si to that of a bare Si wafer, it is evident that the observed KWW behavior of ZDOL/Si is due to the relaxation of ZDOL molecules rather than the possible adsorption of adventitious hydrocarbons. On the basis of the fitting, β is 0.60 and τ is 2.3×10^5 s. The terminal relaxation time constant of the ZDOL polymer chains in the bulk is on the order of 10^{-5} s,¹⁰⁵ and the observed relaxation here is 10 orders of magnitude slower. The data indicate that ZDOL, which is a polymer melt in the bulk, behaves like a polymer glass in nanofilms on an attractive solid substrate, and the relaxation mechanism here is very different from that in the bulk. Interestingly, Z-03 1.3 nm, as well as ZDOL 100% bonded 0.8 nm, shows little relaxation behavior. As shown in Table 10, it was also found that the thickness of bonded ZDOL for ZDOL 1.2 nm increases from 0.1 nm right after dip-coating to 0.5 nm after the relaxation, indicating some mobile ZDOL molecules form hydrogen bonds with the silica surface and become bonded during the relaxation.

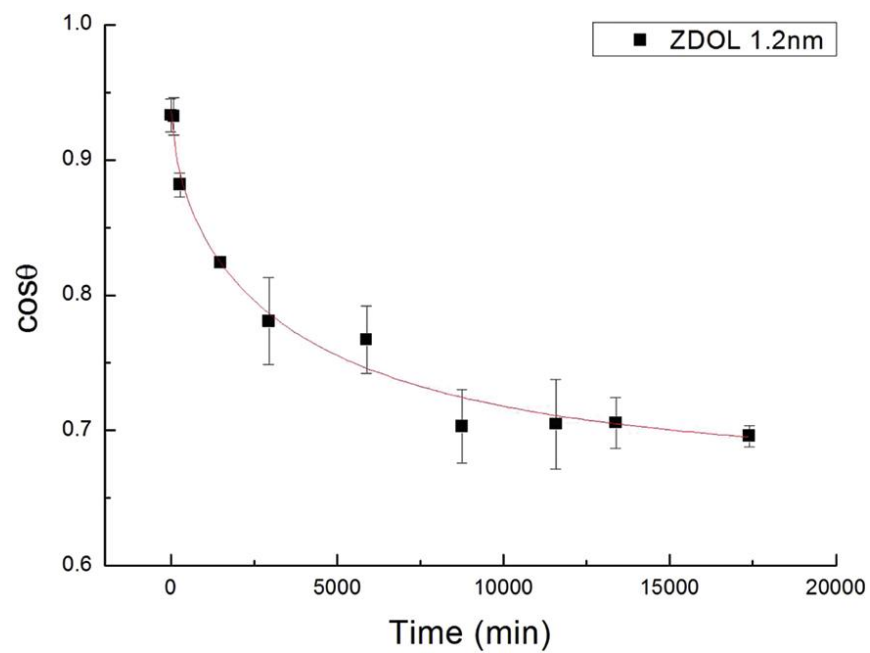


Figure 50. KWW fitting result of the relaxation of ZDOL 1.2 nm ($\cos \theta_0 = 0.93$, $\cos \theta_e = 0.67$, $\tau = 3871$ min, $\beta = 0.60$).

5.5 DISCUSSION

5.5.1 Thermodynamic Driving Force of the Relaxation.

Thermodynamically, what is the driving force for the observed relaxation of ZDOL 1.2 nm? Three observed experimental results are (1) ZDOL 1.2 nm relaxes significantly, while Z-03 1.3 nm does not, suggesting the hydroxyl end groups in ZDOL are critical since that is the only difference between ZDOL and Z-03, (2) ZDOL 100% bonded 0.8 nm does not relax, indicating mobile ZDOL molecules are relaxing species in the ZDOL 1.2 nm sample, and (3) the thickness of bonded ZDOL of ZDOL 1.2 nm increases during the relaxation, indicating mobile ZDOL molecules form hydrogen bonds with the polar sites on the silica surface and become bonded during the relaxation. These results indicate that the relaxation is driven by the attractive interfacial interaction between the polar sites on the silica surface and the hydroxyl end groups of the mobile ZDOL molecules. Our previous study⁴⁶ showed that there are two ways for ZDOL molecules to be coated on a polar surface during the dip-withdraw process, as shown in Figure 51.

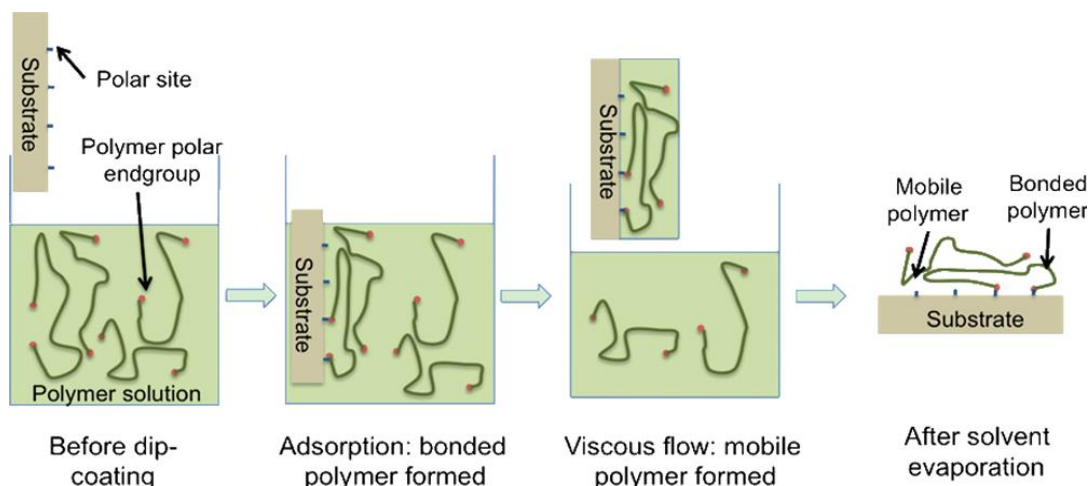


Figure 51. Formation mechanism of ZDOL polymers on the Si wafer during dip-coating (Schematic not shown to scale)

The first one is the solution adsorption in which ZDOL molecules form hydrogen bonds with the polar sites on the surface in solution and become bonded when the solid substrate is immersed into the solution during the dip-coating. The second one is the “viscous flow” mechanism in which a layer of ZDOL solution is forced to go with the solid substrate when the substrate is pulled out of the solution (note that the bonded molecules are already on the surface at this time), simply because the viscosity of the solution is not zero. Via this mechanism, ZDOL molecules become the mobile portion after the solvent evaporates rapidly. Therefore, the mobile molecules are “forced” to stay on the solid surface, and they are not in the equilibrium state. Although it has not been extensively studied, this phenomenon has been reported for polymer nanofilms fabricated by both dip-coating and spin-coating.^{46, 48, 51} To lower the surface energy and approach equilibrium, the hydroxyl end groups of the mobile ZDOL molecules, at the molecular level, tend to move toward the polar sites on the silica surface to form hydrogen bonds. Our previous study⁴⁷ did show that formation of hydrogen bonds between ZDOL and a polar surface will lower the surface energy, possibly due to the fact that the polar hydroxyl groups move away from the polymer/air interface and the polar sites on the silica surface are “covered”

via hydrogen bonding. Therefore, the phenomenon is relaxation in nature at the molecular level, and macroscopically, the measured water contact angle “relaxes” accordingly. With this mechanism, it is easy to understand why the simple water contact angle testing is capable of capturing the relaxation process. This proposed mechanism is shown schematically in Figure 52. Since Z-03 does not have polar end groups, there is no driving force for the relaxation to occur. For 100% bonded ZDOL, all the hydroxyl groups have formed hydrogen bonds with the polar sites on the silica surface, and there is no driving force for the relaxation to occur either. Previously, the change of water contact angle (surface energy) of ZDOL nanofilms with the aging time has been reported,⁴⁴ and the phenomenon has been described as “bonding”. In the current study, the contact angle change has been attributed to the relaxation of mobile polymer molecules, and this mechanism is demonstrated unambiguously by comparing ZDOL to Z-03 and ZDOL 100% bonded samples.

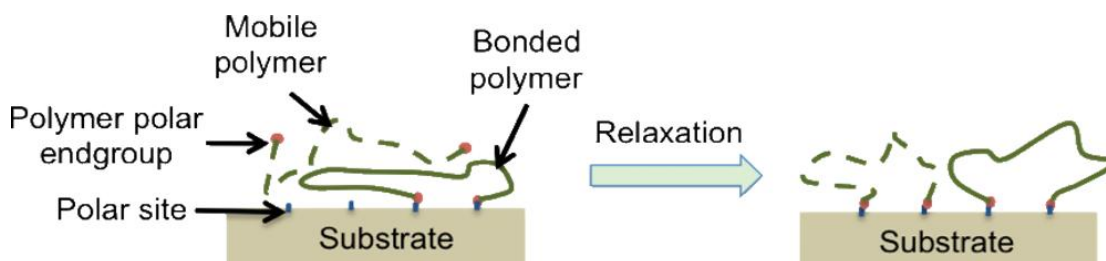


Figure 52. Proposed relaxation mechanism of ZDOL polymers on the Si wafer (schematic not shown to scale).

5.5.2 Kinetics of the Relaxation.

What makes the observed relaxation of ZDOL so slow? Formation of the hydrogen bond between mobile ZDOL molecules and the silica surface must contain two steps. The first step is

the “diffusion” of the end groups of the mobile ZDOL toward the polar sites on the silica surface, and the second step is the “reaction” step in which hydrogen bonding occurs. In physisorption in solution, polymer adsorption is essentially diffusion limited.¹⁰⁶ In our case where there is no solvent present; the diffusion should be even slower and dominate the overall kinetics. Therefore, the slow relaxation should be the result of the slow diffusion of the end groups. Since the end groups are chemically linked to the polymer backbone, other segments (or even the entire polymer chain) of the mobile ZDOL molecule must be involved in the diffusion at the molecular level. Therefore, the slow relaxation indicates that the mobility of the polymer segments (or the entire chain) is low. Can this be explained by previously proposed “spatial confinement” and/or “interfacial interaction” mechanisms? First, the possible effect of the spatial confinement is discussed here. For liquid thin films confined between two solid surfaces, the lower mobility has been explained by the argument¹⁰⁷⁻¹⁰⁸ that the translational entropy available to the molecules under spatial confinement decreases to the point at which it becomes thermodynamically favorable for them to condense as a solid. However, in the current study, ZDOL molecules stay on one solid substrate and there is another ZDOL–air interface that should minimize the entropy loss effect.¹⁰⁹ Therefore, the experimental data cannot be explained by spatial confinement. Second, the possible effect of interfacial interaction is discussed. As described in last section, the relaxing species are mobile ZDOL molecules, rather than bonded ZDOL molecules, and they are not anchored to the solid surface. Therefore, the interfacial interaction (surface adsorption) should not have a direct impact on the observed relaxation. An alternative mechanism, other than spatial confinement and surface adsorption, is proposed here to explain the observed slow relaxation. In ZDOL nanofilms on the silica surface, there are bonded and mobile molecules. The bonded molecules are anchored to the surface by hydrogen bonding, and they have very low

mobility. Since some of the polar sites on the silica surface are blocked by the bonded ZDOL molecules, the mobile ZDOL molecules need the cooperative motion from the bonded ZDOL molecules to “deliver” the end groups to the silica surface (see Figure 52). Because the bonded ZDOL molecules have very low mobility, the overall relaxation rate is limited by this slow step. Therefore, the observed relaxation is very slow, and the interfacial interaction has an indirect effect here. Although this mechanism requires further verification, it does emphasize the importance of the heterogeneity at the polymer–substrate interface and the motional cooperativity in the nanofilms, which has not been presented before.

It is evident that the molecular-level motion behind the observed “contact angle relaxation” is slow. The remaining question is the length scale of the molecular-level motion. Generally, for a polymer, the length scale of the molecular motion can range from very localized motion (such as bond rotation) to segmental motion that involves tens to hundreds of atoms to the entire chain’s motion. The molecular motions of the bonded and mobile ZDOL molecules are discussed separately here. For the bonded ZDOL molecules, the current research suggests that the slow motion, whatever the length scale involved, limits the overall relaxation rate. Torkelson et al.¹¹⁰ found that the rate of structural relaxation of poly(methyl methacrylate) nanofilms on a silica substrate decreases significantly, indicating that the very localized motion (such as bond rotation) is slowed dramatically by the interfacial attraction. The reported increase of the glass transition temperature (T_g) of the supported polymer nanofilms at an attractive polymer–substrate interface¹¹¹⁻¹¹² suggests that the segmental mobility of the polymer molecules is reduced by the interfacial attraction. Scarpulla and Mate¹¹³ reported that the viscosity of the supported PFPE nanofilms is much higher than the bulk value when there is an attractive interfacial interaction, indicating that the entire chain’s mobility is reduced. Therefore, the

mobility at all length scales should be significantly reduced for bonded ZDOL molecules. However, it is highly unlikely that the very localized motion is responsible for the observed relaxation process since the localized bond rotation cannot produce enough “space” to assist the motion of the mobile ZDOL molecules. Meanwhile, the motion of the entire chain is also not likely due to the “anchoring” of both chain ends. As a result, the segmental motion is likely the dominating motion mode for the bonded ZDOL during the relaxation. For mobile ZDOL molecules, the very localized bond rotation should not contribute to the relaxation since this type of motion cannot make the end groups of ZDOL move from the polymer–air to the polymer–silica interface. The entire chain’s motion is likely to be responsible for the observed relaxation if we consider the distance that the end groups have to travel during the relaxation. However, we cannot completely exclude the possibility that the segmental motion is responsible for the relaxation since it is still possible that end groups migrate to the silica surface via a series of cooperative segmental motions without the entire chain involved. Further research on the effect of the temperature and molecular weight, especially when the bonded and mobile ZDOL molecules are decoupled, is needed to clarify the issues.

5.6 CONCLUSION

Contact angle testing on nanometer-thick polymer films shows that the interfacial interaction plays a critical role in the relaxation of the nanoscale polymers on solid substrates. On the one hand, the attractive interfacial interaction is the driving force of the relaxation, during which the end groups of the mobile polymers move from the polymer–air interface to the polymer–substrate interface. On the other hand, the attractive interfacial interaction anchors some of the polymers to the surface and lowers these bonded polymers' mobility greatly. Due to the motional cooperativity between bonded and mobile polymers during the relaxation, the movement of the mobile polymers is slowed significantly by the anchored polymers. As a result, the relaxation of the polymer melt nanofilms becomes very slow.

6.0 SUMMARY & OUTLOOK

6.1 SUMMARY

In the current thesis, the mechanism of simultaneously oleophobic/hydrophilic polymer nano-coatings has been studied and the potential application of the coating in detergent-free cleaning and anti-fogging has been investigated. The key findings are summarized as shown below:

6.1.1 The mechanism of simultaneous oleophobicity/hydrophilicity

It was found experimentally that the HCA on a nanometer-thick amphiphilic perfluoropolyether (PFPE) coated Si wafer, which is more wettable to water than to oil, decreases with time significantly. The change of HCA could be related to the slow relaxation of polymer nanofilm. The results suggest that the previously reported surprising behaviors of some surfaces, which show higher HCA than WCA, are kinetically controlled. By comparing the PFPEs and substrates with different structures, we have proposed that the interaction between the nanometer-thick polymer and the substrate is the key to the appropriate size of the intermolecular “hole” in the polymer layer, which in turn determines the kinetics of the penetration of water and hexadecane. Only when the “hole” size is appropriately small, the large oil molecules penetrate the polymer

layer slowly while the small water molecules penetrate the polymer layer quickly, resulting in a larger OCA than WCA in a short time period, i.e., simultaneous oleophobicity/hydrophilicity.

6.1.2 The applications of simultaneous oleophobicity/hydrophilicity

Simultaneously oleophobic/hydrophilic coatings are highly desirable in many important applications, *e.g.*, anti-fogging, oil-water separation and detergent-free cleaning. The effect of simultaneous hydrophilicity/oleophobicity on the long-term anti-fogging capability has been studied by XPS and the anti-fogging tests in the thesis. The results indicated that the unique simultaneous hydrophilicity/oleophobicity reduces the airborne hydrocarbon contamination and therefore improves the long-term anti-fogging performance. Moreover, we have demonstrated that the simultaneous hydrophilic/oleophobic PFPE coating can be cleaned with just water and no detergent is needed because the surface is more wettable to water than to oil and therefore water can easily replace the oil-type contaminants at the liquid-solid interface and flushes the oil away from the surface.

6.1.3 The photochemical approach of simultaneous oleophobic/hydrophilic substrates

We have developed an UV-based photochemical approach to fabricate nanometer-thick simultaneously oleophobic/hydrophilic coatings using cost-effective perfluoropolyethers (PFPEs) without polar end-groups. The contact angle, ellipsometry and XPS results indicated that the UV irradiation results in the covalent bonding between the polymer and the substrate, which renders more ordered packing of polymer chains and thus the appropriately small inter-chain distance.

As a result, the small water molecules penetrate the polymer network much more quickly than large oil molecules, *i.e.*, the coating shows the simultaneous oleophobicity/hydrophilicity. Moreover, we also demonstrated that this nanometer-thick simultaneously oleophobic/hydrophilic coating has improved long-term anti-fogging performance and detergent-free cleaning capability and is mechanically robust. The photochemical approach established here potentially can be applied on many other polymers and greatly accelerate the development and application of simultaneously oleophobic/hydrophilic coatings.

6.2 OUTLOOK

6.2.1 Clarify the effect of “hole” on simultaneous oleophobic/hydrophilic substrates

The size of the nanoscale “hole” is determined by the packing density of the amphiphilic polymers and can be related to the mass density of the nanofilm. Our results suggested that Z-tetraol has a highly ordered packing structure and have the smallest size of “hole”; Zdol has an ordered packing structure and has an appropriate size of “hole”; Z-03 has a disordered packing structure and has the biggest size of “hole”. However, no direct evidence of the size of each type of “hole” was provided in current work. Other techniques, such as AFM/STM and X-ray Reflectivity (XRR) need to be investigated determine the size of the “hole”.

6.2.2 Optimize the polymer to achieve a better application performance

In this thesis, we have showed that the simultaneously oleophobic/hydrophilic coating can improve the anti-fogging and detergent-free cleaning performance. In the future, more work should be done to tailor the structure of polymers and substrates to optimize the packing structure of polymers and thus further improve the performance of the simultaneously oleophobic/hydrophilic coatings. Moreover, Non-fluorinated materials should be investigated to reduce the cost of the coatings.

APPENDIX A

PUBLICATIONS

1. Wang, Y.; Knapp, J.; Legere, A.; Raney, J.; Li, L., Effect of End-Groups on Simultaneous Oleophobicity/Hydrophilicity and Anti-Fogging Performance of Nanometer-Thick Perfluoropolyethers (Pfpes) RSC Advances **2015**, 5 30570-30576.
2. Z Li*, Y Wang*, A Kozbial, G Shenoy, F Zhou, R McGinley, P Ireland, B ..., Effect of airborne contaminants on the wettability of supported graphene and graphite, Nature materials **2013** 12 (10), 925-931 (*These authors contributed equally)
3. Y Wang, J Sun, L Li, What Is the Role of the Interfacial Interaction in the Slow Relaxation of Nanometer-Thick Polymer Melts on a Solid Surface? Langmuir **2012** 28 (14), 6151-6156
4. Y Wang, KT Williams, L Li, Understanding the Mechanism of Anomalous Viscosity–Molecular Weight Relationships of Diolic Perfluoropoly (Oxyethylene-ranoxymethylene):What is Missing in the Debye–Bueche Model? Macromolecular Chemistry and Physics **2011** 212 (24), 2685-2690

5. X Gong, S Frankert, Y Wang, L Li, Thickness-dependent molecular arrangement and topography of ultrathin ionic liquid films on a silica surface, *Chemical Communications* **2013** 49 (71), 7803-7805
6. A Kozbial, Z Li, S Iasella, A Taylor, B Morganstein, Y Wang, J Sun *et al.* Lubricating graphene with a nanometer-thick perfluoropolyether. *Thin Solid Films* **2013** 549, 299-305.
7. L Li, Y Wang, C Gallaschun, T Risch, J Sun, Why can a nanometer-thick polymer coated surface be more wettable to water than to oil? *J. Mater. Chem.* **2012** 22 (33), 16719-16722
8. A Kozbial, Z Li, J Sun, X Gong, F Zhou, Y Wang, H Xu, H Liu, and L Li. Understanding the intrinsic water wettability of graphite. *Carbon* **2014** 74, 218-225.

APPENDIX B

LIST OF ABBREVIATIONS

Table 11. List of abbreviations

AFM	Atomic force microscopy	PEG	Polyethylene glycol
CCD	Charge-coupled device	PEO	Poly(ethylene oxide)
DI	Deionized	PFPE	Perfluoropolyether
HCA	Hexadecane contact angle	PTFE	Poly (tetrafluoro- ethylene)
HDDs	Hard disk drives	SAMs	Self-assembly monolayers
KWW	Kohlrausch–Williams–Watts	SPM	Scanning probe microscope
MD	Molecular dynamic	TGA	Thermogravimetric analysis
MEMSs	Microelectromechanical systems	UV	Ultraviolet
NEMSs	Nanoelectromechanical systems	WCA	Water contact angle
OCA	Oil contact angle	XPS	X-ray photoelectron spectroscopy

BIBLIOGRAPHY

- (1) Owens, D. K. W., R. C., Estimation of the Surface Free Energy of Polymers. *Journal of Applied Polymer Science* **1969**, 13, 1741.
- (2) Li, D.; Neumann, A., Contact Angles on Hydrophobic Solid Surfaces and Their Interpretation. *Journal of colloid and interface science* **1992**, 148, 190-200.
- (3) Good, R. J., Contact Angle, Wetting, and Adhesion: A Critical Review. *Journal of adhesion science and technology* **1992**, 6, 1269-1302.
- (4) Kloubek, J., Development of Methods for Surface Free Energy Determination Using Contact Angles of Liquids on Solids. *Advances in colloid and interface science* **1992**, 38, 99-142.
- (5) Tavana, H.; Neumann, A., Recent Progress in the Determination of Solid Surface Tensions from Contact Angles. *Advances in colloid and interface science* **2007**, 132, 1-32.
- (6) Shafrin, E. G.; Zisman, W. A. *Upper Limits for the Contact Angles of Liquids on Solids*; DTIC Document: **1963**.
- (7) Extrand, C.; Kumagai, Y., An Experimental Study of Contact Angle Hysteresis. *Journal of Colloid and interface Science* **1997**, 191, 378-383.
- (8) Hutton, S.; Crowther, J.; Badyal, J., Complexation of Fluorosurfactants to Functionalized Solid Surfaces: Smart Behavior. *Chemistry of materials* **2000**, 12, 2282-2286.
- (9) Lampitt, R.; Crowther, J.; Badyal, J., Switching Liquid Repellent Surfaces. *The Journal of Physical Chemistry B* **2000**, 104, 10329-10331.
- (10) Howarter, J. A.; Youngblood, J. P., Self - Cleaning and Anti - Fog Surfaces Via Stimuli - Responsive Polymer Brushes. *Advanced materials* **2007**, 19, 3838-3843.
- (11) Howarter, J. A.; Youngblood, J. P., Self - Cleaning and Next Generation Anti - Fog Surfaces and Coatings. *Macromolecular Rapid Communications* **2008**, 29, 455-466.

- (12) Howarter, J. A.; Youngblood, J. P., Amphiphile Grafted Membranes for the Separation of Oil-in-Water Dispersions. *Journal of colloid and interface science* **2009**, 329, 127-132.
- (13) Yang, J.; Zhang, Z.; Xu, X.; Zhu, X.; Men, X.; Zhou, X., Superhydrophilic–Superoleophobic Coatings. *Journal of Materials Chemistry* **2012**, 22, 2834-2837.
- (14) Chevallier, P.; Turgeon, S.; Sarra-Bournet, C.; Turcotte, R.; Laroche, G. t., Characterization of Multilayer Anti-Fog Coatings. *ACS Applied Materials & Interfaces* **2011**, 3, 750-758.
- (15) Briscoe, B.; Galvin, K., The Effect of Surface Fog on the Transmittance of Light. *Solar Energy* **1991**, 46, 191-197.
- (16) Wang, Y.; Sun, J.; Li, L., What Is the Role of the Interfacial Interaction in the Slow Relaxation of Nanometer-Thick Polymer Melts on a Solid Surface? *Langmuir* **2012**, 28, 6151-6156.
- (17) Li, L.; Wang, Y.; Gallaschun, C.; Risch, T.; Sun, J., Why Can a Nanometer-Thick Polymer Coated Surface Be More Wettable to Water Than to Oil? *Journal of Materials Chemistry* **2012**, 22, 16719-16722.
- (18) Young, T., An Essay on the Cohesion of Fluids. *Philosophical Transactions of the Royal Society of London* **1805**, 65-87.
- (19) Brown, P.; Atkinson, O.; Badyal, J., Ultrafast Oleophobic–Hydrophilic Switching Surfaces for Antifogging, Self-Cleaning, and Oil–Water Separation. *ACS applied materials & interfaces* **2014**, 6, 7504-7511.
- (20) Shimomura, H.; Gemici, Z.; Cohen, R. E.; Rubner, M. F., Layer-by-Layer-Assembled High-Performance Broadband Antireflection Coatings. *ACS applied materials & interfaces* **2010**, 2, 813-820.
- (21) Zhang, L.; Li, Y.; Sun, J.; Shen, J., Mechanically Stable Antireflection and Antifogging Coatings Fabricated by the Layer-by-Layer Deposition Process and Postcalcination. *Langmuir* **2008**, 24, 10851-10857.
- (22) Cebeci, F. Ç.; Wu, Z.; Zhai, L.; Cohen, R. E.; Rubner, M. F., Nanoporosity-Driven Superhydrophilicity: A Means to Create Multifunctional Antifogging Coatings. *Langmuir* **2006**, 22, 2856-2862.
- (23) Lai, Y.; Tang, Y.; Gong, J.; Gong, D.; Chi, L.; Lin, C.; Chen, Z., Transparent Superhydrophobic/Superhydrophilic TiO₂-Based Coatings for Self-Cleaning and Anti-Fogging. *Journal of Materials Chemistry* **2012**, 22, 7420-7426.

- (24) Saperstein, D. D.; Lin, L. J., Improved Surface Adhesion and Coverage of Perfluoropolyether Lubricants Following Far-Uv Irradiation. *Langmuir* **1990**, 6, 1522-1524.
- (25) Vurens, G.; Gudeman, C.; Lin, L.; Foster, J., Mechanism of Ultraviolet and Electron Bonding of Perfluoropolyethers. *Langmuir* **1992**, 8, 1165-1169.
- (26) Vurens, G.; Gudeman, C.; Lin, L.; Foster, J., The Mechanism of Ultraviolet Bonding of Perfluoropolyether Lubricants [Used in Magnetic Recording]. *Magnetics, IEEE Transactions on* **1993**, 29, 282-285.
- (27) Tian, H.; Matsudaira, T., Tribological Characteristics of Liquid Lubricant on Magnetic Disks Treated by Far-Uv Radiation. *Journal of tribology* **1993**, 115, 400-405.
- (28) Zhao, X.; Bhushan, B.; Kajdas, C., Lubrication Studies of Head-Disk Interfaces in a Controlled Environment Part 2: Degradation Mechanisms of Perfluoropolyether Lubricants. *Proceedings of the Institution of Mechanical Engineers, Part J: Journal of Engineering Tribology* **2000**, 214, 547-559.
- (29) Zhao, X.; Bhushan, B., Studies on Degradation Mechanisms of Lubricants for Magnetic Thin-Film Rigid Disks. *Proceedings of the Institution of Mechanical Engineers, Part J: Journal of Engineering Tribology* **2001**, 215, 173-188.
- (30) Zhu, L.; Liew, T.; Chong, T., Pulsed Uv-Laser-Induced Chemistry of Perfluoropolyether Lubricant Film. *Applied Physics A* **2002**, 75, 633-636.
- (31) Chiba, H.; Nakamura, N.; Takeda, M.; Watanabe, K., Effects of Vacuum Ultraviolet Irradiation to Lubricant Layer on Hard-Disk Media. *Magnetics, IEEE Transactions on* **2002**, 38, 2108-2110.
- (32) Chiba, H.; Takeda, M.; Nakamura, N.; Watanabe, K., Improvements of Lubricant Performance in Hard-Disk Media by Vacuum Ultraviolet Irradiation. *Tribology international* **2003**, 36, 367-369.
- (33) Zhang, H.; Mitsuya, Y.; Imamura, M.; Fukuoka, N.; Fukuzawa, K., Effect of Ultraviolet Irradiation on the Interactions between Perfluoropolyether Lubricant and Magnetic Disk Surfaces. *Tribology Letters* **2005**, 20, 191-199.
- (34) Wakabayashi, A.; Shimizu, T.; Kobayashi, M.; Kasai, P., Uv Bonding of Hard Disk Lubricants; Characteristic and Mechanism. *Proceeding of ASIATRIB* **2006**, 603-604.
- (35) Guo, X.-C.; Waltman, R. J., Mechanism of Ultraviolet Bonding of Perfluoropolyethers Revisited. *Langmuir* **2007**, 23, 4293-4295.
- (36) Waltman, R.; Guo, X.-C., The Photodissociation of Perfluoropolyethers by Ultraviolet Light. *Tribology Letters* **2007**, 27, 227-231.

- (37) Nakakawaji, T.; Amo, M.; Matsumoto, H.; Kato, T.; Iimura, K.-i., Mechanism of Perfluoropolyether Chains Bonding on Carbon Overcoat Surface by Ultraviolet Irradiation. *Tribology Online* **2009**, 4, 88-91.
- (38) Zhang, H.; Takimoto, T.; Fukuzawa, K.; Itoh, S., Effect of Ultraviolet Irradiation on Adhesion of Nanometer-Thick Lubricant Films Coated on Magnetic Disk Surfaces. *Magnetics, IEEE Transactions on* **2011**, 47, 94-99.
- (39) Tani, H.; Kitagawa, H.; Tagawa, N., Bonding Mechanism of Perfluoropolyether Lubricant Film with Functional Endgroup on Magnetic Disks by Ultraviolet Irradiation. *Tribology Letters* **2012**, 45, 117-122.
- (40) Alam, M. K.; Zhang, H.; Koga, N.; Iuchi, S., Ultraviolet Bonding of Perfluoropolyethers to Carbon Surfaces Investigated Using Quantum Chemical Methods. *Microsystem technologies* **2013**, 19, 1383-1391.
- (41) J. Waltman, R.; Newman, J.; Guo, X.-C.; Burns, J.; Witia, C.; Amo, M., The Effect of Uv Irradiation on the Z-Tetraol Boundary Lubricant. *Tribology Online* **2012**, 7, 70-80.
- (42) Waltman, R., Evidence for the Unimolecular Decomposition of Cf 3 Ocf 3 to Cof 2 and Cf 4 by High Energy Irradiation. *Journal of Fluorine Chemistry* **2013**, 156, 378-381.
- (43) Tani, H.; Sakane, Y.; Koganezawa, S.; Tagawa, N., External Electric Field Assisted Ultraviolet Irradiation for Bonding of Lubricant Film on Magnetic Disks. *Magnetics, IEEE Transactions on* **2014**, 50, 1-4.
- (44) Tyndall, G.; Waltman, R.; Pocker, D., Concerning the Interactions between Zdol Perfluoropolyether Lubricant and an Amorphous-Nitrogenated Carbon Surface. *Langmuir* **1998**, 14, 7527-7536.
- (45) Waltman, R.; Tyndall, G.; Pacansky, J., Computer-Modeling Study of the Interactions of Zdol with Amorphous Carbon Surfaces. *Langmuir* **1999**, 15, 6470-6483.
- (46) Merzlikine, A.; Li, L.; Jones, P. M.; Hsia, Y.-T., Lubricant Layer Formation During the Dip-Coating Process: Influence of Adsorption and Viscous Flow Mechanisms. *Tribology Letters* **2005**, 18, 279-286.
- (47) Chen, H.; Li, L.; Merzlikine, A. G.; Hsia, Y.-T.; Jhon, M. S., Surface Energy and Adhesion of Perfluoropolyether Nanofilms on Carbon Overcoat: The End Group and Backbone Chain Effect. *Journal of applied physics* **2006**, 99.
- (48) Chen, H.; Guo, Q.; Li, L.; Hsia, Y.-T.; Jhon, M. S., Humidity Effects on the Relaxation of Perfluoropolyether Lubricant Films. *Magnetics, IEEE Transactions on* **2006**, 42, 2531-2533.

- (49) Bhushan, B.; Tao, Z., Lubrication of Advanced Metal Evaporated Tape Using Novel Perfluoropolyether Lubricants. *Microsystem technologies* **2006**, 12, 579-587.
- (50) Tao, Z.; Bhushan, B., Bonding, Degradation, and Environmental Effects on Novel Perfluoropolyether Lubricants. *Wear* **2005**, 259, 1352-1361.
- (51) Tei, Y.; Shirai, S.; Hattori, Y., Liquid Lubricant, Magnetic Recording Medium Using the Same, and Method for Manufacturing Magnetic Recording Medium. Google Patents: **2000**.
- (52) Kwok, D.; Neumann, A., Contact Angle Measurement and Contact Angle Interpretation. *Advances in colloid and interface science* **1999**, 81, 167-249.
- (53) Derjaguin, B.; Muller, V.; Toporov, Y., On Different Approaches to the Contact Mechanics. *Journal of Colloid and Interface Science* **1980**, 73, 293-294.
- (54) Muller, V. M.; Yushchenko, V. S.; Derjaguin, B. V., General Theoretical Consideration of the Influence of Surface Forces on Contact Deformations and the Reciprocal Adhesion of Elastic Spherical Particles. *Journal of Colloid and Interface Science* **1983**, 92, 92-101.
- (55) Pashley, R.; McGuiggan, P.; Horn, R.; Ninham, B., Forces between Bilayers of Cetyltrimethylammonium Bromide in Micellar Solutions. *Journal of colloid and interface science* **1988**, 126, 569-578.
- (56) Claesson, P. M.; Blom, C. E.; Herder, P. C.; Ninham, B. W., Interactions between Water—Stable Hydrophobic Langmuir—Blodgett Monolayers on Mica. *Journal of colloid and interface science* **1986**, 114, 234-242.
- (57) McGuiggan, P.; Pashley, R., A Study of Surfactant Solution Wetting on Mica. *Colloids and surfaces* **1987**, 27, 277-287.
- (58) Jeon, S.; Lee, J.; Andrade, J.; De Gennes, P., Protein—Surface Interactions in the Presence of Polyethylene Oxide: I. Simplified Theory. *Journal of Colloid and Interface Science* **1991**, 142, 149-158.
- (59) Alur, R.; Courcoubetis, C.; Halbwachs, N.; Henzinger, T. A.; Ho, P.-H.; Nicollin, X.; Olivero, A.; Sifakis, J.; Yovine, S., The Algorithmic Analysis of Hybrid Systems. *Theoretical computer science* **1995**, 138, 3-34.
- (60) Starr, D.; Liu, Z.; Hävecker, M.; Knop-Gericke, A.; Bluhm, H., Investigation of Solid/Vapor Interfaces Using Ambient Pressure X-Ray Photoelectron Spectroscopy. *Chemical Society Reviews* **2013**, 42, 5833-5857.
- (61) Nunney, T.; White, R., Characterizing Materials for Energy Generation Using X-Ray Photoelectron Spectroscopy (Xps). *Microscopy Today* **2011**, 19, 22-28.

- (62) Wagner, M.; Horbett, T.; Castner, D. G., Characterizing Multicomponent Adsorbed Protein Films Using Electron Spectroscopy for Chemical Analysis, Time-of-Flight Secondary Ion Mass Spectrometry, and Radiolabeling: Capabilities and Limitations. *Biomaterials* **2003**, 24, 1897-1908.
- (63) Rugar, D.; Hansma, P., Atomic Force Microscopy. *Physics today* **1990**, 43, 23-30.
- (64) Fujiwara, H., *Spectroscopic Ellipsometry: Principles and Applications*. John Wiley & Sons: **2007**.
- (65) Herzinger, C.; Johs, B.; McGahan, W.; Woollam, J.; Paulson, W., Ellipsometric Determination of Optical Constants for Silicon and Thermally Grown Silicon Dioxide Via a Multi-Sample, Multi-Wavelength, Multi-Angle Investigation. *Journal of Applied Physics* **1998**, 83, 3323-3336.
- (66) Tomkins, H. G.; McGahan, W. A., *Spectroscopic Ellipsometry and Reflectometry*. Wiley, New York: **1999**.
- (67) Coats, A.; Redfern, J., Thermogravimetric Analysis. A Review. *Analyst* **1963**, 88, 906-924.
- (68) Shafrin, E.; Zisman, W., Contact Angle, Wettability and Adhesion. *Advances in chemistry series* **1964**, 43, 145-157.
- (69) Timmons, C.; Zisman, W., The Effect of Liquid Structure on Contact Angle Hysteresis. *Journal of Colloid and Interface Science* **1966**, 22, 165-171.
- (70) Mate, C. M.; Novotny, V., Molecular Conformation and Disjoining Pressure of Polymeric Liquid Films. *The Journal of chemical physics* **1991**, 94, 8420-8427.
- (71) Bourges-Monnier, C.; Shanahan, M., Influence of Evaporation on Contact Angle. *Langmuir* **1995**, 11, 2820-2829.
- (72) Hu, H.; Larson, R. G., Evaporation of a Sessile Droplet on a Substrate. *The Journal of Physical Chemistry B* **2002**, 106, 1334-1344.
- (73) Wu, J.; Mate, C. M., Contact Angle Measurements of Lubricated Silicon Wafers and Hydrogenated Carbon Overcoats. *Langmuir* **1998**, 14, 4929-4934.
- (74) Lam, C.; Kim, N.; Hui, D.; Kwok, D.; Hair, M.; Neumann, A., The Effect of Liquid Properties to Contact Angle Hysteresis. *Colloids and Surfaces A: Physicochemical and Engineering Aspects* **2001**, 189, 265-278.
- (75) Tavana, H.; Jehnichen, D.; Grundke, K.; Hair, M.; Neumann, A., Contact Angle Hysteresis on Fluoropolymer Surfaces. *Advances in colloid and interface science* **2007**, 134, 236-248.

- (76) Drelich, J.; Miller, J. D., Examination of Neumann's Equation-of-State for Interfacial Tensions. *Journal of colloid and interface science* **1994**, 167, 217-220.
- (77) Janssen, D.; De Palma, R.; Verlaak, S.; Heremans, P.; Dehaen, W., Static Solvent Contact Angle Measurements, Surface Free Energy and Wettability Determination of Various Self-Assembled Monolayers on Silicon Dioxide. *Thin Solid Films* **2006**, 515, 1433-1438.
- (78) Pollet, I.; Pieters, J.; Verschoore, R., Impact of Water Drops on the Visible Radiation Transmittance of Glazings under Outside Radiant Conditions. *Solar energy* **2002**, 73, 327-335.
- (79) Rangel, E.; Bento, W.; Kayama, M.; Schreiner, W.; Cruz, N., Enhancement of Polymer Hydrophobicity by Sf6 Plasma Treatment and Argon Plasma Immersion Ion Implantation. *Surface and interface analysis* **2003**, 35, 179-183.
- (80) Grosu, G.; Andrzejewski, L.; Veilleux, G.; Ross, G., Relation between the Size of Fog Droplets and Their Contact Angles with Cr39 Surfaces. *Journal of Physics D: Applied Physics* **2004**, 37, 3350.
- (81) Li, L.; Jones, P.; Hsia, Y.-T., Effect of Chemical Structure and Molecular Weight on High-Temperature Stability of Some Fomblin Z-Type Lubricants. *Tribology Letters* **2004**, 16, 21-27.
- (82) Howarter, J. A.; Genson, K. L.; Youngblood, J. P., Wetting Behavior of Oleophobic Polymer Coatings Synthesized from Fluorosurfactant-Macromers. *ACS applied materials & interfaces* **2011**, 3, 2022-2030.
- (83) Wang, Y.; Dong, Q.; Wang, Y.; Wang, H.; Li, G.; Bai, R., Investigation on Raft Polymerization of a Y - Shaped Amphiphilic Fluorinated Monomer and Anti - Fog and Oil - Repellent Properties of the Polymers. *Macromolecular rapid communications* **2010**, 31, 1816-1821.
- (84) Leng, B.; Shao, Z.; de With, G.; Ming, W., Superoleophobic Cotton Textiles. *Langmuir* **2009**, 25, 2456-2460.
- (85) Xu, F.; Neoh, K.; Kang, E., Bioactive Surfaces and Biomaterials Via Atom Transfer Radical Polymerization. *Progress in polymer science* **2009**, 34, 719-761.
- (86) Kobayashi, M.; Terayama, Y.; Yamaguchi, H.; Terada, M.; Murakami, D.; Ishihara, K.; Takahara, A., Wettability and Antifouling Behavior on the Surfaces of Superhydrophilic Polymer Brushes. *Langmuir* **2012**, 28, 7212-7222.
- (87) Wang, Y.; Knapp, J.; Legere, A.; Raney, J.; Li, L., Effect of End-Groups on Simultaneous Oleophobicity/Hydrophilicity and Anti-Fogging Performance of Nanometer-Thick Perfluoropolyethers (Pfpes) *RSC Advances* **2015**, 5 30570-30576.

- (88) Granick, S.; Kumar, S. K.; Amis, E. J.; Antonietti, M.; Balazs, A. C.; Chakraborty, A. K.; Grest, G. S.; Hawker, C.; Janmey, P.; Kramer, E. J., Macromolecules at Surfaces: Research Challenges and Opportunities from Tribology to Biology. *Journal of Polymer Science Part B: Polymer Physics* **2003**, 41, 2755-2793.
- (89) Luengo, G.; Schmitt, F.-J.; Hill, R.; Israelachvili, J., Thin Film Rheology and Tribology of Confined Polymer Melts: Contrasts with Bulk Properties. *Macromolecules* **1997**, 30, 2482-2494.
- (90) Rowland, H. D.; King, W. P.; Pethica, J. B.; Cross, G. L., Molecular Confinement Accelerates Deformation of Entangled Polymers During Squeeze Flow. *Science* **2008**, 322, 720-724.
- (91) Vogel, M., Rotational and Conformational Dynamics of a Model Polymer Melt at Solid Interfaces. *Macromolecules* **2009**, 42, 9498-9505.
- (92) Gellman, A. J., Vapor Lubricant Transport in Mems Devices. *Tribology Letters* **2004**, 17, 455-461.
- (93) Mate, C. M., Atomic-Force-Microscope Study of Polymer Lubricants on Silicon Surfaces. *Physical review letters* **1992**, 68, 3323.
- (94) Priestley, R. D., Physical Aging of Confined Glasses. *Soft Matter* **2009**, 5, 919-926.
- (95) Huu, C. H.; Vu-Khanh, T., Effects of Physical Aging on Yielding Kinetics of Polycarbonate. *Theoretical and applied fracture mechanics* **2003**, 40, 75-83.
- (96) De Gennes, P.-G., *Scaling Concepts in Polymer Physics*. Cornell university press: **1979**.
- (97) Alsten, J. V.; Granick, S., Shear Rheology in a Confined Geometry: Polysiloxane Melts. *Macromolecules* **1990**, 23, 4856-4862.
- (98) Cho, Y.-K.; Watanabe, H.; Granick, S., Dielectric Response of Polymer Films Confined between Mica Surfaces. *The Journal of chemical physics* **1999**, 110, 9688-9696.
- (99) Aoyagi, T.; Takimoto, J.-i.; Doi, M., Molecular Dynamics Study of Polymer Melt Confined between Walls. *The Journal of chemical physics* **2001**, 115, 552-559.
- (100) Borodin, O.; Smith, G. D.; Bandyopadhyaya, R.; Bytner, O., Molecular Dynamics Study of the Influence of Solid Interfaces on Poly (Ethylene Oxide) Structure and Dynamics. *Macromolecules* **2003**, 36, 7873-7883.
- (101) Zhang, H.; Mitsuya, Y.; Fujikawa, Y.; Fuwa, A.; He, Y.; Fukuzawa, K., Changes in Friction Properties of Monolayer Lubricant Films Induced by Development of Molecules' Bonding. *Tribology Letters* **2007**, 28, 163-170.

- (102) Choi, J.; Morishita, H.; Kato, T., Frictional Properties of Bilayered Mixed Lubricant Films on an Amorphous Carbon Surface: Effect of Alkyl Chain Length and Sam/Pfpe Portion. *Applied surface science* **2004**, 228, 191-200.
- (103) Cotts, P. M., Solution Properties of a Group of Perfluoropolyethers: Comparison of Unperturbed Dimensions. *Macromolecules* **1994**, 27, 6487-6491.
- (104) Evans, S. D.; Sharma, R.; Ulman, A., Contact Angle Stability: Reorganization of Monolayer Surfaces? *Langmuir* **1991**, 7, 156-161.
- (105) Jhon, M. S.; Choi, H. J., Rheological Analysis of Oligomeric Perfluoropolyethers. *Polymer* **2010**, 51, 1882-1886.
- (106) Ben, O.; Vavylonis, D., Non-Equilibrium in Adsorbed Polymer Layers. *Journal of Physics: Condensed Matter* **2005**, 17, R63.
- (107) Granick, S., Motions and Relaxations of Confined Liquids. *Science* **1991**, 253, 1374-9.
- (108) Hu, H.-W.; Carson, G. A.; Granick, S., Relaxation Time of Confined Liquids under Shear. *Physical review letters* **1991**, 66, 2758.
- (109) Mate, C. M.; Marchon, B., Shear Response of Molecularly Thin Liquid Films to an Applied Air Stress. *Physical review letters* **2000**, 85, 3902.
- (110) Priestley, R. D.; Ellison, C. J.; Broadbelt, L. J.; Torkelson, J. M., Structural Relaxation of Polymer Glasses at Surfaces, Interfaces, and in Between. *Science* **2005**, 309, 456-459.
- (111) Richard, A., Interface and Surface Effects on the Glass-Transition Temperature in Thin Polymer Films. *Faraday Discussions* **1994**, 98, 219-230.
- (112) van Zanten, J. H.; Wallace, W. E.; Wu, W.-l., Effect of Strongly Favorable Substrate Interactions on the Thermal Properties of Ultrathin Polymer Films. *Physical Review E* **1996**, 53, R2053.
- (113) Scarpulla, M. A.; Mate, C. M.; Carter, M. D., Air Shear Driven Flow of Thin Perfluoropolyether Polymer Films. *The Journal of chemical physics* **2003**, 118, 3368-3375.